SYNTHESIS AND LEACHATE ANALYSIS OF DRY SYNTHESIZED SUBSTITUTED FLUORAPATITE NUCLEAR SURROGATE WASTE FORMS FOR MOLTEN SALT REACTORS

A Dissertation

by

RICHARD J. LIVINGSTON

Submitted to the Graduate and Proffessional School of
Texas A&M University
in partial fulfillment of the requirements for the degree of

DOCTOR OF PHILOSOPHY

Chair of Committee,	Sean McDeavitt
Committee Members,	Pavel Tsvetkov
	Patrick Shamberger
	Luis Ortega
Head of Department,	Michael Nastasi

May 2022

Major Subject: Nuclear Engineering

ABSTRACT

The development of commercialized molten salt reactors nuclear reactors (MSR), a nuclear reactor where the fuel is in a liquid state dissolved in carrier salt, is underway throughout the nuclear power community. With this renewed interest in MSRs multiple unresolved issues need to be addressed before commercialization is to occur. One area is waste management of spent fuel. However, this is a complex scenario for MSRs, as the fuel is dissolved within a carrier salt. Further complications arise once operation begins and fission product buildup begins to occur in the carrier salt. Various removal methods have been proposed depending on the needs of the fuel, carrier salt, and state of the fission product: whether they are a gas, soluble compound, or insoluble metal. The aforementioned waste streams will culminate in a final waste product that will require adequate and safe disposal methods.

A direct dry conversion process is presented for synthesizing fluorapatite minerals from soluble fission products, carrier salt, and the fuel for fluorine salt bearing MSRs. A lithium fluoride and beryllium fluoride salt (FLiBe) was combined with tricalcium phosphate (TCP) and sintered to produce substituted fluorapatites. Upon verification of apatite formation, additional fission product substituted apatites were fabricated using the same conversion process to incorporate cesium fluoride (CsF), strontium fluoride (SrF_2), gadolinium fluoride (GdF_3) and uranium tetrafluoride (UF_4): these compounds are representative of the fuel and represent a gamut of fission products expected from this waste stream.

The apatites are characterized using Powder X-Ray Diffraction (XRD) methods to determine phases present in the sintered apatites. Additionally, scanning electron microscopy and energy dispersive spectroscopy (SEM-EDS) techniques were employed to verify XRD predictions and to determine the nature of any additional phases found during SEM and XRD analysis. Afterwards the XRD data were updated and Rietveld refinement techniques were employed to quantify the phases.

The synthesized surrogate waste form minerals were subjected to a common leach testing pro-

cedure devised by the American Society for Testing and Materials (ASTM), specifically ASTM's C1285, commonly known as the Product Consistency Test (PCT). The leach testing is used to determine leaching rates of the constituents to quantify leaching behavior on directly fluorapatite surrogate waste forms. Leachate from the PCTs were subjected to analytical chemistry techniques to quantify the leached cations and anion concentrations. From the chemical concentration data normalized concentrations (NC_i) and normalized elemental mass loss (NL_i) were tabulated. The NC_i of the elements of interest ranged from 5.27X10^{-4} to 1.08 g/L and NL_i ranged from 7.76X10^{-9} to 20.3 g/m^2. The calculated values were then compared to other waste form studies to show the efficacy of fluorapatite waste forms.

ACKNOWLEDGMENTS

I would like to thank Dr. McDeavitt and my committee for their guidance and support throughout my studies at Texas A&M. As well as the fellow students of the FCML for their support throughout this study.

I would also like to thank Dr. Ragusa of Texas A&M's Nuclear Department for facilitating and managing the NuSTEM IRP and the rest of NuSTEM team for their support and the opportunities and experiences that have presented themselves through this work.

Finally, I would like to thank my family and friends for their support and encouragement throughout my education and research at Texas A&M University.

CONTRIBUTORS AND FUNDING SOURCES

Contributors

This research was supported by a dissertation committee consisting of Professor Sean McDeavitt (advisor), Professor Pavel Tsvetkov, and Dr. Luis Ortega of the Department of Nuclear Engineering and Professor Patrick Shamberger of the Department of Material Science.

The inductively coupled plasma mass spectrometry (ICP-MS) presented in this work was conducted by Dr. Bryan Tomlin of the Department of Chemistry at Texas A&M University.

All other work conducted for the dissertation was completed by the student independently.

Funding Sources

This study was funded by the United States Department of Energy's Office of Nuclear Energy, Univeristy Program grant No. DE-NE0008651.

NOMENCLATURE

ρ	Density (g/cm^3)
AEC	Atomic Energy Commission
ARE	Aircraft Reactor Experiment
ASTM	American Society of Testing and Materials
ATR	Aircraft Test Reactor
BeF_2	Beryllium Fluoride
°C	Degrees Celsius
$CaCO_3$	Calcium Carbonate
$CaHPO_4$	Calcium Hydrogen Phosphate
CsF	Cesium Fluoride
FAp	Fluorapatite
FLiBe	Lithium Fluoride and Beryllium Fluoride Salt in a 66.6-33.4mol% (LiF-BeF_2) Composition
g	Grams
GdF_3	Gadolinium Fluoride
in	Inch
LiF	Lithium Fluoride
ml	Milliliter
mm	Millimeter
MCC	Materials Characterization Center
MCF	Materials Charaterization Facility
MPa	Megapascal

MSBR	Molten Salt Breader Reactor
MSR	Molten Salt Fueled Reactor
MSRP	Molten Salt Reactor Project
NaF	Sodium Fluoride
NaOH	Sodium Hydroxide
NC_i	Normalized Concentration. The total mass fraction of ion *i* in the waste form that dissolves into the solution
NH_4HF_2	Ammonium Bifluoride
NHO_3	Nitric Acid
NL_i	Normalized Elemental Mass Loss. The total mass of waste form element *i* dissolved into the leachant over the duration of the test
ORNL	Oak Ridge National Laboratory
PCT	Product Consistency Test
PFA	Perfluoroalkoxy Alkane
PTFE	Polytetrafluoroethylene
Sa	Surface Area
SrF_2	Strontium Fluoride
TCP	Tricalcium Phosphate
UF_4	Uranium Tetrafluoride
UF_6	Uranium Pentafluoride
V_i	Volume With Respect to Variable *i*
VHT	Vapor Hydration Test
ZrF_4	Zirconium Fluoride

TABLE OF CONTENTS

Page

LIST OF FIGURES

FIGURE Page

LIST OF TABLES

TABLE Page

1. Introduction

The aim of this study is to investigate the efficacy of synthesized fluorapatite as a potential waste form or waste form precursor for molten salt reactors. Fluorapatite was selected as a waste form for its capacity to incorporate fluoride salts components, salts typically proposed for use in thermal molten salt reactors, and a wide variety of cations into the apatite structure leading to various substituted fluorapatites. The following sections in this chapter detail the molten salt reactor and the issues particular to waste generated from this style of reactor, Section 1.1. An overview of the history of the molten salt reactor and project motivation is presented in Section 1.2. While Section 1.3 outlines the scope of the work conducted in this study.

A direct dry synthesis method was modified for the production of substituted fluorapatites. While various apatites have been created using similar methods, this work is the first to produce apatites containing uranium and multiple surrogate waste products at once. Further, it is the first work to conduct leach testing and subsequent analysis on synthetic fluorapatites in the context of a nuclearn waste form. The leach testing is foundational work needed in order begining to undertsand the behavior of the waste form to retain structural and radioactive components. It is the first major step in moving fluorapatite from a hypothetical waste form into a position of waste form candidacy for molten salt reactors.

1.1 The Molten Salt Reactor

The molten salt reactor (MSR) is a class of fission reactors in which the primary coolant, or carrier salt, and the fuel are a molten mixture. This means as the reactor is in operation fission products will develop within this carrier salt alongside the fuel. Thus, the primary loop will contain salt, fuel, and fission products. These fission products fall into various classes depending on the element or proceeding compound that may form: they are fission product gases, insoluble noble metals, and soluble fission products.

All of the aforementioned fission product categories produce issues within the system and may

require their own unique removal path and managment method within the fuel system. A high-level representation of a molten salt reactor with removal of each of these fission product categories is shown in Figure 1.1. However, these removal systems fall into design requirements and decisions that have been left to the vendors that are developing molten salt reactors.

Many questions are left to vendors and industry decisions how, when, the compostion of these waste stream, however questions may be asked for the final waste package that will be disposed of. What are the essential elements which require removal of waste produced so that a pathway to waste disposal may be resolved. Again, a separate answer for each category of waste stream may be required as the waste for each will have its own procedure and challenges to a final waste product. This research seeks to begin to solve one of these waste streams, that of the carrier salt, fuel, and dissolved fission products. While no treatment of the spent fuel salt is an option, this has lead to criticality concerns at Oak Ridge National Laboratory in the past, and will be discussed in the follow section. Requiring removal of the fuel from the salt, thus some method of conditioning the salt must happen for before long term storage of the waste.

Removal and separation of the fission products itself is an engineering challenge, it is not one covered here as this a reactor design question. Instead, the research performed here focuses on establishing the foundation of a waste form to contain the extracted soluble fission products, carrier salt, and spent fuel that will be removed during the period of operation or at end of life. However, currently it is unknown what the composition of this waste stream will be and had to be estimated for the work.

1.2 Molten Salt Reactor History and Motivation

The first major implementation of the molten salt reactor concept started in the late 1940s to aid in the US Aircraft Nuclear Propulsion Program conducted under the US Army Air Force which was to design a nuclear-powered bomber. The first project under this effort was the Aircraft Reactor Experiment (ARE). The reactor's main loop, constructed at Oak Ridge National Laboratory (ORNL), comprised NaF-ZrF_4-UF_4. The ARE operated for 462 hours, split between non-critical and critical operation [1]. In the mid-1950s the experiment came to a close and the reactor disman-

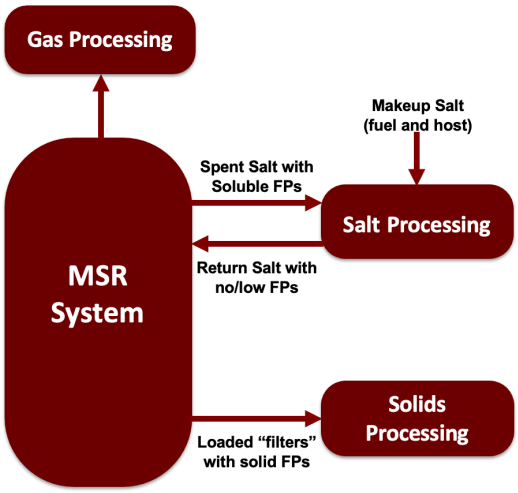

Figure 1.1: Diagram representing high-level waste stream for molten salt reactors.

tled. A second program, the Aircraft Test Reactor proceeded the ARE and site preparation began at ORNL however, the program had been canceled before construction of the reactor began [2].

This was not the end of the molten salt reactor, towards the end of the 1950s the Atomic Energy Commission (AEC) shifted molten salt reactor research to focus on civilian use and power production by funding the Molten Salt Reactor Experiment (MSRE) at Oak Ridge National Laboratory, using the facilities that were designated for the ARE [3]. The MSRE main loop comprised LiF-BeF_2-ZrF_4-UF_4 (65-29-5-1 mol%) and was designed to operate at 10-MW_{th} [4]. Construction of the reactor finished in 1964 with fuel salt loading beginning soon after. The MSRE obtained first criticality in 1965 with the reactor remaining in operation until 1969.

Upon completion of the MSRE in 1968, the Experimental Breeder Reactor Program was established, however, full funding hadn't been procured from the AEC, which subsequently terminated the MSRE program and further MSR research. After final shutdown of the MSRE, ORNL decommissioned the reactor and moved the fuel laden salt into long-term storage containers. It was later discovered that at low temperatures radiolysis liberated fluorine from the salt and waste constituents producing fluoride gas. To ease fluorine generation the salt was heated to 150°C annually until 1989. Yet concerns grew over fluoride gas production which could lead to uranium tetrafluo-

ride (UF_4) complexing to uranium hexafluoride (UF_6, a volatile form of uranium fluoride, leading to migration of the fuel components in the stored waste [5].

In 1994 it was discovered that UF_6 production had been occurring and that upper sections of the storage tanks were comprised of UF_6 and fluoride gases, leading to a potential criticality accident [5]. Research to decontaminate and decommission the storage tanks soon followed culminating in removal of the uranium compounds from the salt: with work begining in 2003 and finishing in 2009. While the uranium was removed, the carrier salt and fission products from operation are still in the long-term storage tanks at ORNL [6].

In recent years, numerous independent firms and governmental laboratories have demonstrated renewed interest in advancing towards commercialization of molten salt reactors. Many challenges were never resolved during previous investigations that were conducted on molten salt reactors, including a long term waste solution of the spent salt. This led to under developed waste management strategies and methods that solely deal with the salt, fuel, and fission products. Development of a suitable waste form will be necessary in moving the reactor class into commercialization, a waste form that allows not merely the capability to integrate the fuel but the fission products and carrier salt into a single waste package will assist in promoting the molten salt reactor out of research phase into commercial operation.

1.3 Objective

The objective of this work is to determine the efficacy of fluorapatite (FAp) and substituted fluorapatite minerals via a direct disposal immobilization route to sequester fluorine salts, dissolved fluorinated fission products, and fuel employed in thermal molten salt reactors containing fluorine salts. Previous research conducted by Lexa established that direct conversion of a LiF-BeF_2 salt into FAp could be accomplished [7]. Building upon this past work, fluorapatite was synthesized from tricalcium phosphate (TCP) and a lithium-beryllium fluoride (FLiBe), 66-34 mol% (LiF-BeF_2), salt. The resulting crystal structures were determined using Powder x-ray diffraction techniques (XRD).

Upon completion, FLiBe salt was doped with small amounts of UF_4 and various representative

soluble fission products for formation of substituted FAp. The resulting substituted FAp waste forms were subjected to additional powder x-ray diffraction measurements in conjunction with scanning electron microscopy and energy dispersive spectroscopy to characterize and quantify the microsctructures developed in each the apatites.

Finally, a common leach test procedure devised for glass and glass-ceramic nuclear and hazardous waste was conducted on the FLiBe salt, synthesized FAp, and substituted FAp. Leachate from the procedure was analyzed for pH differences, and fluoride and cation concentrations. Samples from each experiment were subjected to pycnometer measurements to determine the densities, once obtained the surface area was calculated to obtain a leach rate for the ions of interest. The leach rates are then normalized and compared to various other waste form studies.

2. Background

The following section establishes the foundation for work performed in this study. Section 2.1 outlines the development process of a nuclear waste form. Section 2.2 details the framework of fluorapatite as a potential waste form. Previous work conducted on synthesized fluorapatite waste forms is presented in Section 2.3 While the final section, Section 2.4, reviews the major nuclear waste form leach testing protocols.

2.1 Overview of Waste Form Development

Development of waste disposal technologies has been a crucial issue for nuclear energy where a balance must be taken with emphasis on safety, economics, and waste minimization. Fundamentally a complete waste package contains the waste form and possible other structural binding methods, such as vitrification which as has been demonstrated in chloride salt waste work [8, 9]. Further, the waste form must function to contain and isolate the radioactive and hazardous components from the environment for long term storage within the waste package [8].

In a recent article by Riley et al., numerous direct disposal immobilization techniques have been proposed for the soluble fission product waste stream in MSRs [10]. These consist of direct disposal, vitrification, metal-composite, and mineralization. Direct disposal is one of two current methods for nuclear waste disposal for the operating light water reactors in the United States, here direct retention of the nuclear fuel and the fuel cladding is simply moved to long term storage. Direct disposal of the waste in a molten salt reactor may not be an answer to this problem, as demonstrated with the issues that developed after the MSRE was dismantled at Oak Ridge National Laboratory. Additionally, many of the proposed fluoride salts dissolve or disassociate in the presence of water.

Vitrification, the second method used for waste disposal in the current nuclear fleet, involves removing the fuel from the cladding and processing the spent fuel. With an end product that encases the spent fuel and non-gaseous fission products in borosilicate glass. While conversion to

borosilicate glass is an option, studies have shown that borosilicate glass does not support significant loading of fluorides and not retain the halogens that comprise a majority of the carrier salts proposed for MSRs [11]. Fluorite glasses are an option; however, they demonstrate low chemical durability requiring additives to function long term [10].

Multiple minerals have been identified that accept various ions into their crystal structure with the three principal candidates for salt waste disposal. They are titanites, sodalites, and apatites [10]. Titanites were first explored in the 1970s for waste treatment in the United States nuclear defense program, utilizing a complex process called SYNROC [12]. Titanite is a composite formed of zirconolite (eg. $CaZrTi_2O_7$), perovskite (eg. $CaTiO_3$), and hollandite (eg. $BaAl_2Ti_6O_16$) and can incorporate a broad assortment of alkalis, alkali-earth metals, transition metals, metals, and actinides into its structure [13, 12].

Sodalite was developed during the pyroprocessing initiative as part of the Experimental Breeder Reactor II program culminating in sodalite-glass waste forms, however stability at elevated temperatures is known to degrade the structure [14]. The sodalite mineral has the general structure:

$$R_8^{+1}(R^{+3}R^{+4}O_4)_6A_n \tag{2.1}$$

Where R denotes cations with the respective valence +1, +3, +4 state and A are anions with -1 valence state [15]. Like titanite, sodalite possess the ability to accept a variety of elements into its structure.

Apatites have been explored for a host of nuclear waste forms depending on the halogen ranging from chloride, fluoride, and iodine apatites [7][9][16]. Apatites have the general form:

$$R_{(4-x)}^{+1,+2}R_{(6+x)}^{+3,+4}[(Si,P,V)O_4]_6A_2 \tag{2.2}$$

Where R denotes cations with the respective valence of +1 through +4 and A any -1 or -2 anion [17][18]. Just as the previous minerals presented apatites accept a wide variety of ions into their structures.

Metal composites are composed of waste particles in a ceramic form or encased in a ceramic and are immobilized in a metal matrix. Common metal composites are cermet and halmet however, limited research exists on their applicability for work with halogen salts and are in need of further study to determine if they may be effective at sequestering molten salt waste.

2.2 The Fluorapatite Mineral

Support of apatites as a waste form can be seen at the Oklo Natural Reactor site where apatites containing fission products are observed within the rock structures. While no longer active, the Oklo site is a rare natural event where sufficient natural uranium was present under precise environmental conditions that allowed spontaneous nuclear fission to occur roughly 1.7 million years ago. Within these apatites isotopes of rubidium, barium, and rare earth elements characteristic of fission have been found. When compared to the quantity of uranium found within these samples researchers concluded that the formation of the apatites formed due to migration of the fission product isotopes into the apatites after fission of uranium had occurred [19]. This migration and immobilization of the fission products supports the basis for use of apatites as a waste form.

Apatites are typically described as a mineral containing phosphate, cations, and an anion such as fluorapatite, $Ca_{10}(PO_4)_6F_2$, and are described by Elliot as a mineral with a hexagonal structure with a space group of $P6_{3/m}$ and lattice parameters a = 9.367 and c = 6.884 Å. The structure of apatites consists of columns of cations spaced one and a half the distance of the c parameter and are designated Ca_1, often called the columnar site, these are connected to neighboring cations above and below with three shared oxygen atoms [17]. The columns are linked together by phosphates in phosphate-oxygen tetrahedras. The resulting three-dimensional structure results in two distinct channels throughout the structure. The first of theses sites lays between the parallel oxygen planes while the second lies within the triangularly bonded oxygen: in these channels sit the second cation and the anion. The first channel contains the second cation, Ca_2, and the anion is nested in the second channel [17]. A diagram of the apatite structure is provided in Figure 2.1.

The resulting structure allows for a wide variety of substitutions at the Ca_1, Ca_2, and anion sites. At the anion site, substitutions have been observed for hydroxide ions, other halogens, peroxide,

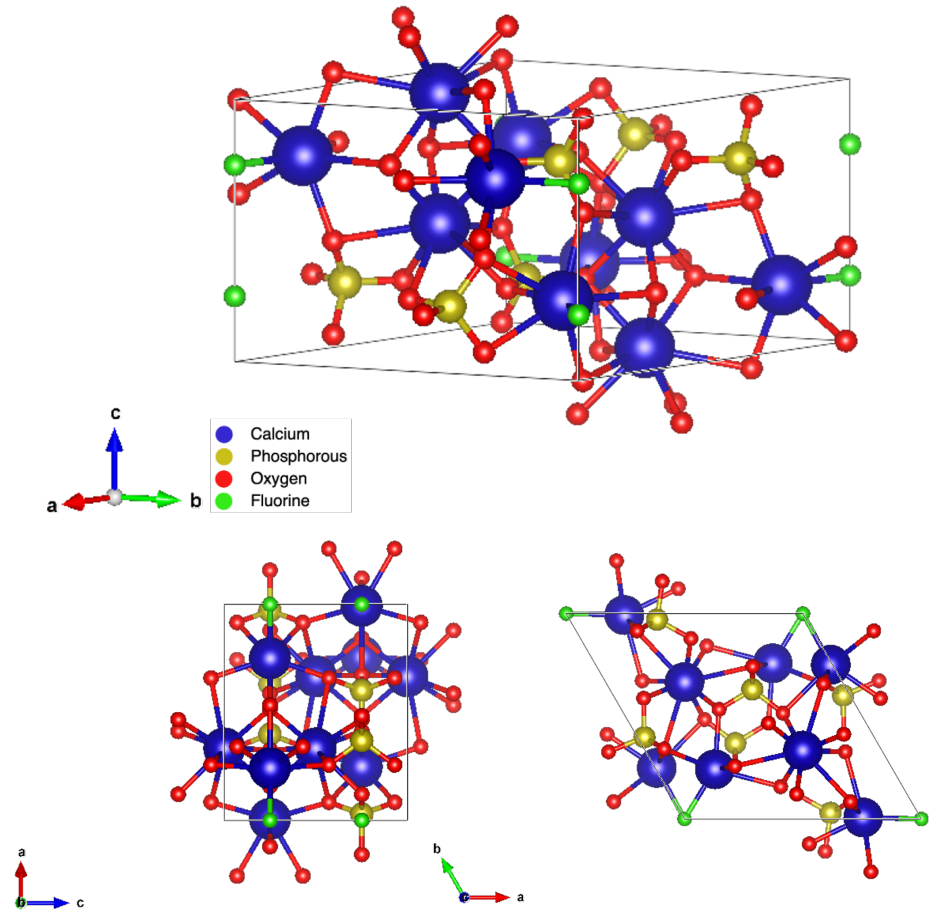

Figure 2.1: The isometric view (top), and perpedicular views from the b axis and the c axis (bottom) of the fluorapatite structure.

cyanamide, carbonate, and sulfates [17]. These substitutions are the basis for other apatites with the charge balance, size, and electronegativity affecting the resulting produced structure.

Cation substitutions can be relatively complex as there are two locations for substitution, typically substitutions are described with respect to calcium. Resulting in an unequal distribution of substitutions at the sites. Further, if the replacement cation carries a +2 or a +4 charge, the substitution is expected to site select by the size of the ion compared to the calcium ions location size, although other circumstances may influence this. Based on coordination number, it is predicted that cations smaller than calcium will fill the Ca_2 site while larger ions will occupy the Ca_1 site [17].

For ions of +1 an +3-valence state, they must overcome charge compensation mechanism to fit within the apatite structure and generally appear at the Ca_2 site when the size of the cation is close to that of calcium. However, Elliot notes that when multiple replacement elements are presented, indiscriminate occupation of both sites may occur [17]. While there may be some grounds for prediction of which site cations substitutions will replace. There is presently no general rule that will predict where a cation will rest. Some use an expansion of apatite definition which contain to 17 minerals that include the phosphates, arsenates, and vanadates. Additionally, sulphates and silicates can form similar structures and compounds to the apatites.

2.3 Previous Work on Fluorapatite Waste Forms

Fluorapatites have been investigated for some time with initial adoption in the medical and dental fields [20, 21, 22]. Fluorapatite use in the nuclear field emerged as a possible waste form solution for the waste salt left over from the MSRE project. In which, lithium fluoride (LiF) and beryllium fluoride (BeF_2) salts are mixed into tricalcium phosphate (TCP) and heated treated. Powder X-Ray Diffraction patterns confirmed the presence of fluorapatite structures. Differential scanning calorimetry identified two thermal incidents were appearing within the samples. The first peak was determined to be the melting point of the LiF and BeF_2 salt used. While the second, a sharp exothermic peak, at 527°C was determined to be the required temperature to convert the constituents to fluorapatite [7].

Wet synthesis of fluorapatite, and strontium and neodymium apatites have also been conducted. In this work calcium nitrate or strontium hydroxide were mixed with phosphoric acid and ammonium bifluoride. Ammonium hydroxide was then added to reach a pH of 7, at this time the apatites would precipitate out of the solution [23]. The apatite was separated, dried, and pressed into pellets for further processing and analysis using XRD. The fluorapatite samples were estimated to contain 95-97% apatite with a minor phase assumed to be calcium fluoride. While the strontium apatite, $Sr_2(PO_4)_2$, contained impurities of approximately 15% strontium phosphate and approximately 1% $Sr_2P_2O_7$ [23]. The neodymium apatites were produced in a similar manner and contained significantly less neodymium apatite at roughly 13% [23].

Further work focused on substitutions of calcium ions with heavy metals conducted using dry processing techniques, similar to Lexa. One such study sequestered cesium and neodymium in an apatite known as britholite [24]. Fluorapatite substituted synthesis using strontium was performed utilizing a blend of strontium fluoride, calcium fluoride, and calcium phosphate yielding an apatite with a strontium content up to 10%. The same study reacted strontium hydrogen phosphate, calcium oxide, and calcium fluoride forming a strontium bearing fluorapatite with loading up to 70% [25]. In both occasions, Raman spectra, XRD, and scanning electron microscopy (SEM) with energy dispersive spectroscopy mapping (EDS) were employed for verification. Further activity within the same group modified the process to achieve a 100% loading of strontium creating $Sr_{10}(PO_4)_6F_2$[26].

2.4 Waste Form Testing Methods

To evaluate the capability of a waste form's immobilization ability two approaches are commonly employed, leach testing and modeling. Leach testing is used in waste form characterization as the major failure mechanism identified for nuclear waste forms is leaching of the structural or radioactive components from the waste form or waste package. Leach testing is used throughout development cycles of nuclear waste forms. Modeling is emerging as a viable testing method in many material engineering applications, allowing users to develop computer models that can predict the behavoir under a given scenario and has begun to be implemented in waste form testing. Modeling is not covered in the following study.

Many standards have been developed for leach testing and provide for an ample variety of parameters, such as sample size and environment. Once one of the leach tests are completed the leachate can be analyzed using standard analytical chemistry methods such as anion or cation concentraion analysis. While many governing bodies exist, leach test methods proposed by the Americas Society for Testing and Materials (ASTM) will be covered.

The most fundamental leach test and the typcal starting point to determine viability of a waste form for further investigation is the Product Consistency Test (PCT), ASTM C1285, a static leach test developed to test ceramic and glass nuclear and hazardous waste forms. The PCT contains two

methods, method A and B, where method A restricts the environment, duration, particle size, and temperature during tests. While method B allows for easing of the constraints. A PCT is conducted by processing the waste form to a defined particle size, and deposited into a sealable vessel with a liquid, typically ASTM Type-1 water, a regagnt grade water with little to no contamination and low electrical properties. The test is usually conducted over 7-days at 90°C.

Next is monolith testing, comprising of larger cylinders or cubes of a waste form. Monloith testing is a similarly to method B of the PCT. Originally developed as Matierals Characterization Center (MCC) 1 & 2, or MCC-1 and MCC-2, further advancement shifted into what is now ASTM C1220. Monolith testing is conducted from 1-day to 1-month at room temperature and can be completed under differing environments with temperatures up to 100°C.

Non-static testing under a flowing environment is covered in ASTM C1662 and recognized as the single-pass flow-through or SPFT method. In C1662, various waste form sizes are tested utilizing a single pass-through flow of water or other liquid. The technique provides for temperatures up to 100°C and can likewise accommodate various pHs using different liquids. An advantage of this method is that surface analysis of the material can identify additional corrosion mechanisms.

Accelerated leach testing methods are also available, such as ASTM C1308. In this method, monoliths are simultaneously tested at 20°C and at an elevated temperature in water. Results can then be used to determine the increased rate of corrosion between the standard temperature and the elevated temperature.

Vapor hydration testing (VHT), ASTM C1663, is applied to investigate waste form deterioration, typically under high temperatures up 300°C. Here the environmental conditions allow for vapor or a thin film to cover a waste form monolith. The elevated, or in some cases reduced, temperatures allow for phase changes that may arise in extreme storage conditions. Therefore providing for not just simple leaching information but knowledge regarding possible phase changes and their respecting leaching characteristics.

3. Experimental Methods

The following chapter outlines the experimental equipment and methods employed to conduct the experiments. Sections 3.1 through 3.3 summarize the synthesis of compounds that were not commercially available: with Section 3.1 describing FLiBe salt fusing, Section 3.2 summarizing production of tricalcium phosphate, and 3.3 describing the fluorination of uranium oxide (UO_2) to produce uranium tetrafluoride (UF_4). Section 3.4 outlines fluorapatite and substituted fluorapatite production methods. Section 3.5 describes the PCT procedure adopted for leach testing. Section 3.6 introduces the density measurement techniques employed. While Section 3.7 describes the methods employed to calculate the normalized leaching rates, and finally Sections 3.8 and 3.9 summarize the procedures for preparing the waste forms for powder x-ray diffraction and scanning electron microscopy with energy dispersive x-ray spectroscopy techniques, respectively.

All work conducted with the salt components lithium fluoride (LiF) and beryllium fluoride (BeF_2) as well as the fused FLiBe salt were completed inside an inert atmosphere MBraun glove-box using a helium atmosphere under negative pressure. While infiltration of oxygen and water is a concern for salt quality, safety of the user and lab personnel are the predominant consideration as BeF_2 and LiF are easily aerosolized. Furthermore, beryllium fluoride is a known carcinogenic and associated with serious chronic lung and breathing complications. While lithium fluoride is a corrosive compound that can diffuse through skin and can lead to severe skin and eye damage. In addition, all activity conducted using fluorinated compounds are treated in the same manner. When moved outside of the glovebox, samples were handled only by authorized personnel with no other personnel in the immediate laboratory space, and placed an air tight container until use. Proper protective equipment was donned at this time, including a full-face respirators, and placed within a secondary sealed container to reduce contamination to the laboratory during transportation to designated beryllium work areas.

In Chapter 2 waste form and waste package were discuessed, asserting the two terms have different definitions for the final waste product. The aim of this research is to determine the efficacy

of the fluorapatite mineral not to define the waste form or the waste package. Additionally, the waste forms synthesized are infact not true waste forms as they do not contain waste from a reactor but are instead surrogate waste forms doped with representative elements. To fully define the fluorapatite as a waste form or waste package will require further study that this investigation lays the ground work for. However, to facilitate discussion the fluorapatite may be referred to as a waste form or surrogate waste form throughout this document.

3.1 FLiBe Salt Fusing

At the time of this research, fused lithium fluoride and beryllium fluoride salts were not commercially available. To produce the FLiBe salt, 99.99% pure powdered LiF was procured from ProChem and >99% pure powdered BeF_2 was bought from BOC Sciences. The BeF_2 shipped sealed under argon atmosphere and upon delivery, both chemicals were stored in an MBraun LABmaster Pro glovebox under helium atmosphere until use, the glove box and working are are shown in Figure 3.1.

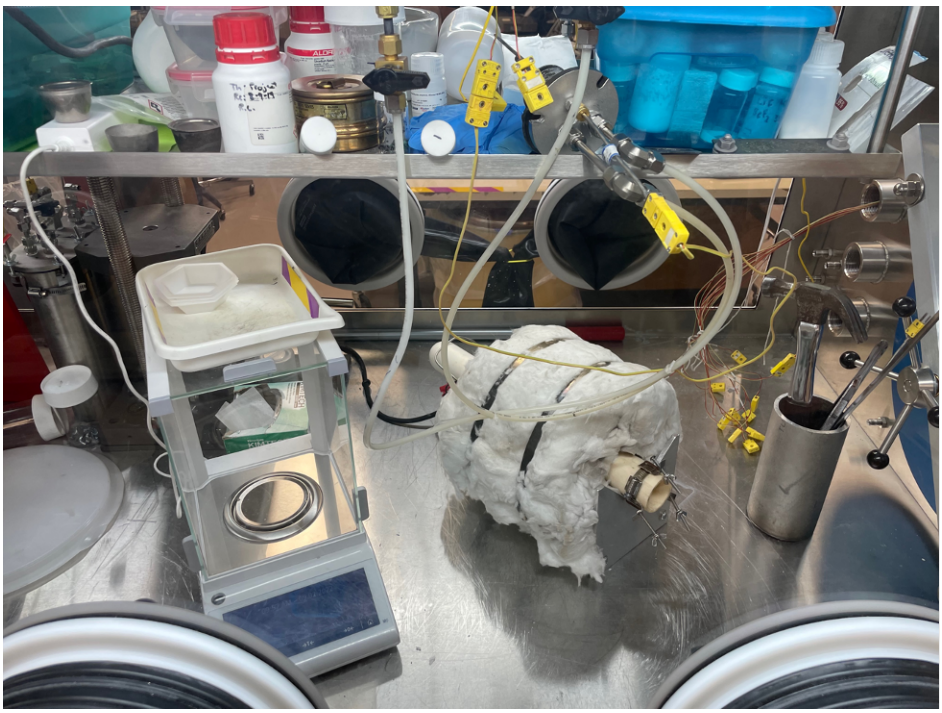

Figure 3.1: Working area of the MBraun glove box showing the furnace and scale used.

Before fusing the salt, all equipment that may have the potential to interact with the salt was replaced and constructed out of nickel or nickel-based alloys, as FLiBe salt is known to be corrosive to steels and many other substrates under certain conditions. A 20-ml nickel crucible and lid were purchased from VWR, modification of the crucible was needed to reduce the height of the crucible so that it would fit inside a 50.8-mm alumina furnace tube chosen for FLiBe salt use and acquired from McDaniels Ceramics. To seal the tube, a custom nickel end-cap was designed and fabricated from alloy 620: with two 6.35-mm (1/4-in) NTP taps and one 3.175-mm (1/8-inch) NPT tap. The taps were fitted with Inconel 620 Hy-Lok tube fittings obtained from Southwest Process Control to secure cover gas lines and to observe the internal conditions of the tube during operation. Of the fittings, the larger ports are fitted for cover gas flow stream while the smaller port was equipped with a 3.175-mm (1/8-in) Type-K thermocouple made with an Inconel sheath provided by Nanmac. Five heat shields were cut from 1.5875-mm (1/16-in) Inconel with holes drilled for the gas flow lines and thermocouple. The heat shields were fitted to the gas lines and pressed into position. Finally, a custom gasket made of Viton was cut to seal the end of the tube to the end cap.

Synthesis of the salt took place in the glovebox using a 120-volt, 101.6-mm diameter ceramic tube furnace, model VC404AOGA, manufactured by Waltow, using a Watlow SA controller. Lithium fluoride and beryllium fluoride were mixed at a ratio of 66.4-33.4-mol% (LiF-BeF_2) and the resulting amalgam placed into the nickel crucible. The nickel lid was placed on the crucible and the assembly inserted into the tube furnace, the end cap secured, and helium cover gas introduced. The tube furnace was heated to an internal temperature of 600°C at 10°C/min and maintained for 2-hours then allowed to cool to ambient conditions. The resulting pellet of fused salt was crushed using an agate mortar and pestle, a sample of crushed fused salt is shown in Figure 3.2.

3.2 Tricalcium Phosphate Synthesis

Tricalcium phosphate (TCP), $Ca_3(PO_4)_2$, was commercially available. However, further investigation found that the products listed were hydroxyapatite, $Ca_5(PO_4)_6(OH)_2$, which is not suitable for the conversion of FLiBe into fluorapatite. A straight forward manner has been detailed by Elliot for synthesizing TCP [17]. Here calcium carbonate ($CaCO_3$) and calcium hydrogen phos-

Figure 3.2: Fused FLiBe salt powdered for use in proceeding experiments.

phate ($CaH(PO_4)$) are heat treated at 1000°C for over 20-hours, and is described by the following chemical equation:

$$2CaHPO_4(s) + CaCO_3(s) \rightarrow Ca_3(PO_4)_2(s) + H_2O(g) + CO_2(g) \tag{3.1}$$

Calcium carbonate and calcium hydrogen phosphate were obtained from Alfa Aesar with 99.5% and >98% purities respectively. The compounds were mixed using a NORTON rolling mill for 5-minutes at ratio of 66.67-33.33 mol% ($CaH(PO_4)$-$CaCO_3$). The amalgamation was transferred to alumina crucibles and heat treated in a Lynnberg Blue open atmosphere furnace at 1000°C for 20-hours.

Once cooled to ambient conditions, the resultant material was powdered by hand using an agate mortar and pestle. A sintered pellet of TCP is shown in Figure 3.3. A sample of the powder was then analyzed via XRD using a Rigaku Miniflex II, Figure 3.4, to confirm the presence of a non-hydrated TCP structure. Verifying that TCP was indeed created.

Figure 3.3: Heat treated sample of calcium hydrogen phosphate and calcium carbonate creating tricalcium phosphate.

3.3 Uranium Tetrafluoride Fluorination

One essential objective of this research is to establish if spent fuel and other fission products present in MSRs would substitute into fluorapatite (FAp) or an apatite in general. Typically, uranium tetrafluoride (UF_4) is used as the fuel in this reactor class and needed to be procured or produced. Synthesis of uranium tetrafluoride was conducted using a process known as dry fluorination using depleted uranium dioxide (UO_2). Dry fluorination uses ammonia bifluoride (NH_4HF_2) to convert oxides to fluorides and is frequently utilized for small batch fluorinations. Multiple research studies demonstrate the methods effectiveness on a range of metal oxides [27, 28, 29, 30].

Dry fluorination works by NH_4HF_2 reacting at room temperature with UO_2 to form UF_4 and

Figure 3.4: The Rigaku Miniflex II Powder-XRD used throughout the study.

various byproducts [29]. A moderate increase in temperature can increase the rate of transformation by converting the ammonium bifluoride to a liquid phase, however doing so will volatilize small amounts which may no longer take part in the fluorination process. Increasing the temperature further removes excess ammonium bifluoride and unwanted byproducts. The reactions associated with the fluorination UO_2 to UF_4 are presented in the stoichiometric equations below adobted from Wani, et. al. [29]:

$$UO_2 + NH_4HF_2 \rightarrow UF_8(NH_4)_4 + 2H_2O \tag{3.2}$$

$$UF_8(NH_4)_4 \rightarrow UF_7(NH_4)_3 + NH_4F \tag{3.3}$$

$$UF_7(NH_4)_3 \rightarrow UF_6(NH_4)_2 + NH_4F \tag{3.4}$$

$$UF_6(NH_4)_2 \rightarrow UF_5(NH_4) + NH_4F \tag{3.5}$$

$$UF_5(NH_4) \rightarrow UF_4 + NH_4F \tag{3.6}$$

Depleted-uranium UO_2 with a purity of 99.99% was obtained from International Bio-Analytical Industries, Inc., and 99.999% NH_4HF_2 was acquired from Sigma Aldrich for UF_4 synthesis. The compounds were placed into the inert atmosphere glovebox and blended in a 5:1 mass ratio of NH_4HF_2 to UO_2 inside a nickel crucible, the crucible was then set into the alumina tube furnace and sealed.

To facilitate the reaction, the internal temperature of the tube was increased to 120°C and maintained for 2-hours to fluorinate the uranium described by equation 3.2. A helium cover gas was then introduced and the temperature raised to 425°C to extract non-reacted ammonium bifluoride, ammonium fluoride, and any remaining water for 2-hours and is described by equations 3.3 through 3.6. Upon cooling, a visual inspection of the resulting compound presented a rich green material that is characteristic of UF_4, and is shown in Figure 3.5. A sample of the material was placed into an inert atmosphere XRD sample holder, shown in Figure 3.6, and characterized with the Rigaku Miniflex II. Analysis determined that the only structure present after conversion was that UF_4.

3.4 Fluorapatite Manufacturing

The general procedure adopted to synthesize fluorapatite (FAp) and substitute fluorapatite (X-FAp) pellets used in this study is covered in the following section. A complete chart of the molar compositions, temperature, ramp rate, and ball-milling and sintering duration utilized for each

Figure 3.5: Uranium tetrafluoride converted from uranium oxide using ammonium bifluoride.

fluorapatite can be located in Table 3.1 at the end of this chapter.

As the beryllium and fluorine compounds used contain various health hazards work conducted with the materials was performed in the MBraun glovebox with a helium atmosphere under negative pressure. However, milling was not feasible inside the glovebox, therefore samples were sealed with the milling media in 20-ml or 80-ml polymer sample vessels inside the glovebox. The sample was then transferred out of the glovebox and the cap further secured with Parafilm and placed into a secondary containment vessel. The secondary vessel consisting of the sample, milling media, and sample container was placed on the NORTON roller mill for the milling duration. Once the desired time transpired, to reduce the chance of contamination the sample was promptly moved back into the glovebox where the parafilm was removed and milling media was seperated from the powder using a US3-14B sieve obtained from Dual Manufacturing.

The initial apatite production consisted of 66.89-33.11 mol% (TCP-FLiBe), and was weighed using a Mettler Toledo MS304TS/00 scale. The compounds were ball milled for 1-hour using 6-

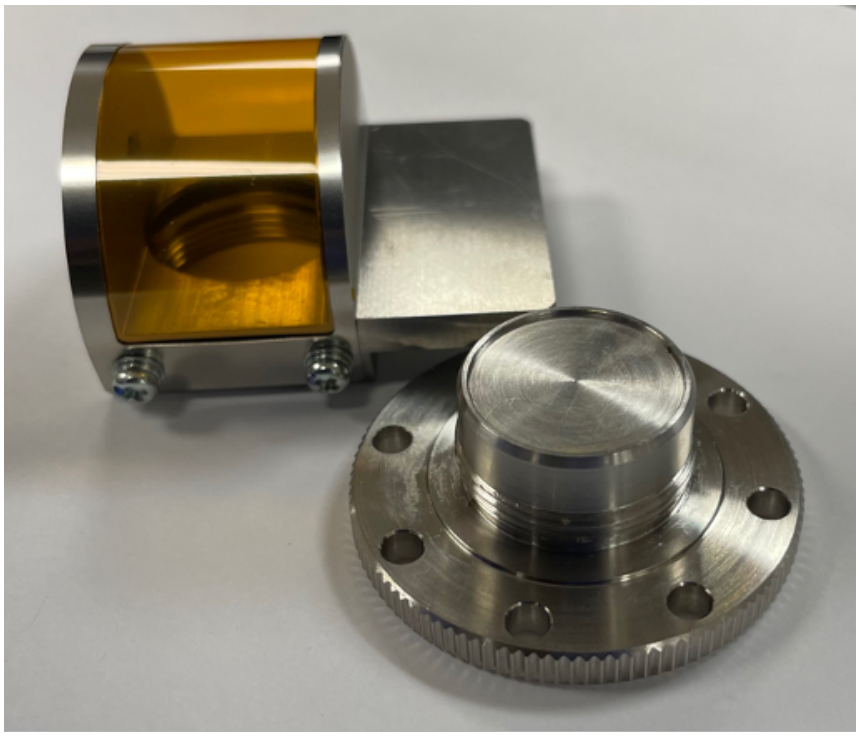

Figure 3.6: The Rigaku MiniFlex II inert atmosphere sample holder used for air sensative samples.

mm zirconia milling balls purchased from MSE Supplies. To produce a green pellet, 3.5-g of the milled powder was deposited into a 20-mm stainless steel press die acquired from Precision Press Die Sets. To reduce friction during pressing a saturated zinc stearate-benzene solution was applied to all surfaces that may be in contact with the powder and or each other before powder addition. The loaded die was pressed on a Carver 3912 uniaxial press, shown in Figure 3.8,and 152-MPa of pressure was applied for 45-seconds. A green pellet from U-FAp-3 resting on a nickel slide is presented in Figure 3.8.

The green pellet was removed from the die and set on an alloy 620 slide to reduce possible interactions of the FLiBe salt with the slide surface during heat treatment. The alloy 620 slide was cut from a larger 1.5875-mm thick sheet of Inconel and measured 101.6-mm long by 34.925-mm wide and heat treated inside the glovebox using the supplied tube furnace for 6-hours at 600°C before use. The pellet and slide were then loaded into the tube furnace and enclosed with the Inconel end-cap.

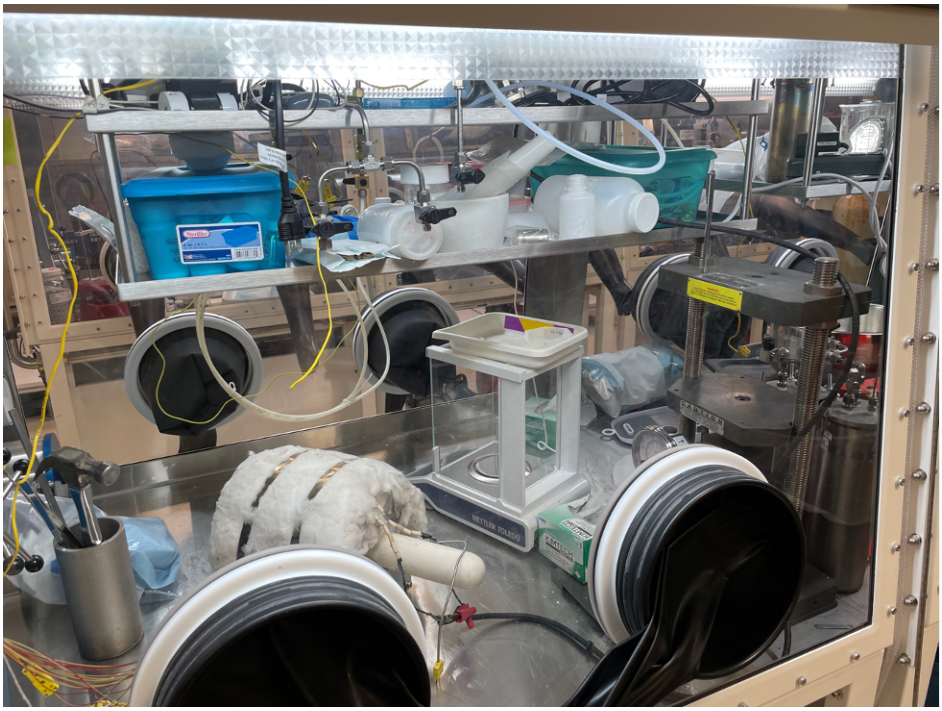

Figure 3.7: Back side of glovebox working area showing the carver press.

For sintering of FAp-1 the furnace was heated to an internal temperature of 700°C with a ramp rate of 5°C/min for 3-hours with no cover gas. Previous investigations had discovered that the helium cover gas that was procured contained excessive amounts of oxygen. It is believed the oxygen interacted with the exterior surface of the pellet. A cross section from such a pellet is shown in Figure 3.9 where a visible dark outer layer has formed on the surface that gradually dissipated towards the center of the pellet. While a sintered pellet from the FAp-1 experiment is shown in Figure 3.10.

Visual inspection identified few surface defects and delamination of the pellet. Visible inclusions were present, a pellet is shown in Figure 3.11. The pellet was crushed into a powder using an agate mortar and pestle for XRD analysis. The initial XRD evaluation identified that fluorapatite was the major component of the resulting waste surrogate.

In order to enhance the conversion to fluorapatite the sintering temperature was increased to 800°C with a ramp rate of 10°C/min and held for 3-hours. Visual inspection found that the pellet

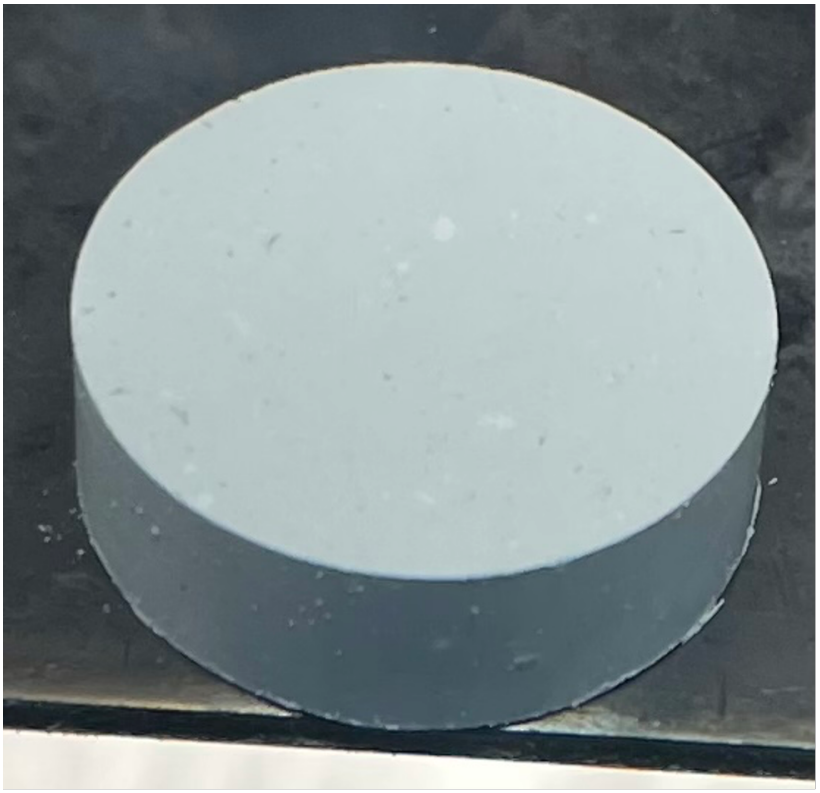

Figure 3.8: A pressed green pellet containing tricalcium phosphate, FLiBe salt, and uranium tetrafluoride ready for sintering of a U-FAp-3 waste pellet on a nickel slide.

had begun to delaminate and had a very rough surface with pores resembling boiling and possilbe inclusions of additional phases, as seen in Figure 3.11. The initial XRD data determined that the conversion to fluorapatite was much higher than FAp-1, closer to 90%.

To further investigate the conversion to apatite and reduce the surface defects the FAp-3 waste form was synthesised. In FAp-3 both the milling and sintering durations were increased to 10-hours. Like FAp-1 the sintering temperature was 700°C with 5°C/min ramp rate. The resulting pellet showed few surface defects and little or no delamination, with a slight decrease in the appearance of inclusions, a pellet from FAp-3 is shown in Figure 3.12. The initial XRD pattern showed a greater conversion to fluorapatite than FAp-2 with a small minor phase.

Once fluorapatites were created using FLiBe salt and confirmed additional substituted apatites were made. The initial substituted fluorapatite experiments were conducted using UF_4, the doping was accomplished by adding sufficient UF_4 such that a FLiBe salt to UF_4 ratio of 95-5 mol%

Figure 3.9: Cross section of a pellet created under helium cover gas showing a possible oxidation gradient.

(FLiBe-UF_4) was achieved, which is similar to propsoed fuel loading ratios found in literature. Experiments 4 through 6 (U-FAp-1 through U-FAp-3), followed the same methods as FAp-1 through FAp-3 respectively. Just as FAp-2 contained surface defects and delamination issues so did U-FAp-2, inclusions can be seen in Figure 3.13. U-FAp-3 pellets appeared similar to U-FAp-2, however the inclusions were darker and larger.

Initial XRD analysis of U-FAp samples determined that uranium substituted fluorapatites were synthesized.

The final pellets were only processed using 10-hour milling and sintering durations at 700°. FAp-4 increased the quantity of FLiBe to a ratio of 48.9-51.1 mol% (TCP-FLiBe). The fission product dopted apatites are denoted as X-FAp, with X denoting the fluorine fission product that was added. The fission product fluorapatites contained either cesium fluoride (CsF), strontium fluoride (Sr_2), gadolinium fluoride (GdF_3), or a mixture of CsF and GdF_3. The final surrogate waste form, M-FAp, contained CsF, SrF_2, GdF_3, and UF_4. The fission product apatite, X-FAp,

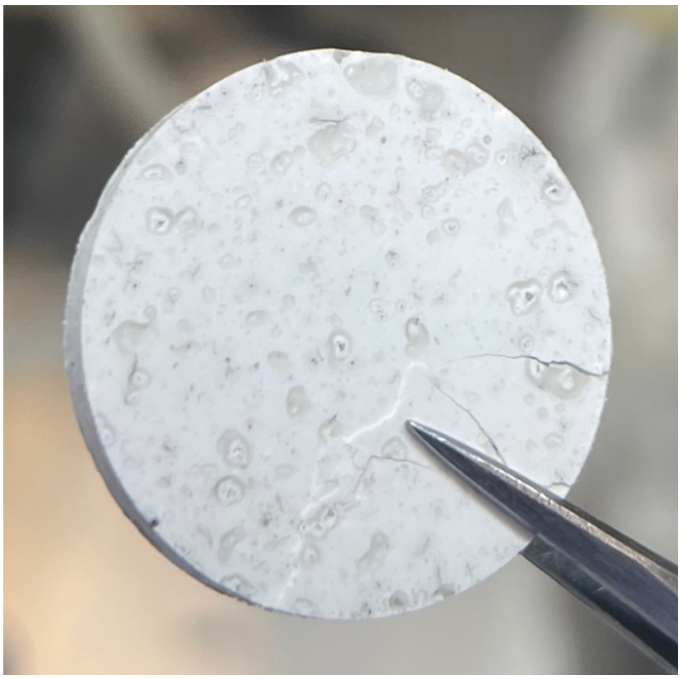

Figure 3.10: A FAp-1 pellet heated treated at 700°C for 3-hours.

were mixed in a ratio of 95-5 mol% (FLiBe-X) and split evenly amongst the constituents fluorine fission products if multiple fission products were used.

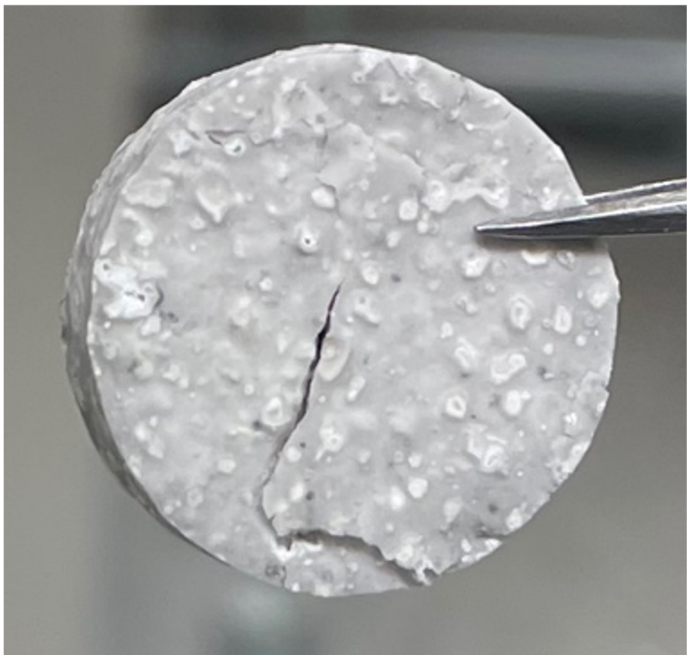

Figure 3.11: A pellet created for FAp-2, heated to 800°C for 3-hours, showing the rough surface and delamination present at this sintering temperature.

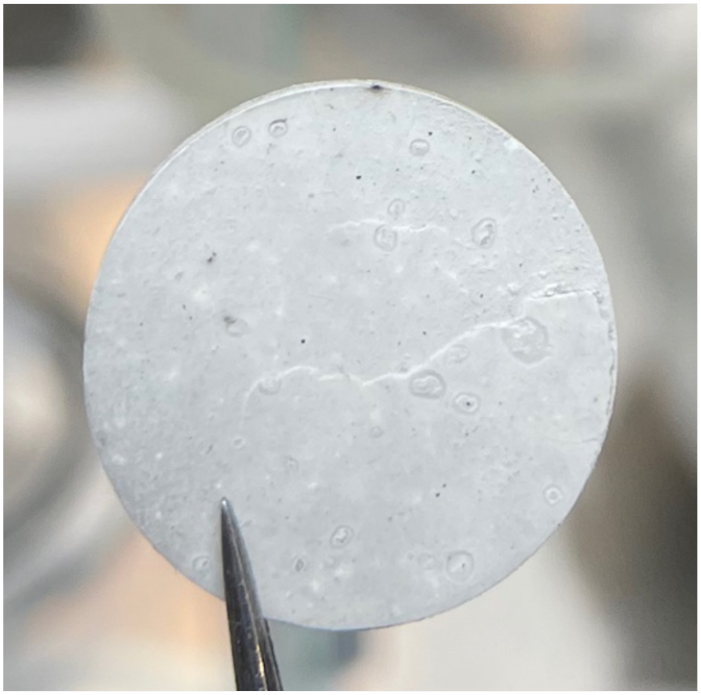

Figure 3.12: A FAp-3 pellet heated to 700°C for 10-hours.

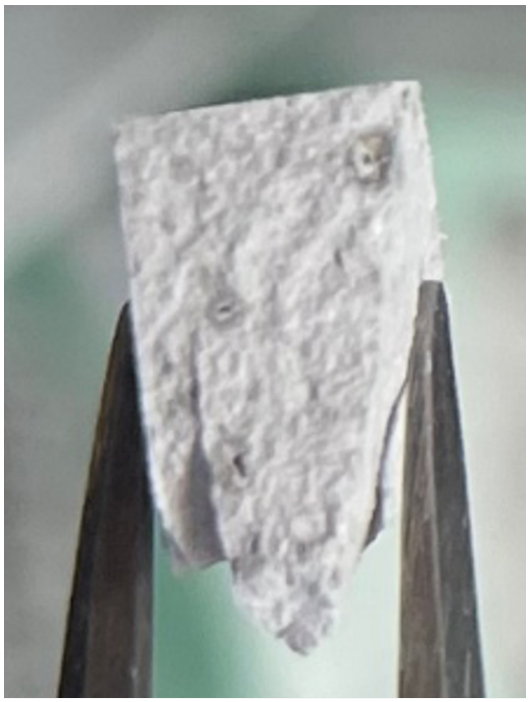

Figure 3.13: The cross section of a U-FAp-1 pellet, heated to 700°C for 3-hours, note the darker inclusions.

3.5 Product Consistency Test Procedures (PCT)

To investigate the capacity of the apatites to retain the surrogate waste and surrogate waste form structural components the leach test ASTM-C1825 "Standard Test Methods for Determining Chemical Durability of Nuclear, Hazardous, and Mixed Glasses and Multiphase Glass Ceramics: The Product Consistency Test (PCT)" was utilized. The PCT is a fundamental static leach test used to test the efficay of waste forms, and often used as a preliminary study before more extensive research on a waste form is carried out. The subsection 3.5.1 outlines the methods and equipment utilized to conduct the leaching experiments. While cleaning of the test vessels and equipment is discussed in subsection 3.5.2.

3.5.1 PCT Procedures

To administer the PCT tests, twelve 60-ml perfluoroalkoxy alkane (PFA) digestion vessels were bought from Savillex that met the specifications for PCT Method B. Before use each vessel and cap was etched using a mechanical indenter to identify and track each vessel's use and cleaning. The vessels are shown during a cleaning procedure inside the Yamato oven in Figure 3.14. The vessels initial cleaning is discussed in subsection 3.5.2.

Five to six 20-mm 3.5-g pellets were made for each substituted fluorapatite and cracked inside the glovebox using the agate mortar and pestle before being deposited into a glass sample vial and sealed. The container and sample were transferred out of the glovebox and placed into a secondary transfer box which was carried to a designated beryllium fume hood, shown in Figure 3.15, for further processing. The sample vials were removed from the transfer container and decontaminated twice using ethanol before preparing the sample for a PCT.

Processing began by putting 2-g of substance into an agate mortar and crushed inside a fume hood with the agate pestel. The crushed material was deposited into a 76.2-mm brass ring 100-mesh (0.149-mm) stainless steel sieve. The 100-mesh sieve was placed onto a 200-mesh (0.074-mm) sieve with catch pan and a lid added: the sieves, pan, and lid were procured from Dual Manufacturing. All seams on the sieve stack were sealed using electrical tape and fixed onto a

Figure 3.14: Savillex vessels inside the Yamato oven on the final stage of a cleaning process.

sieve shaker, aquared from Dual Manufacturing model D-4326, for 20-minutes. Once finished, the 200 to 100-mesh material was then placed into a fresh glass sample container. Material greater than 100-mesh was reprocessed with additional waste form until all of the sample was processed below 100-mesh. Sub 200-mesh material was put into a glass sample vial and kept for powder XRD analysis.

As leach rates are sensitive to surface area, the sieved material required that any adhered fine particles be removed ensuring that the material used for the PCT was between 100 and 200-mesh. Thus, the sieved material needed to be washed. TO wash the sample was deposited into a 80-ml glass beaker and ASTM Type-1 water injected into the beaker using a squirt bottle, such that the water volume was two and half times the volume of solid. The liquid was decanted and process repeated an additional time. After the second flush, a volume of ASTM Type-1 water equal to two times the volume of solid material was sprayed into the beaker, swirled for a few seconds to

Figure 3.15: The designated beryllium fume hood used throughout this study.

agitate and placed into a PC3 bath sonicator manufactured by L&R. After 2-minutes the beaker was removed, and the contents allowed to settle for 15-seconds then the liquid decanted, the process was repeated an additional time. Once the second sonication with ASTM Type-1 water was decanted, the same process was conducted using absolute ethanol and repeated until the decanted ethanol was clearn then dried over night on a hot plate at 90°C. In most instances, this was 25 to 30 times. Processing in this manner yielded 30% to 40% of original mass usable for a PCT. A fully washed sample of PCT ready material is shown in Figure 3.16.

During sieving, it became evident that crushed material was having issues passing through the 200-mesh sieve. The fine particles were conglomerating, creating small spheres on the sieve surface and not passing through. It is thought to be due to electrostatic forces in the powder and humidity conditions inside the laboratory. Thus, the sieving protocol after U-FAp-3 was modified: as before, 2-g of material was crushed and deposited onto the 100-mesh sieve and loaded onto the 200-mesh sieve and base shook by hand for 1 to 2-minutes. Material not moving though the

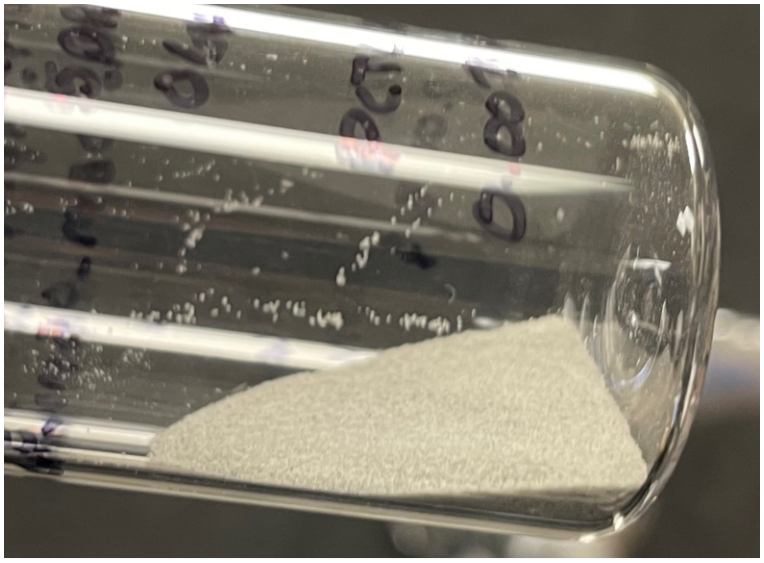

Figure 3.16: Fully processed and washed surrogate waste form material ready for a product consistency test.

100-mesh sieve was reprocessed with additional material until all of the sample passed onto the 200-mesh sieve. The material that remained on the 200-mesh sieve was periodically removed and stored in a glass specimen jar while additional material was processed. Once all material was processed, the 200-mesh material was deposited back onto the 200-mesh sieve and wet sieved.

The wet sieving was conducted by spraying absolute ethanol onto the sample while tilting the sieve over a beaker. The sieve was turned throughout the process, and conducted until the liquid dripping form the sieve appeared clear, typically taking 150-ml of ethanol to do so. After wet sieving, the sample was transferred into a clean 80-ml glass beaker and dried on a hotplate overnight at 90°C. The next morning the dried sample's weight was obtained and then stored in a new glass vial until until cleaning to removed the fine grains could be removed. Changing to wet sieving reduced sieving and cleaning time from 1-day per apatite to 3-hours and increased the yield closer to 50%.

To perform each PCT, four vessels and lids are needed, three for the sample of interest to be tested and one utilized as a control or blank. The control serves to determine if ions are leaching from the walls of the test vessel, typically associated to improper cleaning, or are present within

the liquid used. Each PCT vessel and lid were initially weighed, using an A&D GR-202 scale. Three of the four vessels were loaded with 1-g of the washed sample material which was measured on a Sartorius GD-503-NTEP scale.

The PCT was conducted using ASTM Type-1 water, a standardized reagent water with limits on contaminates and electical properties, however before addition, an aliquot of the water was analyzed for temperature, pH, and fluoride content to determine a baseline. The pH probe was an Oakton model 01X099314 with an Oakton pH5+ reader that was three-point calibrated using 4, 7, and 10 pH buffers purchased from Oakton. The fluoride content was obtained using an Oakton model UX-27504-14 ion-selective probe and interpreted via an Oakton Ion pH6+ reader. Three-point calibration was performed by serial dilution of a 10-ppm fluoride standard solution stabilized with TISAB-II, procured from RICCA, using 0.1, 1.0, and 10 ppm. The temperature was recorded using the supplied thermocouple that shipped with the pH 6+ reader, using the Okaton Ion pH 6+.

All four vessels were then filled with 10-ml of ASTM Type-1 water pipetted into the vessel 1-ml at a time using a Eppendorf Research Plus 1000 pipette. The vessels were secured with their respective lids and fixed using supplied wrenches from Savillex. The total weight of the vessels was obtained for each vessel using the A&D scale. Each vessel and lid's tightness were checked, then swirled to ensure wetting of the material and placed in to a preheated Yamato ADP-21 oven at 90°C for 7-days. Between 4 and 16-hours after placing the vessels inside the oven the vessels and lids were again tested for tightness and tightened if required by quickly removing each vessel from the oven. After the check, the vessels remained in the oven for the duration of the test. Temperature data of the oven was recorded throughout the test duration every thirty seconds using an OMEGA RDXL4SD thermocouple data logger and a 1.588-mm OGEMA Type-K thermocouple.

Upon conclusion the vessels were removed from the oven and allowed to cool to room temperature, typically taking 4-hours. Once cooled, the vessel's final weight was recorded and lids removed, contents of the the vessel are shown in Figure 3.17. The leachate was filtered using individually sealed 25-mm diameter 0.45-μm PVDF model 13-100-105 syringe filters with a 20-ml oil free, sterile, individually packaged syringes, model 14-955-460, both acquired from VWR.

The filter was removed and placed in sealable plastic bags and identified for further analysis if desired. The leachate was injected into individual 15-ml disposable Fisherbrand polypropylene beakers and the temperature, pH, and fluoride content obtained and recorded from three-point calibrated pH and fluoride selective ion probes. Leachate was then stored in new glass sample vials with PTFE sealed lids and saved for cation analysis, shown in Figure 3.18. Before cation analysis (ICP-MS) any leachate having a pH above 10 was acidified with 1-μl 70% Nitric acid.

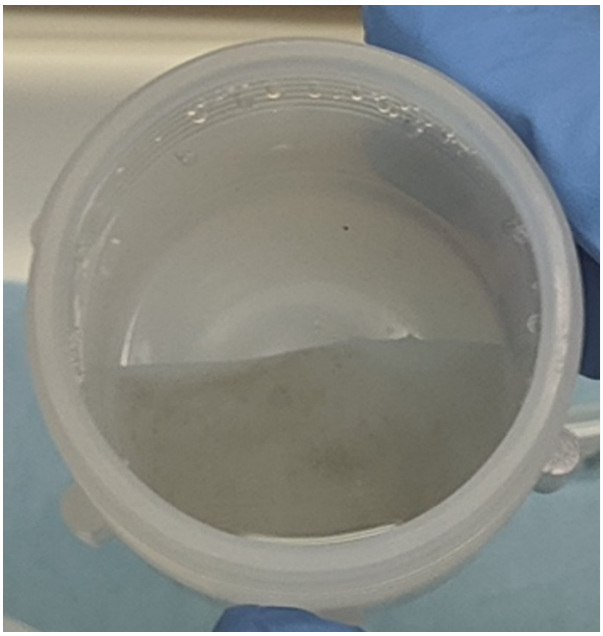

Figure 3.17: A cooled open vessel after a PCT showing leachate and insoluble products.

3.5.2 Cleaning Procedures

Once received, all twelve vessels were initially cleaned under ASTM C1825 guidelines to remove any fluoride present on the interior surface from manufacturing. Vessels were washed with ambient temperature ASTM Type-1 water, then filled to 90% with a 5-wt% sodium hydroxide (NaOH) solution and secured with their respective lids. The vessels were placed into the Yamato oven preheated to 110 °C for 7-days. After 12 hours, the lids were tightened and process allowed to finish. Upon completion, the vessels were removed from the oven and allowed to cool to room

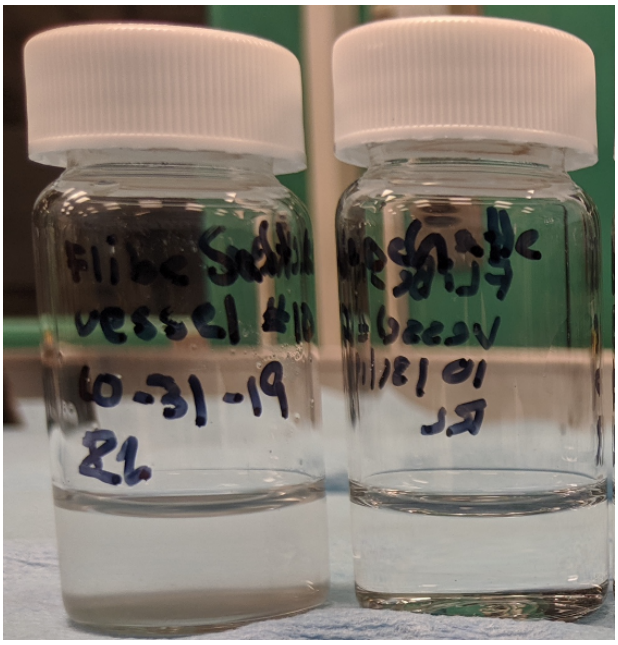

Figure 3.18: Leachate after a PCT test: the left sample is before filtering and the right sample is after filtering.

temperature and the NaOH solution disposed of.

The vessels were again washed twice with ASTM Type-1 water before being placed into boiling ASTM Type-1 water for 1-hour and 30-minutes then removed and washed with ASTM Type-1 water. This process was then repeated. After the second boiling, the vessels were filled 90% with ASTM Type-1 water, sealed, and placed into a preheated 90°C for 16-hours.

Once removed, the vessels were cooled to room temperature and aliquots of the water were analyzed for pH and fluoride content using three-point calibrated meters. According to the ASTM guidelines, if the pH is between 5 to 7 and the fluoride content <0.5 ppm, the vessels were considered clean. If out of these ranges, the process was redone from the beginning. During the initial cleaning, fluoride concentrations and pH did not satisfy the conditions, and the process was conducted a second time for all twelve vessels, passing the criteria on the second cleaning.

After each use, the PFA vessels required cleaning of residual contamination left from the waste form tested. This was carried out by first rinsing the vessels and lids with ASTM Type-1 water. The cleaned vessels were placed into 0.16 M nitric acid (NHO_3) solution heated on a hotplate to

90°C for 1-hour and 30-minutes. The vessels were removed and rinsed with fresh ASTM Type-1 water and placed into ASTM Type-1 water heated on a hotplate to 90°C for 1-hour and 30-minutes. The vessels were then flushed and filled to roughly 90% with fresh ASTM Type-1 water, sealed, and placed into a preheated 90°C oven for at least 16-hours. Upon removal the vessels were cooled to room temperature and the pH and free fluoride content obtained. As before, if the pH is between 5 to 7 and the fluoride content <0.5 ppm, the vessels were clean. If out of these ranges, the process was redone from the beginning.

To reduce cross contamination from one fluorapatite to another, all sieves were cleaned after use. Precautions were taken as the sieve inside the MBraun was contaminated with raw materials and needed to be removed from the MBraun for proper cleaning. This specific sieve was wiped down inside the glovebox using ChemWipes, then transferred outside the MBraun and placed into a cleaning vessel then into a secondary container for transport. The container was moved to the beryllium designated fume hood and a sufficient volume of ethanol added to the cleaning vessel so ethanol covered the sieve surfaces, and the cap placed back onto the containment vessel. The vessel was bath sonicated for 10-minutes then moved back into the fume hood where the ethanol was removed and process was repeated. After the second ethanol sonication, a final sonication using distilled water was performed. After decanting the water, the sieve was removed from the vessel left open inside the fume hood overnight dry. The next morning the vessel was secured and transported back to the glovebox where the sieve was transferred back into for further use.

Sieves that were utilized to prepare pellets for PCT testing were cleaned by sonication in ethanol in a large beaker twice, and a final sonication using distilled water. After water sonication, the sieves were sprayed with ethanol and allowed to dry overnight before further use.

3.6 Density Measurements

Density was obtained using two methods, first after sinterting geometric dimensional information, height(h) and diameter(d), was obtained using a set of Mitutoyo model CD-6"PSX calipers. The post sintered weight was then obtained using the Mettler Toledo scale inside the glovebox and a density was calculated from the following equation:

$$\rho = \pi h \left(\frac{d}{2}\right)^2 \tag{3.7}$$

This was conducted for all pellets produced and an average density was then obtained for each fluorapattite synthesized.

Additional and more accurate density information was also obtained. To do so 0.5 to 0.7-g pieces of each waste form were removed from the sintered pellets. The pieces were then subjected to gas pycnometry measurement by use of a Quantachrome ULTRAPYC 1200e, displayed in Figure 3.19.

Pycnometers do not directly measure density, instead they determine the volume of the sample via pressure changes inside a blank sample cell and a loaded sample cell using a standardized gas. The device then calculates the density from the volume difference and a supplied mass. The governing equation for the volume is as follows:

$$V_s = V_c + \frac{V_r}{1 - \frac{P_1}{P_2}} \tag{3.8}$$

Where V_s is the sample volume, V_c is the sample cell volume, V_r, is the reference volume (obtained before running the samples), P_1 is the pressure inside the sample chamber, and P_2 is the pressure inside the sample chamber and the reference chamber.

The fluorapatites were placed into the supplied "nanocell" and the experiment conducted using nitrogen gas. A maximum of nine runs were conducted for each fluorapatite or until the average over 3 runs was less than 0.1%. Masses for the apatite samples were obtained using the Sartorius GD-503-NTEP scale.

3.7 Normalized Leaching Behavior

Once a PCT is complete cation analysis of the leachant may be conducted to determine ions that are dissolving into solution. The results from the chemical analysis may then be normalized according to the ASTM C1825 guidelines, this allows for comparison of leach rates from one waste form to another. Two normalizations figures are presented, the first is normalized concentration,

Figure 3.19: The Ultrapyc 1200e used to obtain densities of the FAp waste forms.

NC_i in g/L, which estimates the total mass fraction of ion *i* in the waste form that dissolves into the solution, following equations are used to determine the normalized concentrations:

$$NC_i = \frac{C_i(s)}{f_i} \tag{3.9}$$

Where:

$C_i(s)$ = concentration of element *i* in the solution, in g/L

f_i = mass fraction of element *i* in the original waste form

And $C_i(s)$ is calculated from:

$$C_i(s) = \frac{C_i(n)V_f(n)}{V_o(n)} - C_i(control) \tag{3.10}$$

Where:

C_i	= the concentration of element *i* obtained, in g/L
V_f	= final leachate volume, in L
V_o	= initial leachate volume, in L
n^{th}	= the number of tests
C_i(control)	= is the average concentration of element *i* in the blank, in g/L

While C_i(control) is calculated from:

$$C_i(control) = \left(\sum_{l=1}^{m} C_i(l) \frac{V_f(l)}{V_l(n)}) \right) \frac{1}{m} \tag{3.11}$$

Where:

C_i	= the concentration if element *i* found in the blank, in g/L
V_f	= final leachate volume, in L
V_o	= initial leachate volume, in L
m	= the number of replicate blanks
l	= the l^{th} blank.

The second normalization is the normalized elemental mass loss, NL_i in g/m^2, and is the total mass of waste form element *i* dissolved into the leachant over the duration of the test. Assuming that the components dissolve congruently with element *i* and that the surface area remains constant. NL_i is determined from:

$$NL_i = \frac{C_i(s)}{f_i(Sa/V)} = \frac{NC_i}{(Sa/V)} \tag{3.12}$$

Where:

C_{si}(s) = the concentration of element *i* in the sample, in g/L

f_i = mass fraction of element *i* in the waste form

Sa/V = surface area divided by the leachant volume, in m^2/L

And surface area (Sa) may be obtained from:

$$Sa = mass\frac{6}{\rho d} \tag{3.13}$$

Where:

mass = the total mass, in g

d = the average particle diameter, in cm

ρ = the density of the waste from, in g/cm^3

3.8 Powder X-ray Diffraction

Powder x-ray diffraction was conducted using a Rigaku Miniflex II powder x-ray diffractometer. The samples were powdered and placed onto the standard provided 24-mm sample holders (unless otherwise noted), shown in Figure 3.12. The powder was pressed with a glass slide to ensure a smooth, flat, height appropriate surface for analysis. The Miniflex uses a 600-kW Cu x-ray tube, with a k_α wavelength of 1.5418-Å operating at a current of 40-kV at 15-mA as a line focus. The divergent slit used was the standard 1.25° slit provided by Rigaku, while the scatterring slit was the provided 8 mm slit with a k_β filter. Additionally, a variable knife edge filter was installed to reduce scattering and a direct beam absorber installed. The detector was Rigaku's D/teX Ultra 1-D silicon strip detector. All runs were conducted in range of 15° to 80° with a step size 0.001 2θ.

The XRD was controlled via Rigaku's supplied SmartLab Studio II software. Phase identification and crystal information were obtained using the SmartLab software's search and identification functions using the Open Crystallopgrahic Database. Rietveld refinement was conducted using SmartLab studios whole powder pattern fitting module.

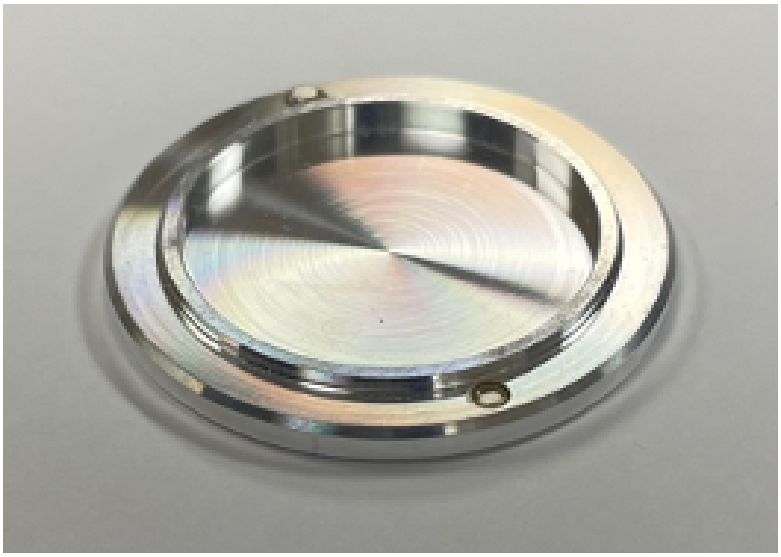

Figure 3.20: The Rigaku MiniFlex II XRD sample holders used in this study.

3.9 Scanning Electron Microscopy and Energy Dispersive X-ray Spectroscopy

Scanning electron microscopy (SEM) images were aquired at the Material Characterization Facilities (MCF) at Texas A&M using a JEOL JSM-7500F cold field emision SEM with an Oxford ULTIM MAX EDS detector with the capability to detect trace elements as low as 0.1-mass% within a sample. To esnure adaqute vaccum through-out the imaging liquid N_2 was used to reduce off gasing of the samples. Images were captured using 10-KeV accelerattion voltage and 10-μA emision current. For the energy dispersive x-ray spectrometry (EDS) mapping the volage and emision current were set to 20-KeV and 20-μA. The EDS was used to investigate components of each phase. Additional details can be found on each SEM image presented in Chapter 4.

To prepare samples for SEM-EDS fragments of every pellet were placed into LECO 25-mm mold cups, model 513-018, coated with Buehler mold releasing agent, model 20-8186. The mold cups were then filled with Buehler EpoKwick epoxy consisting of EpoKqick hardner, model 20-8136, and EpoKwik Resin, model 20-8136, until the pellets were covered. Multiple pieces were placed into epoxy at once to image multiples samples at a time during SEM-EDS imaging. Once the expoy was set, the samples were removed from the molds and rough upper edges scrapped off

using a file and placed into plastic zip-locking bags and labeled until polishing was conducted.

Polishing was conduced with Buehler 76.2-mm (3-in) glass platens, model 69-1510, inside the designated berullium fume hood. Polishing was conducted using Buehler CarbiMet abrasive paper at 180 (model 36-02-180), 240 (model 36-02-240), and 600 (model 36-02-600) grits. After polishing with 600 grit Buehler MicroCut pads were used at 800 grit (model 36-02-0800) and 1200 grit(model 36-02-1200). The final polishing stage was conducted with Buehler 1-μ monocrystalline diamond suspension, model 40-6530, using a Buehler TexMet, model 40-6032, polshing surface. All polishing pads were PFA backed and supplied with adhesive applied. To reduce friction Buehler MetaDi fluid, model 40-6032, was used during polishing at all stages except with the 1-μ diamonds which are in suspendion. Between grit sizes the samples were placed into ethanol filled glass beakers and sonicated for 2 to 3-minutes in a L&R PC3 ultrasonic cleaner. Then removed and allowed to dry, the ethanol was disposed of and replaced after each sonication.

Once a sample was fully polished it was placed back into its respective plastic bag and stored until SEM-EDS imaging. Prior to imaging samples were placed inside the MBraun's small antechamber under vacuum to remove moisture and trapped gasses at least 5-days before imaging was to be conducted.

As the samples are ceramics and non-conducting a conductive film needed to be applied to the polished surface to obtain adaquate images. The coating was applied at the MCF using a cressington 208HR high resolution sputter coater to apply a 5-nm palladium and platinum conducting layer controlled via a Cressington 20 thickness contoller. Once applied the sample was mounted into a 25-mm SEM mount and secured. Copper tape was then applied to ground the sample to the sample holder, Figure 3.21 and Figure 3.22 show polished and coated samples with copper tape applied to the sample surface ready for the SEM-EDS.

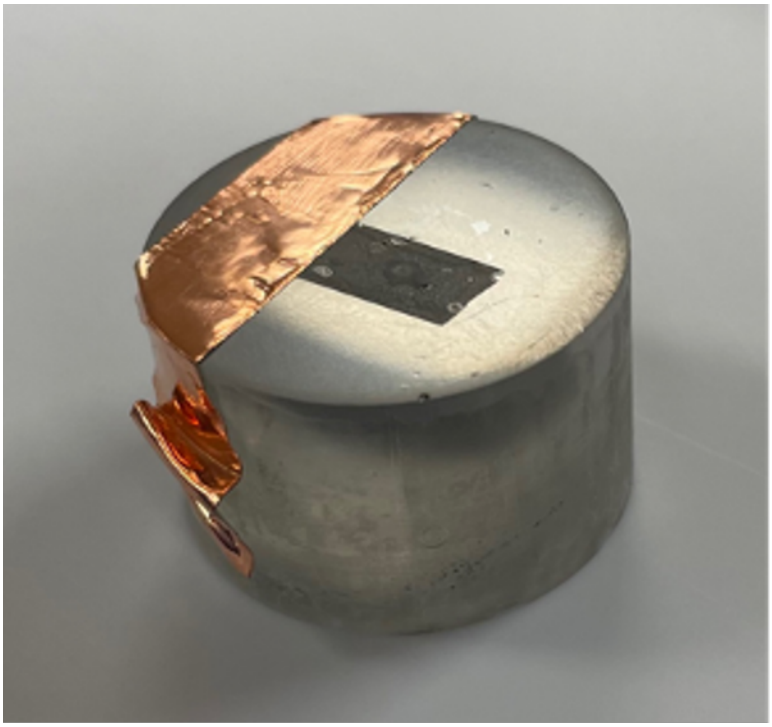

Figure 3.21: A single uranium fluorapatite waste sample in expoy prepared for SEM-EDS work.

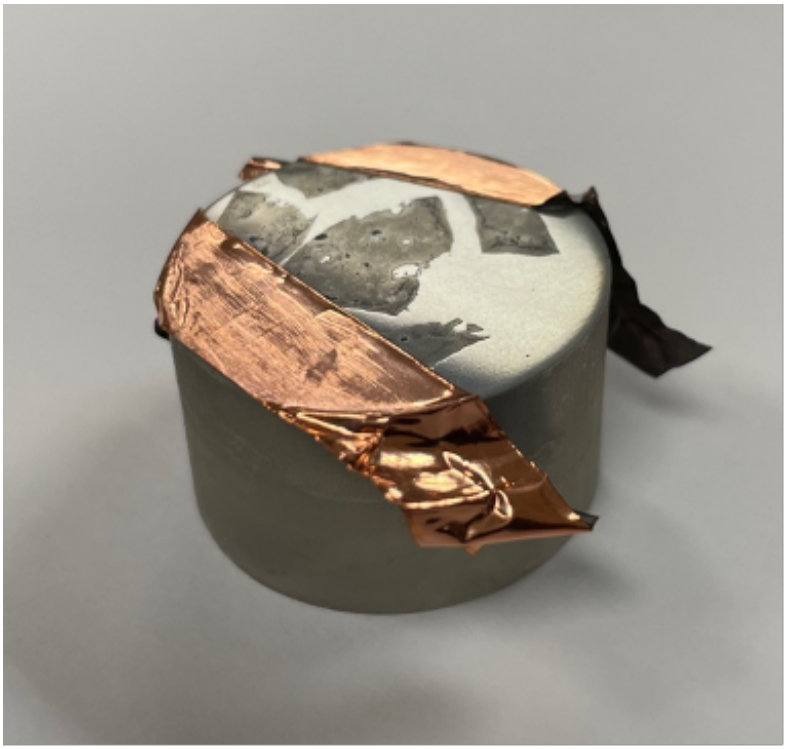

Figure 3.22: Gadolinium doped waste form samples that were preppared for SEM-EDS analysis.

Table 3.1: Summary of experimental compositions and environmental conditions for fabrication of surrogate waste form pellets.

Experiment	Composition Component	mol%	Milling Time (hr)	Temp (°C)	Sinter Time (hr)	Ramp Rate (°C/min)
FAp-1	TCP*	66.89	1	700	3	5
	FLiBe	33.11				
FAp-2	TCP	66.89	1	800	3	10
	FLiBe	33.11				
FAp-3	TCP	66.89	10	700	10	5
	FLiBe	33.11				
U-FAp-1	TCP	74.20	1	700	3	5
	FLiBe	24.48				
	UF_4	1.29				
U-FAp-2	TCP	74.24	1	800	3	10
	FLiBe	24.48				
	UF_4	1.29				
U-FAp-3	TCP	74.20	10	700	10	5
	FLiBe	24.48				
	UF_4	1.29				
FAp-4	TCP	48.9	10	700	10	5
	FLiBe	51.1				
Cs-FAp	TCP	70.43	10	700	10	5
	FLiBe	28.10				
	CsF	1.47				
Sr-FAp	TCP	69.71	10	700	10	5
	FLiBe	28.78				
	SrF_2	1.50				
Gd-FAp	TCP	72.01	10	700	10	5
	FLiBe	26.59				
	GdF_3	1.39				
CsGd-FAp	TCP	71.26	10	700	10	5
	FLiBe	27.30				
	CsF	0.72				
	GdF_3	0.72				
M-FAp	TCP	71.63	10	700	10	5
	FLiBe	26.88				
	UF_4	0.36				
	CsF	0.29				
	SrF_2	0.60				
	GdF_3	0.25				

*TCP = Tricalcium Phosphate

4. Results

Chapter 4 presents the results of the various data collected in this study. Section 4.1 presents the SEM images and EDS maps. The XRD patterns and refinement are shown in Section 4.2, while the densities are displayed in Section 4.3. The Product Consistency Test results for pH and free fluoride are presented Section 4.4, while the ICP-MS data is shown in Section 4.5. Data in section Chapter 4 is presented in naming convention adopted in Table 3.1 for the produced fluorapatite samples. To reassess the differences in the produced minerals, please refer to Table 3.1 at the end of Chapter 3 on the preceding page.

4.1 Scanning Electron Microscopy & Energy-Dispersive X-Ray Spectroscopy

To understand the microstructure scanning electron microscopy with energy dispersive spectroscopy (SEM-EDS) maps were collected using the JOEL JSM-7500 SEM and the Oxford ULTIM MAX EDS. Within the fluorapatite surrogate waste forms, several distinct phases were present depending upon the sintering temperature, duration, ball-milling duration and chemical content, such as fluorapatite, calcium phosphate, phosphate or fluorophosphate, and calcium fluoride. The observed surfaces comprised of dense regions with randomly sized voids, to larger open porous regions. Within the porous structures and in the regions immediately surrounding the voids under high magnification, crystals were observed ranging in size from 20-μm to 100-μm.

The same phenomenon was also observed in the U-FAp waste forms. In samples of the U-FAp and fission product doped apatites, inclusions of metal oxides were observed, such as uranium oxide (UO_2), and were roughly 100-μm in length and 70-μm in width. The fission product cations were observed to be spread throughout the bulk material, with a few metal deficient regions appearing. The SEM and EDS maps are shown in Figures 3.1 through Figure 3.19 presenting the features observed within the waste forms.

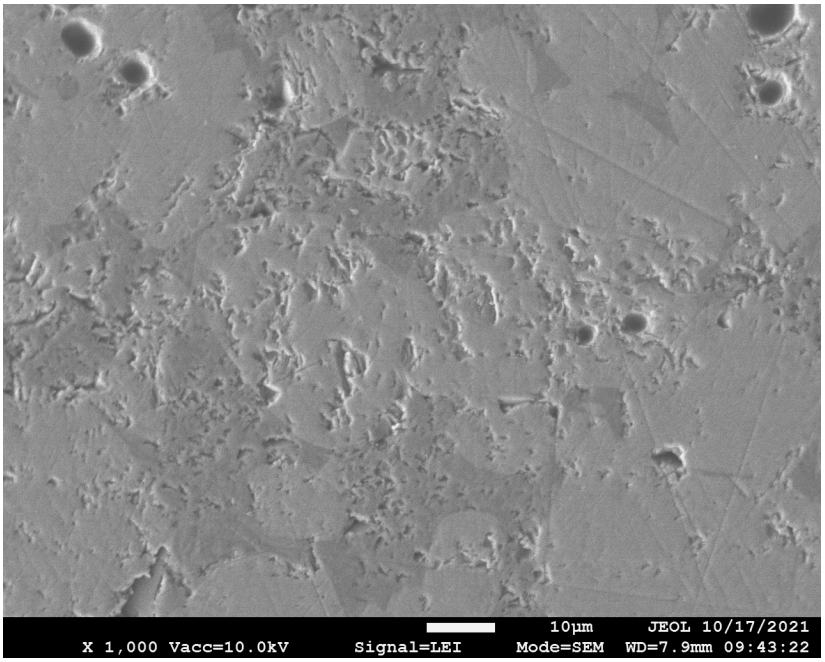

Figure 4.1: Dense region found in the 10-mol% FLiBe surrogate waste form, note the gradients of possible phases and the large voids in the upper quadrants.

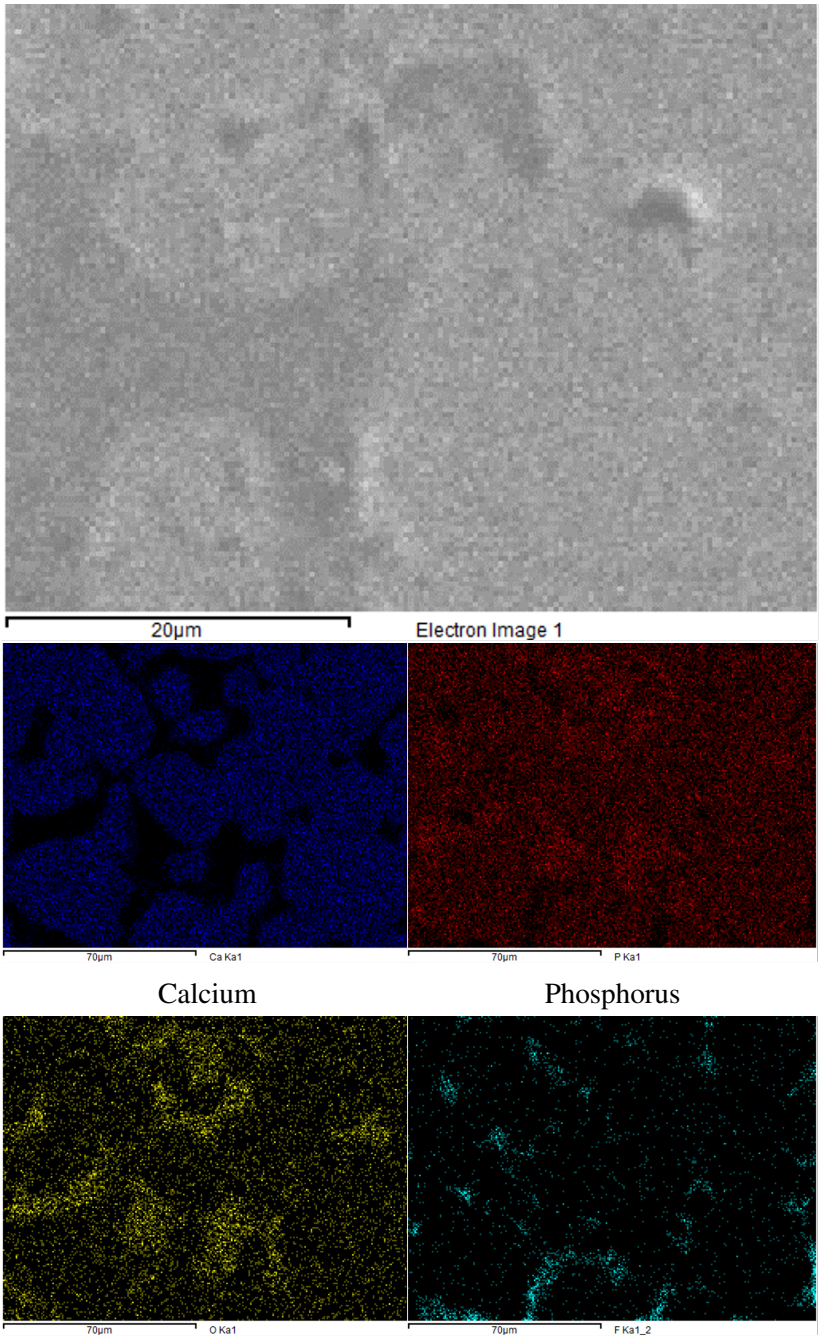

Figure 4.2: Section of 10-mol% FLiBe EDS showing the differences in the dark and light regions found in Figure 4.1.

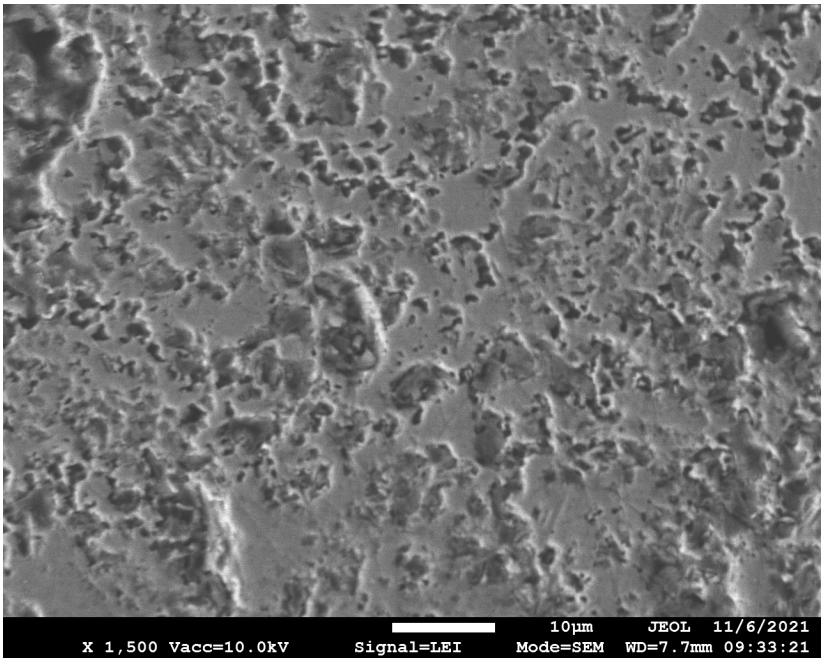

Figure 4.3: Dense region of a gadolinium surrogate waste form sample.

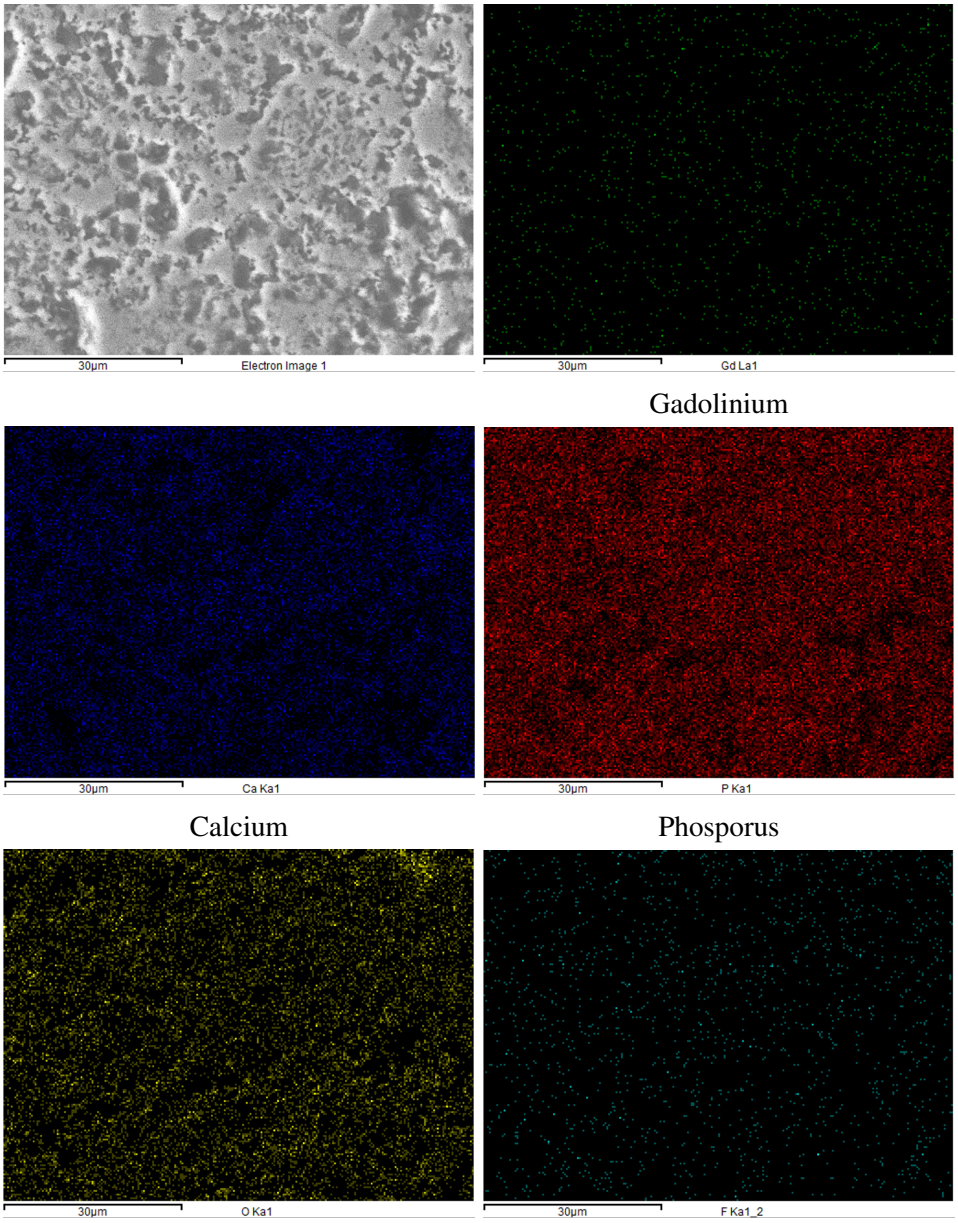

Figure 4.4: The EDS of Gd-FAp sample showing the disperstion of gadolinium through out the sample.

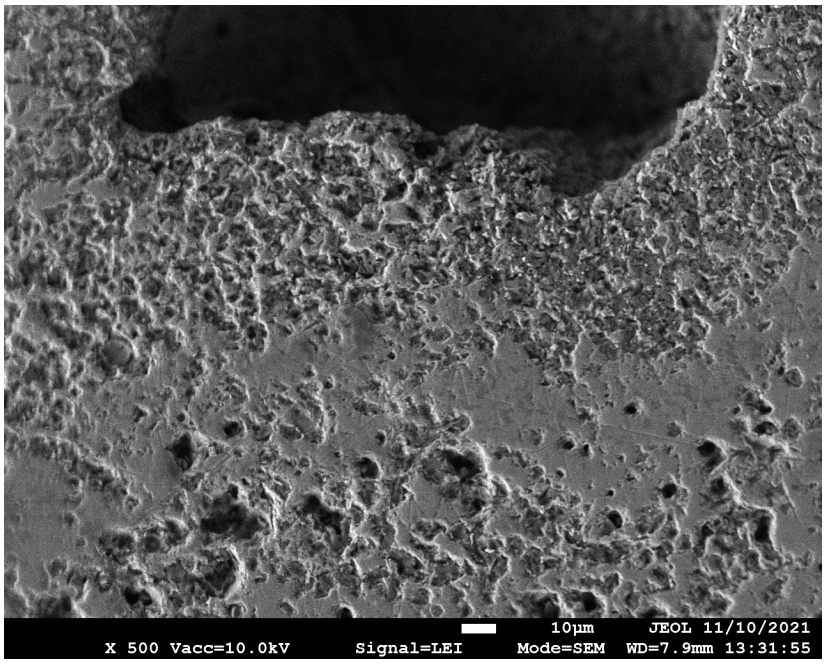

Figure 4.5: Dense region (bottom) and porous region surrounding a large void found in a U-FAp-2 surrogate waste sample.

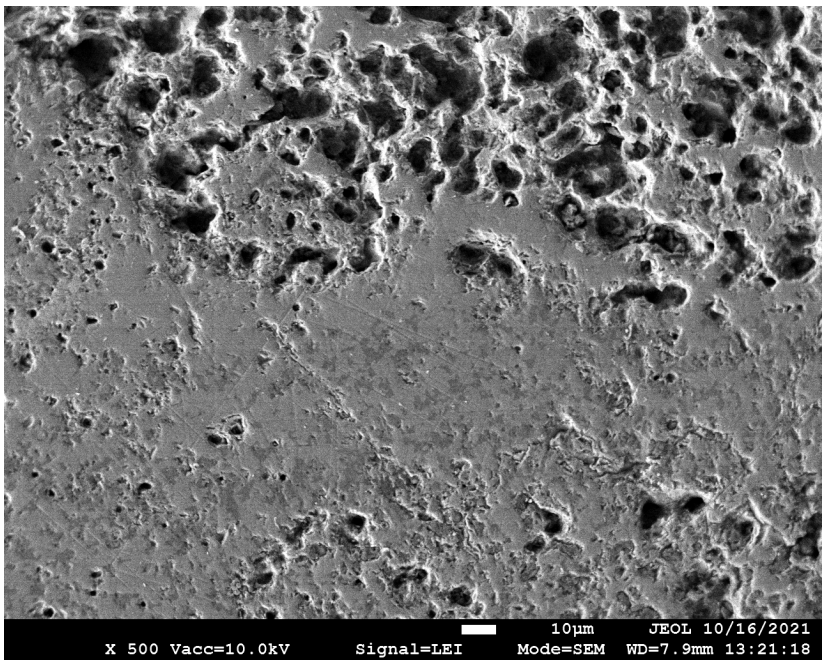

Figure 4.6: Dense region (bottom) and porous region (top) leading to a large void above the porous region.

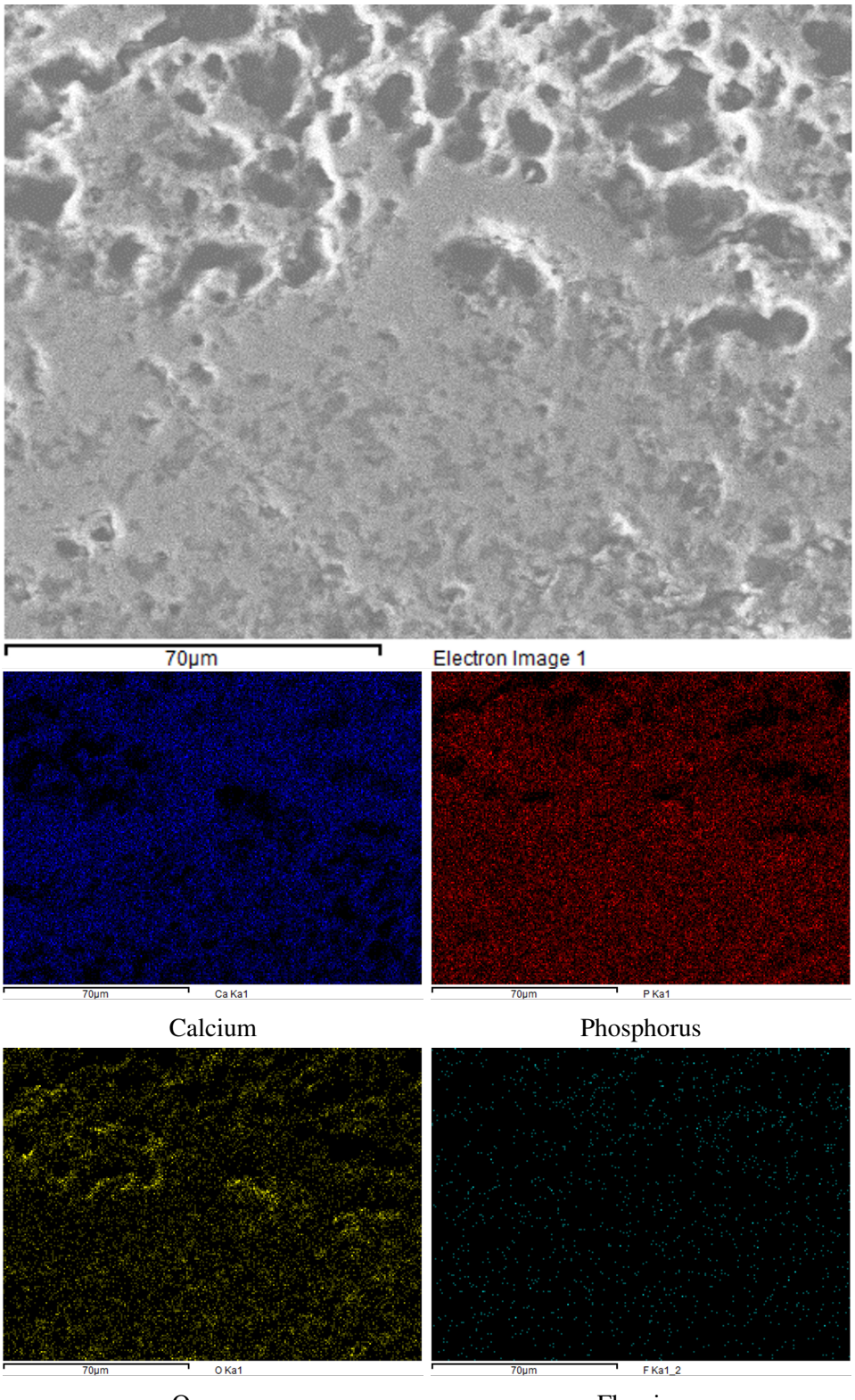

Figure 4.7: Section of the FAp-2 surrogate waste form shown in Figure 4.6 with maps EDS showing the difference in the dense bulk region.

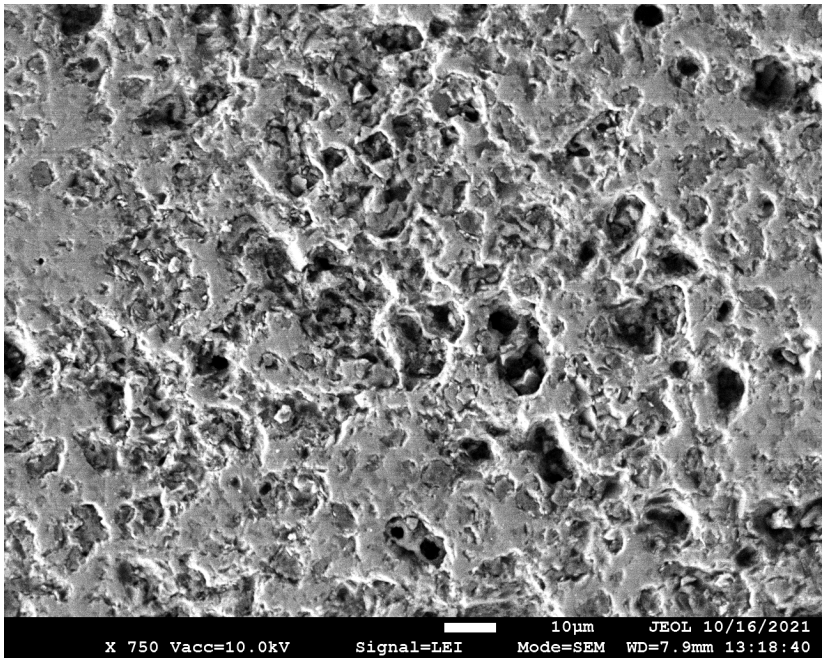

Figure 4.8: A sample of porous region found in a FAp-2 sample.

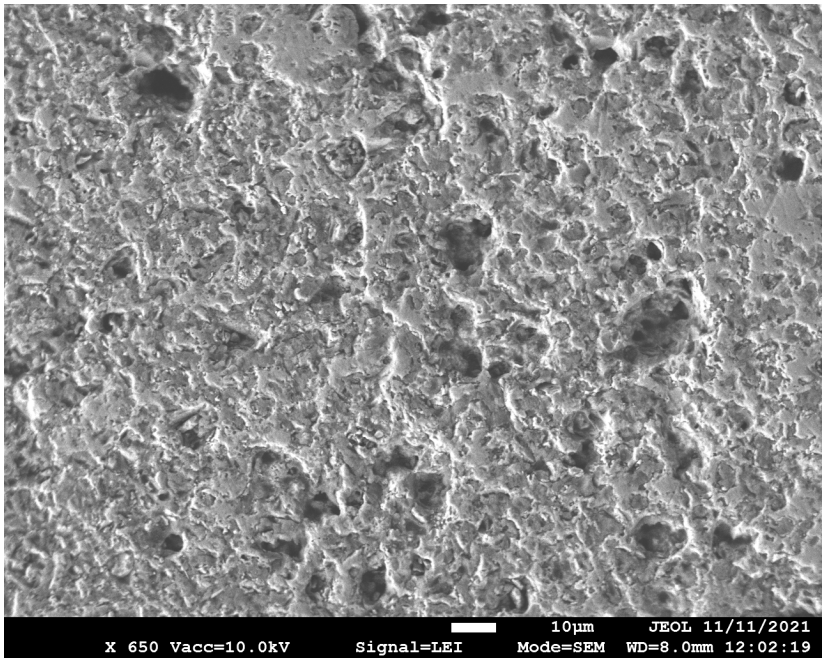

Figure 4.9: An additional porous region found in a M-FAp sample, which appear in all the surrogate waste forms.

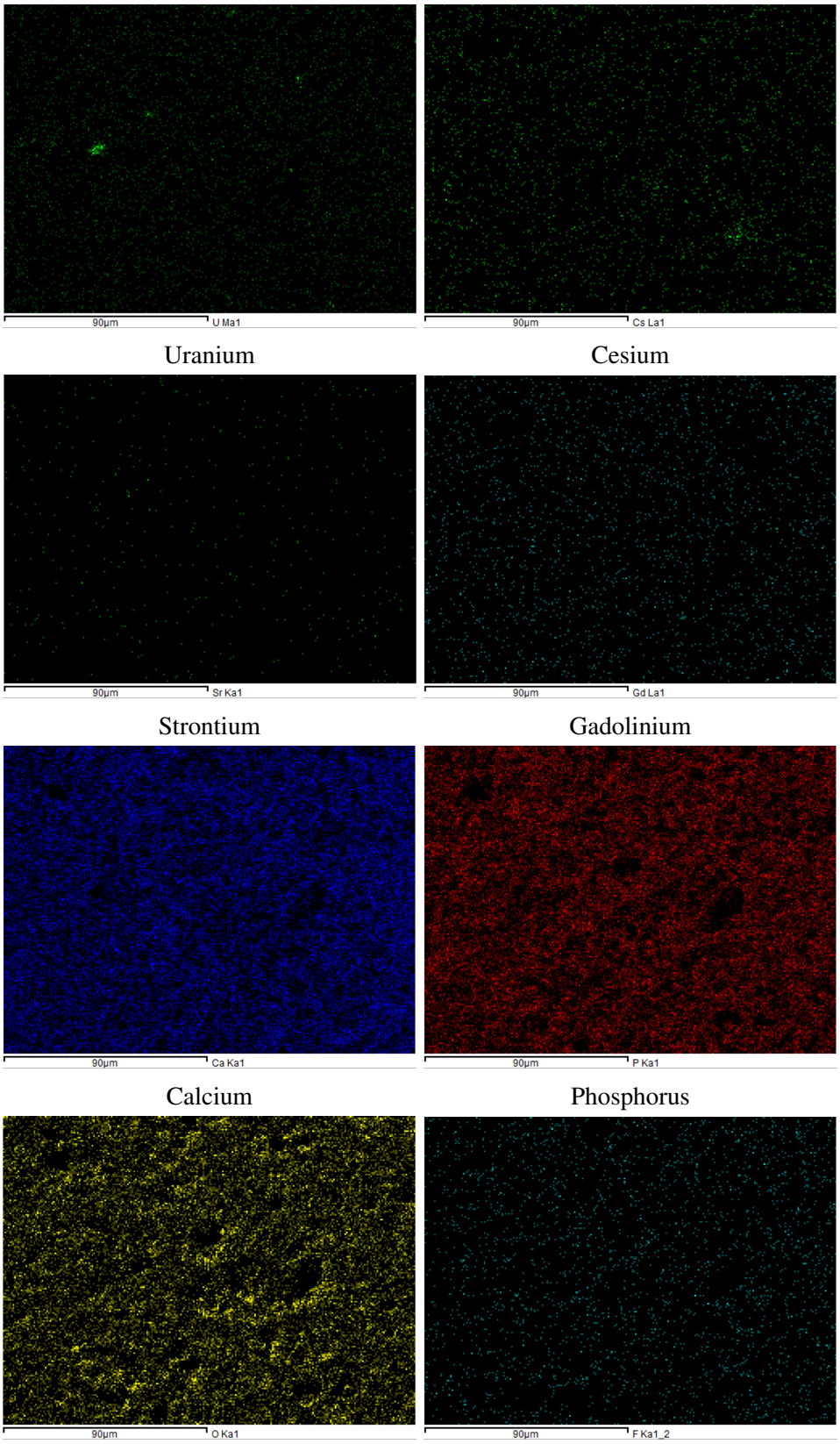

Figure 4.10: EDS mapping of the porous region found in M-FAp surrogate waste forms.

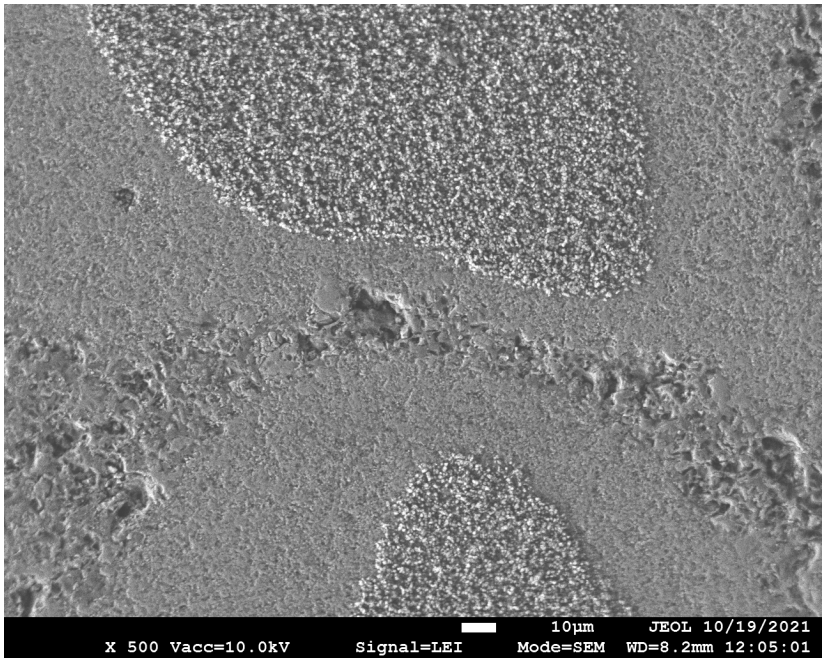

Figure 4.11: Two regions of like phases, surrounded by additional phasess found in FAp-1, and represatative of regions found in all the fluorapatites.

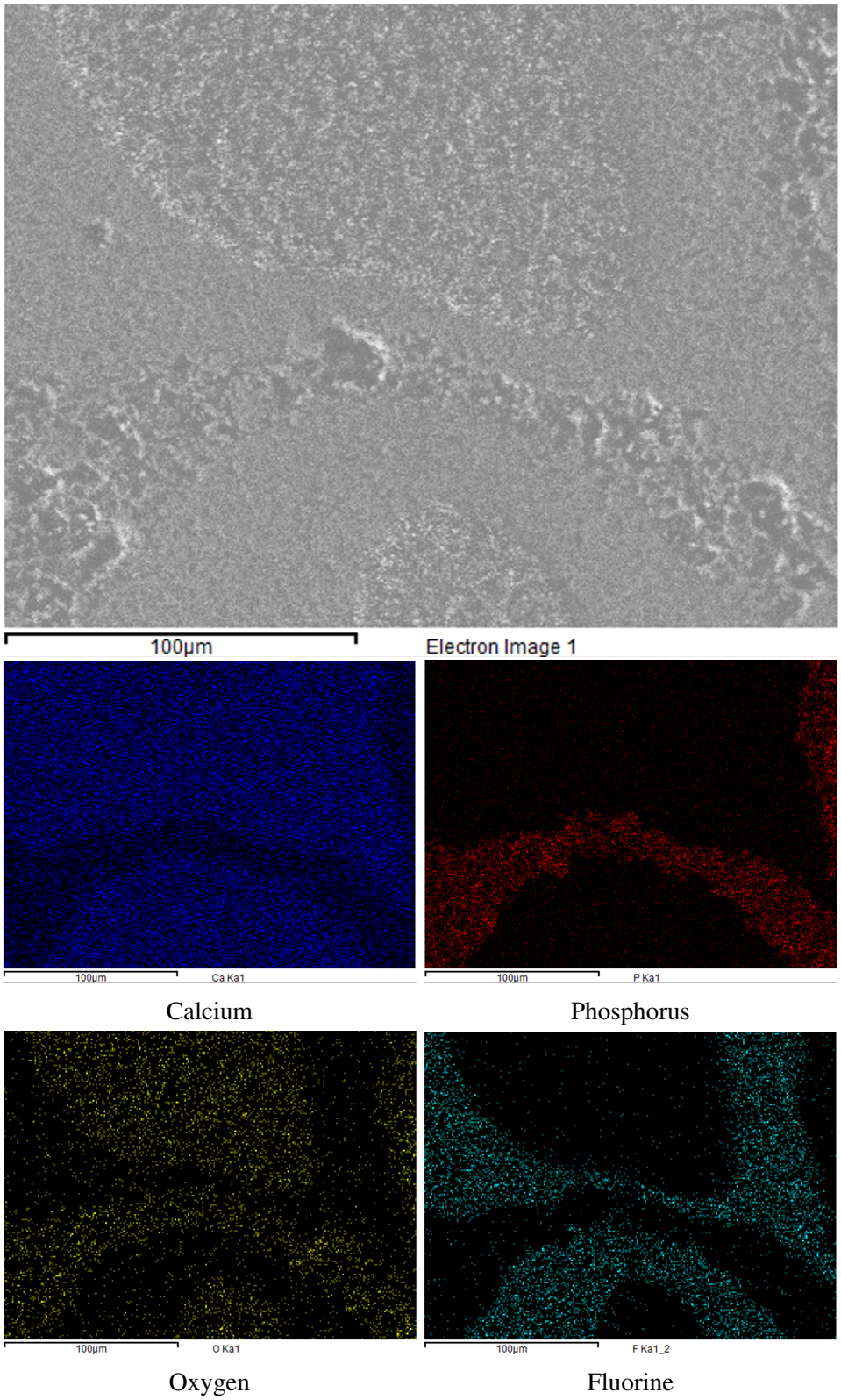

Figure 4.12: The EDS mapping of the three phases, showing a distinct of fluorine, phosphorus, and oxygen content, with increased concentraion of calcium and fluourine.

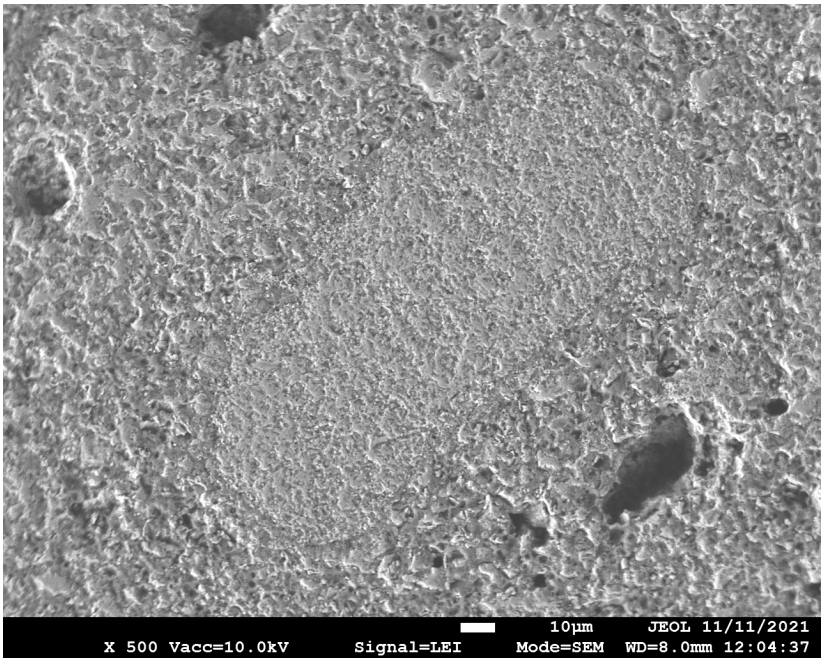

Figure 4.13: Small inclusion found in a M-FAp surrogate waste form sample.

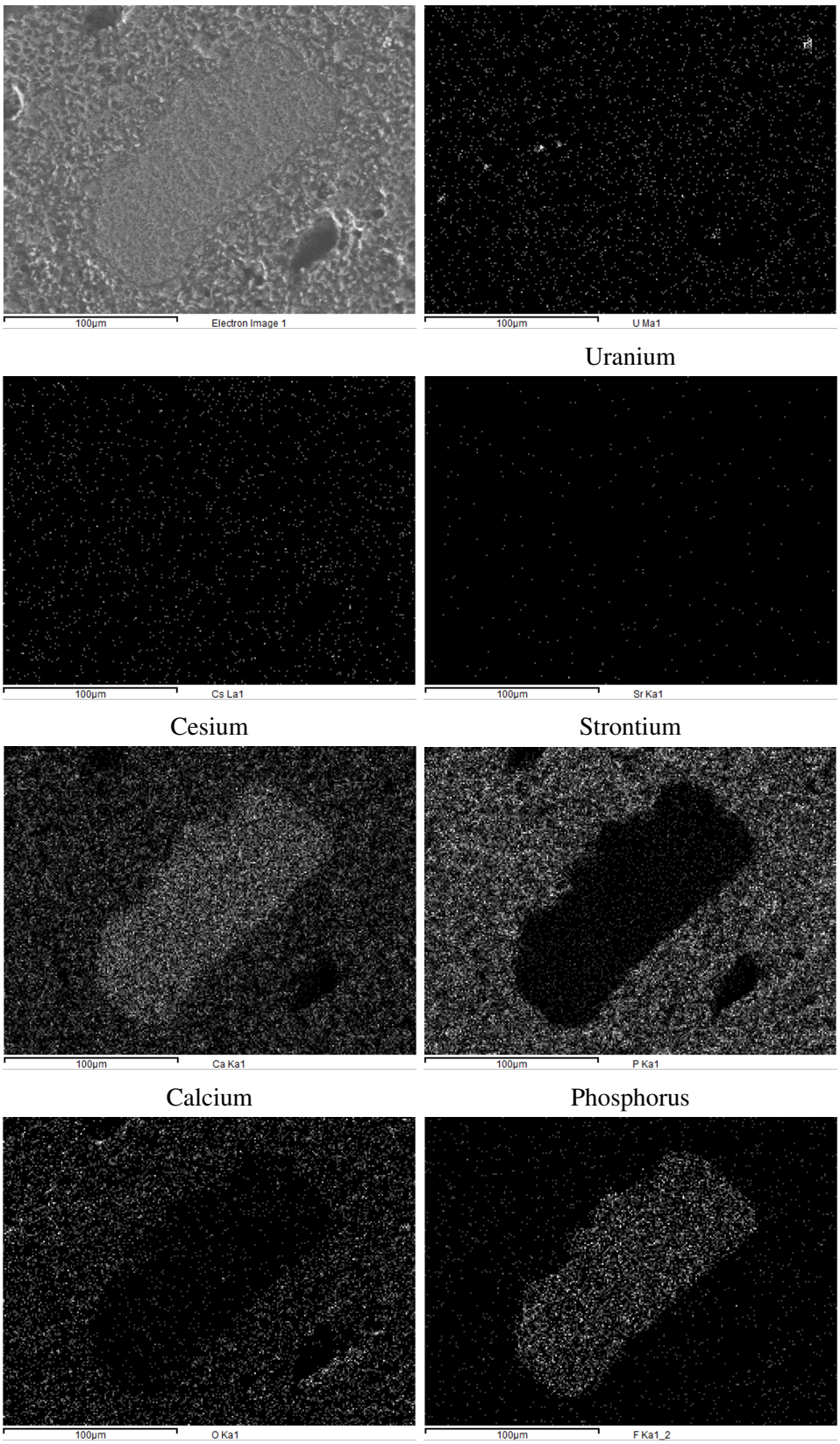

Figure 4.14: The EDS mapping of the inclusion in Figure 4.13, in a M-FAp sample, showing the lack of oxygen and phosphorus and increase in calcium and fluorine concentrations.

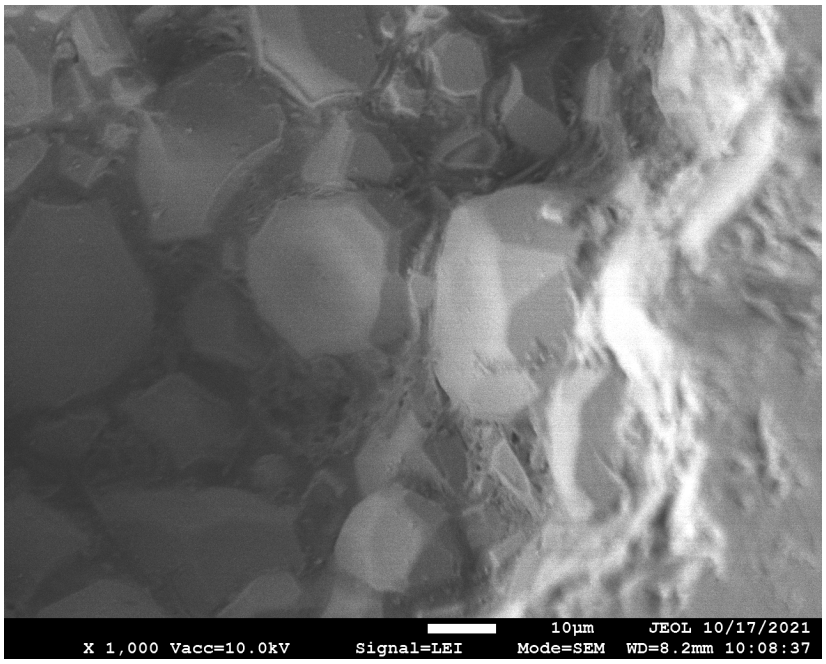

Figure 4.15: Large crystal structures found in a well inside a FAp-4 surrogate waste form.

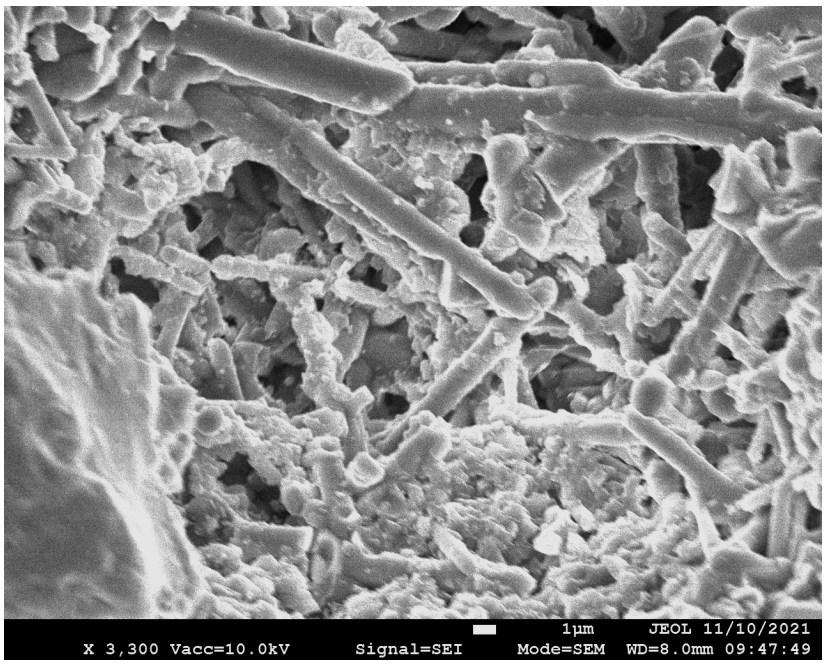

Figure 4.16: Dendritic features found in a U-FAp-3 surrogate waste samples.

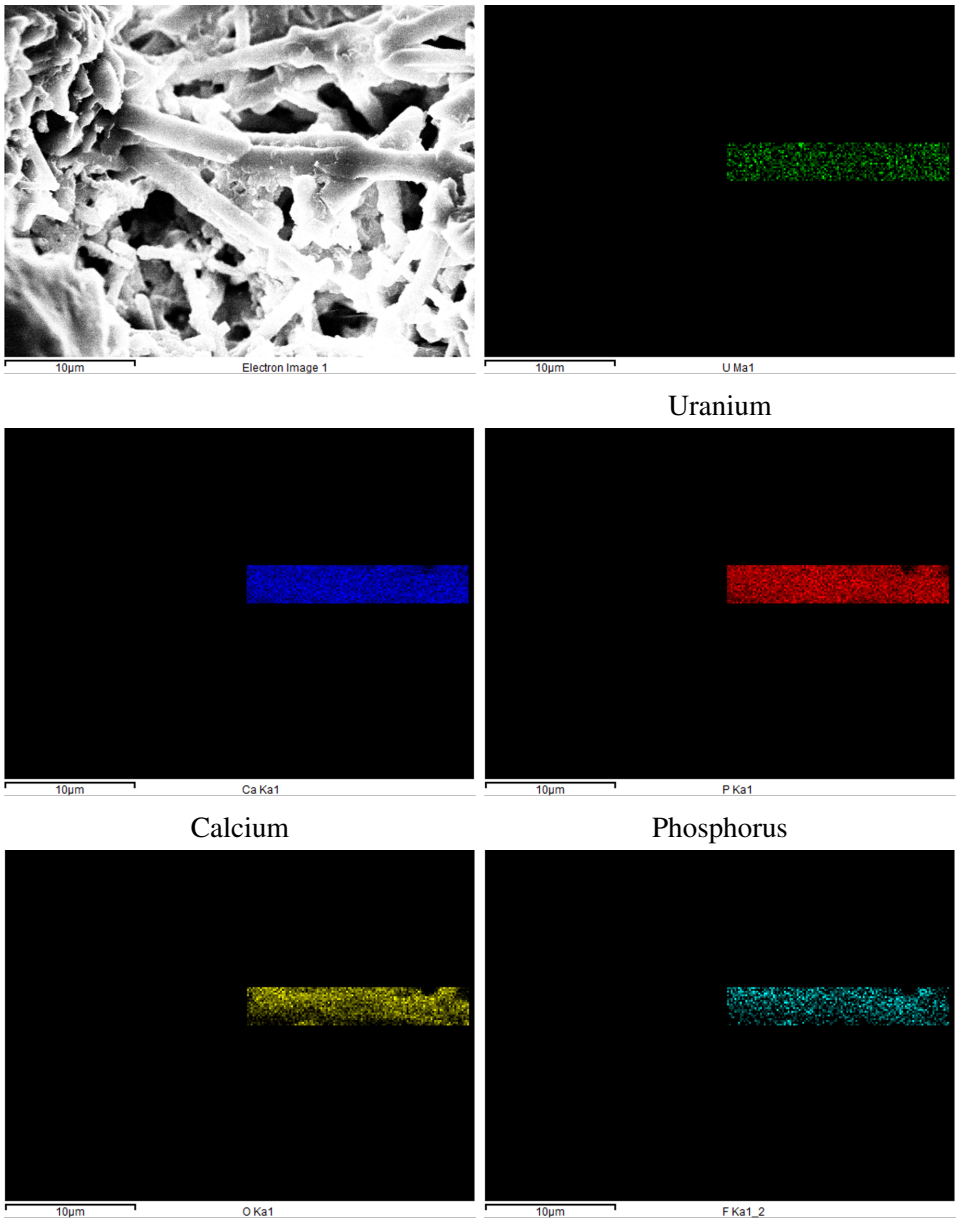

Figure 4.17: EDS of a single crystal found in the U-FAp-3 crystal structure.

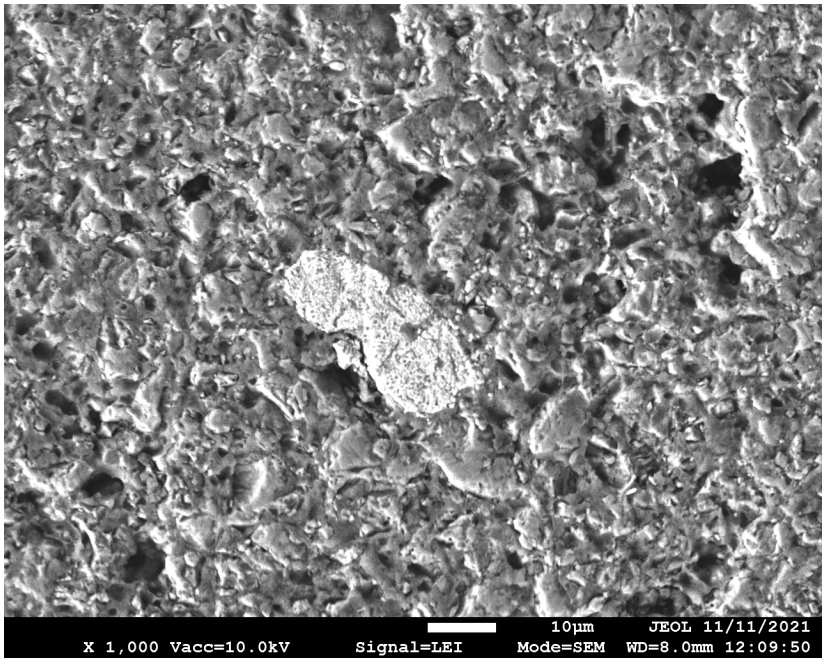

Figure 4.18: A metal inclusion found in a M-FAp sample.

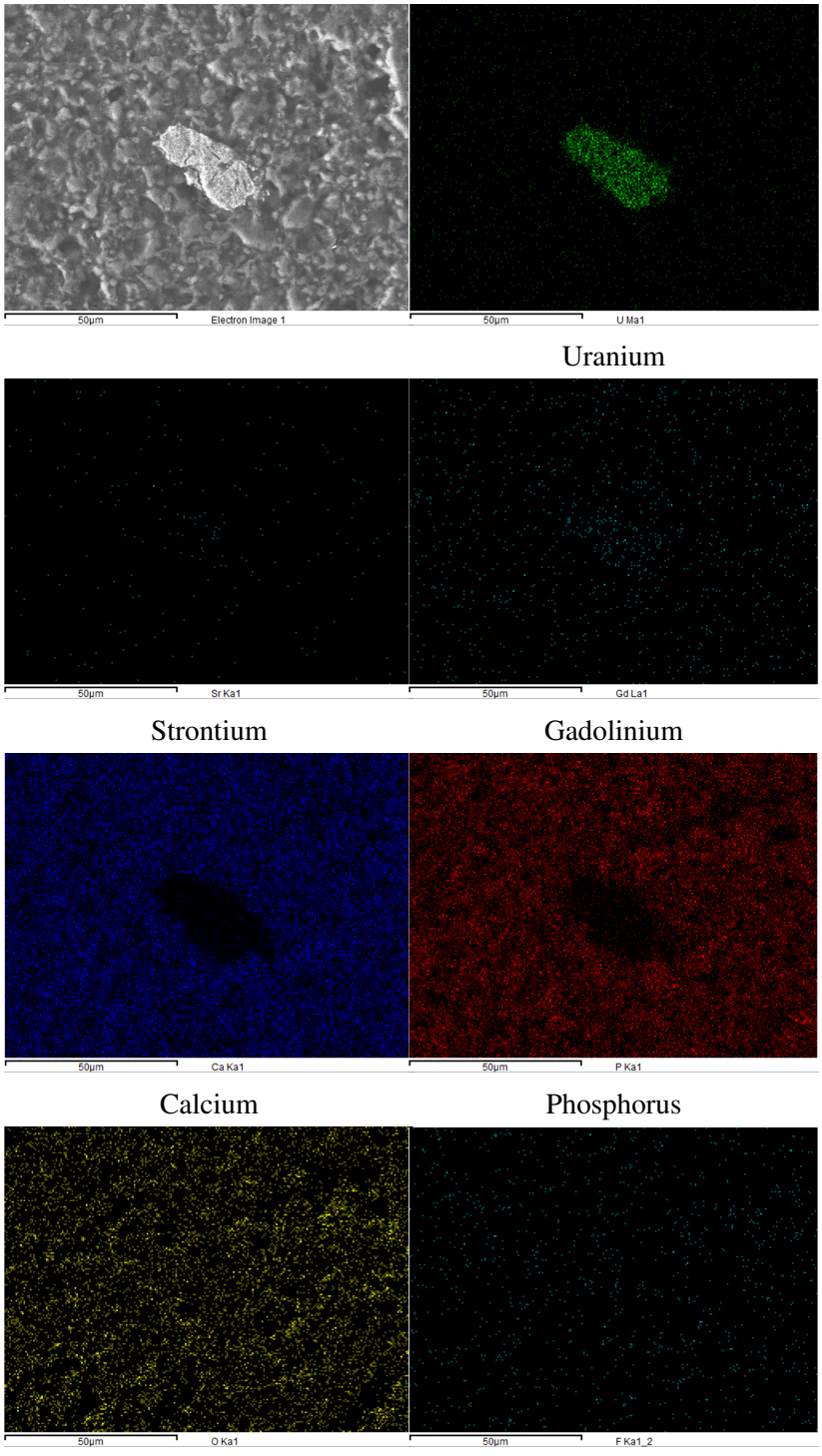

Figure 4.19: The EDS of the metal inclusion found in an M-FAp surrogate waste form, displaying the increase in uranium and oxygen concentration with a corresponding decrease in the concentration of calcium and phosphorus.

4.2 Powder X-Ray Diffraction

Powder X-ray diffraction was conducted using a Rigaku MiniFlex II with SmartLab Studio to identify crystal structures using NIST and Open Crystallography Database and was used to perform Rietveld refinement on the synthesized apatite minerals. The observed XRD patterns and corresponding structures are presented below in Figure 4.20 through Figure 4.31.

The phases present in FLiBe salt samples are: in FAp-1 contained fluorapatite, calcium triphosphate, dicalcium phosphate, and fluorite [31, 32, 33, 34]. FAp-2 contained fluorapatite, fluorite, and hurlbutite [31, 34, 35]. FAp-3 contained fluorapatite and fluorite [31, 36]. FAp-4 contained fluorapatite, dicalcium phosphate and fluorite [31, 33, 37].

For the uranium surrogate waste forms the phases for each waste form were: U-FAp-1 contained uranium substituted fluorapatite, tricalcium phosphate, and uranium oxide [38, 32, 39]. U-FAp-2 contained uranium substituted fluorapatite, tricalcium phosphate, and uranium dioxide [38, 32, 40]. Finally, U-FAp-3 contained uranium substituted fluorapatite, tricalcium phosphate, uranium dioxide, fluorite, and dicalcium phosphate [38, 32, 41, 34, 33].

For the fission product surrogate waste forms the phases observed were: Cs-FAp contained fluorapatite, tricalcium phosphate, and fluorite [31, 32, 36]. While Sr-FAp contained fluorapatite, tricalcium phosphate, fluorite, and fluorostrophite [31, 32, 36, 42]. While the Gd-FAp contained fluorapatite, tricalcium phosphate, and fluorite [31, 32, 36]. The CsGd-FAp contained fluorapatite and tricalcium phosphate [31, 43]. Finally, M-FAp contained fluorapatite, fluorite, uranium oxide, and tricalcium phosphate [31, 36, 41, 44].

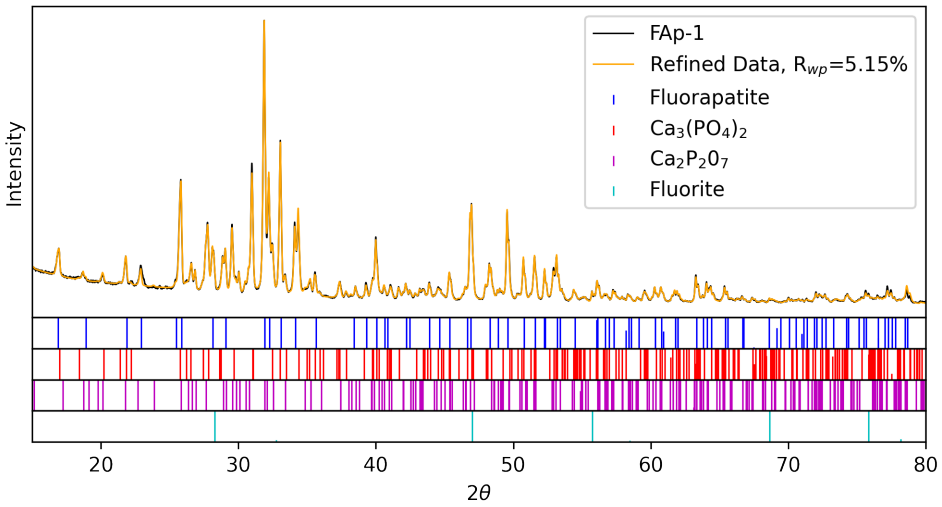

Figure 4.20: Observed XRD patterns and refinment of FAp-1 surrogate waste form with associated phases.

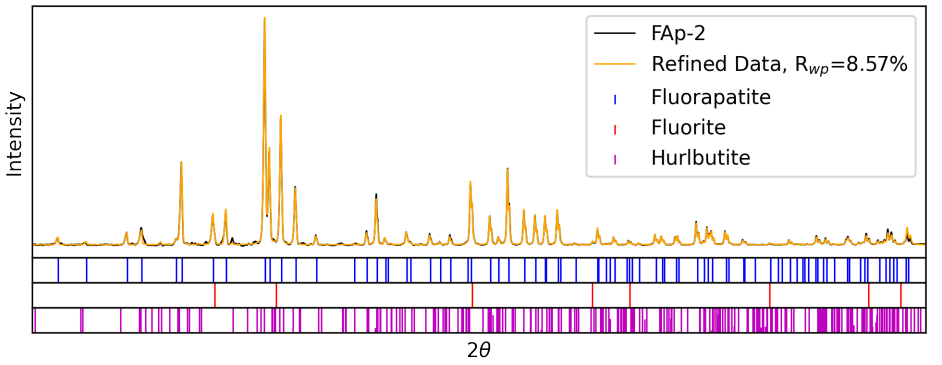

Figure 4.21: Obtained XRD pattern and refinement of FAp-2 fluorapatite with associated phases.

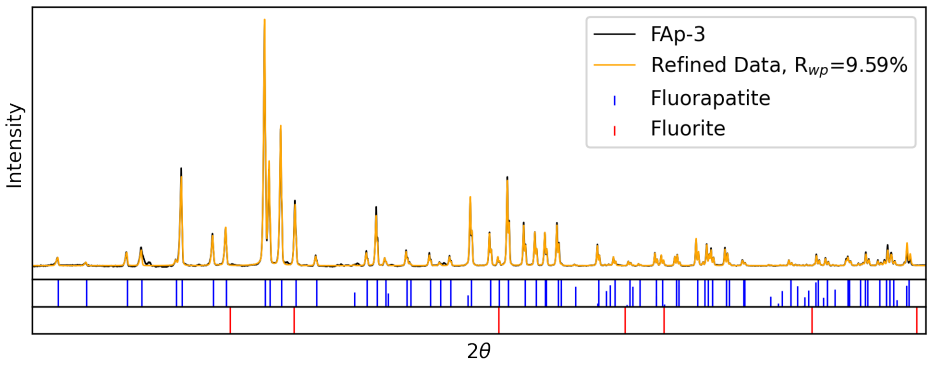

Figure 4.22: Obtained XRD pattern and refinement of FAp-3 waste form with associated phases.

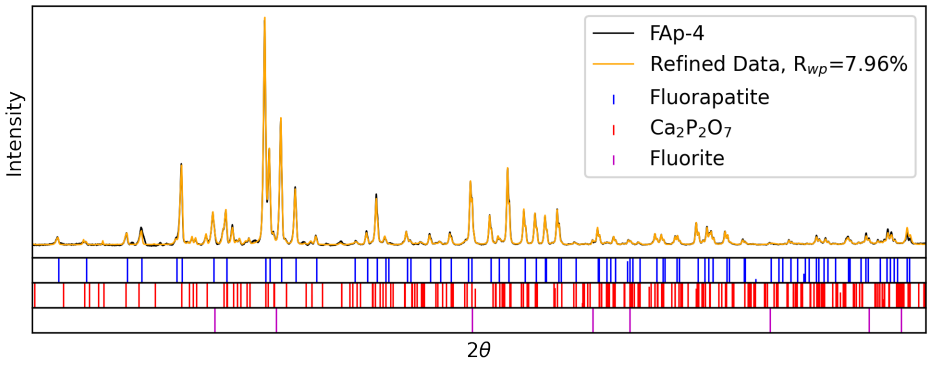

Figure 4.23: Obsered XRD pattern and refienment of FAp-4 fluorapatite with associated phases.

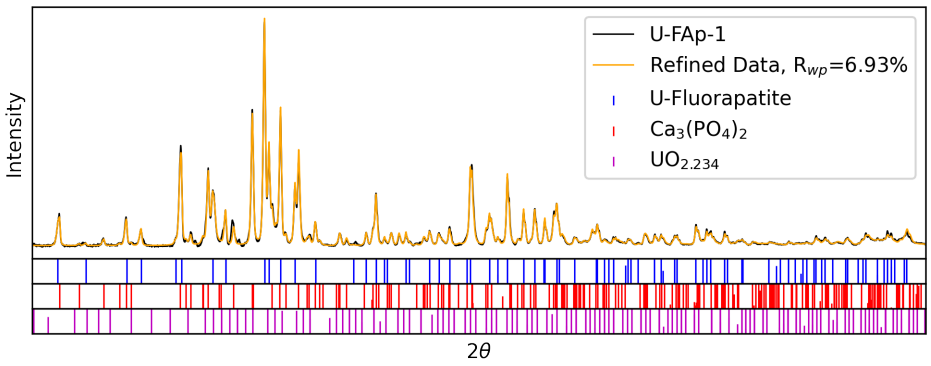

Figure 4.24: Obtained XRD pattern and refinement of U-FAp-1 surrogate waste form with associated phases.

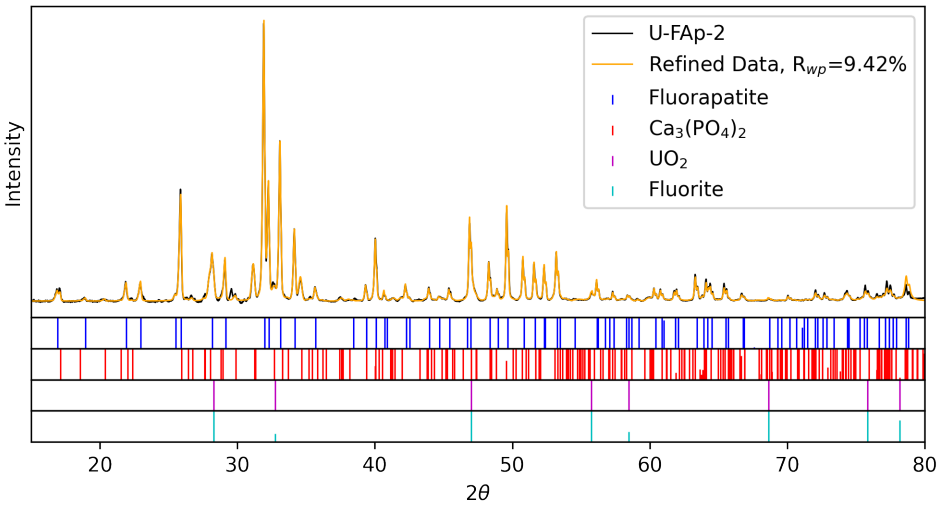

Figure 4.25: Obtained XRD pattern and refinement of U-FAp-2 waste mineral with associated phases.

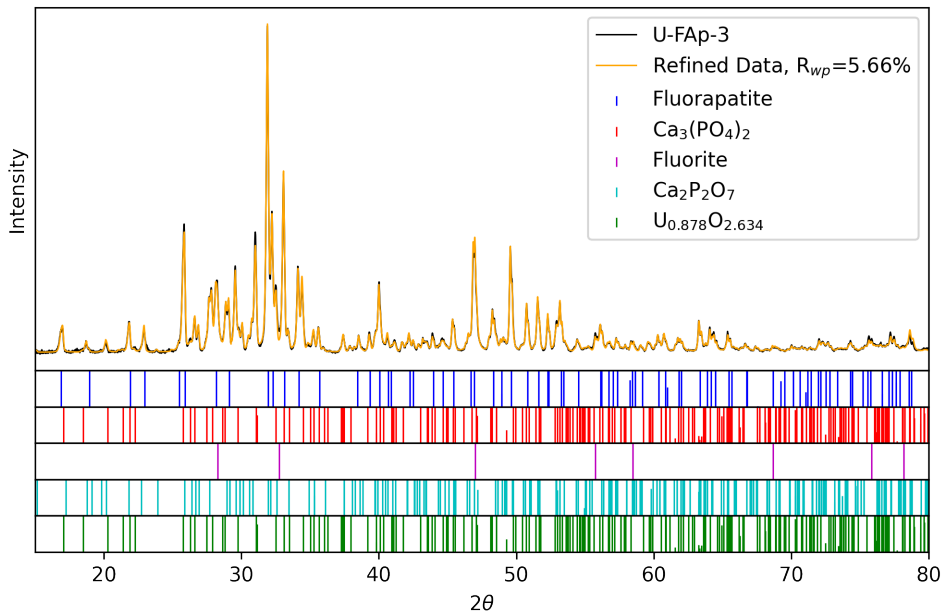

Figure 4.26: Observed XRD pattern and refinement of U-FAp-3 surrogate waste form with associated phases.

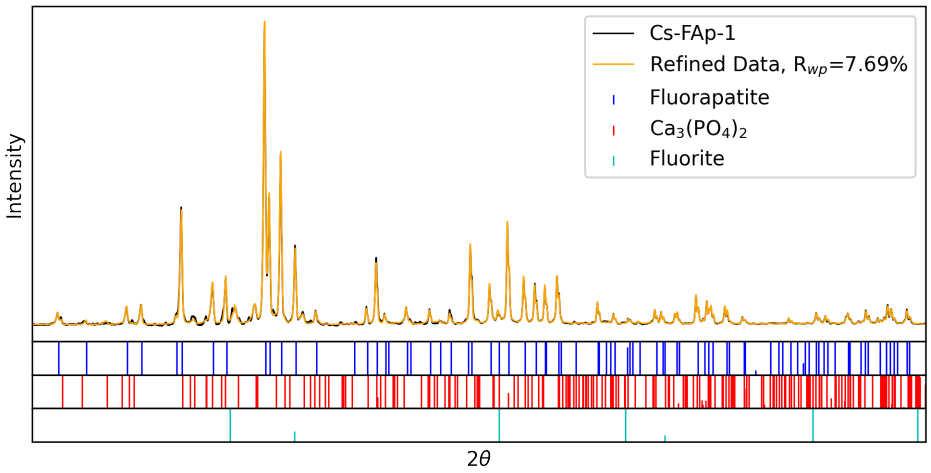

Figure 4.27: Obtained XRD pattern and refinement of Cs-FAp surrogate waste form with associated phases.

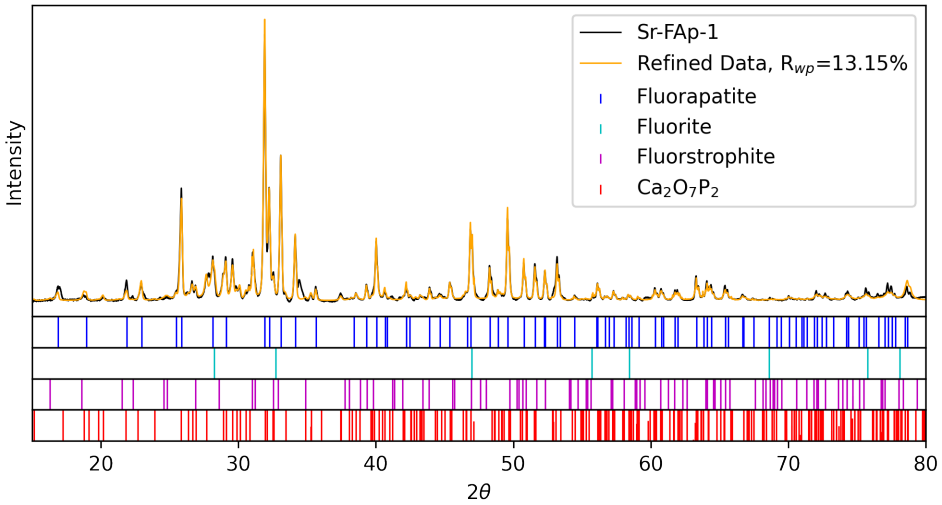

Figure 4.28: Obtained XRD pattern and refinement of Sr-FAp waste mineral with associated phases.

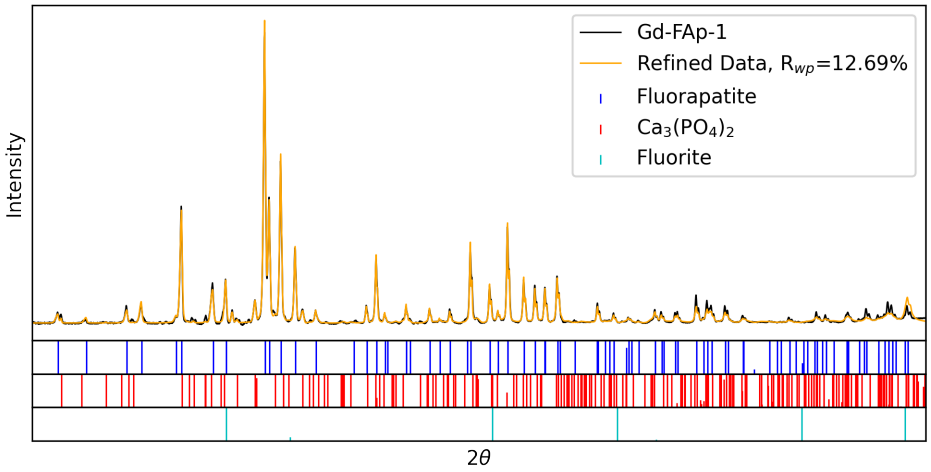

Figure 4.29: Obtained XRD pattern and refinement of Gd-FAp waste mineral with associated phases.

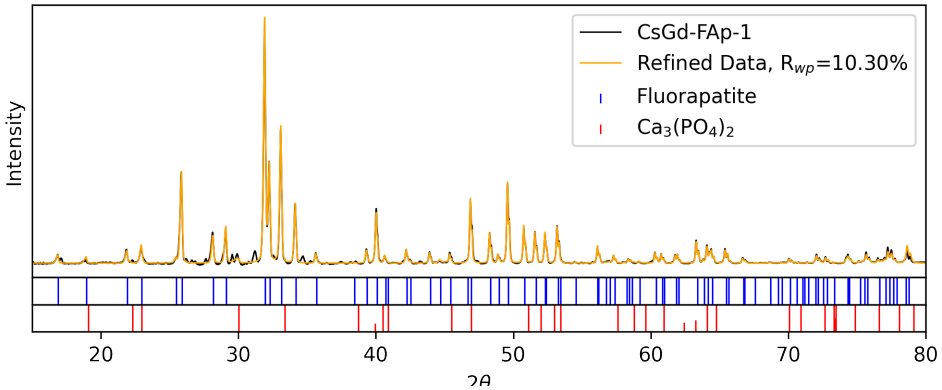

Figure 4.30: Observed XRD pattern and refinement of CsGd-FAp surrogate waste form with associated phases.

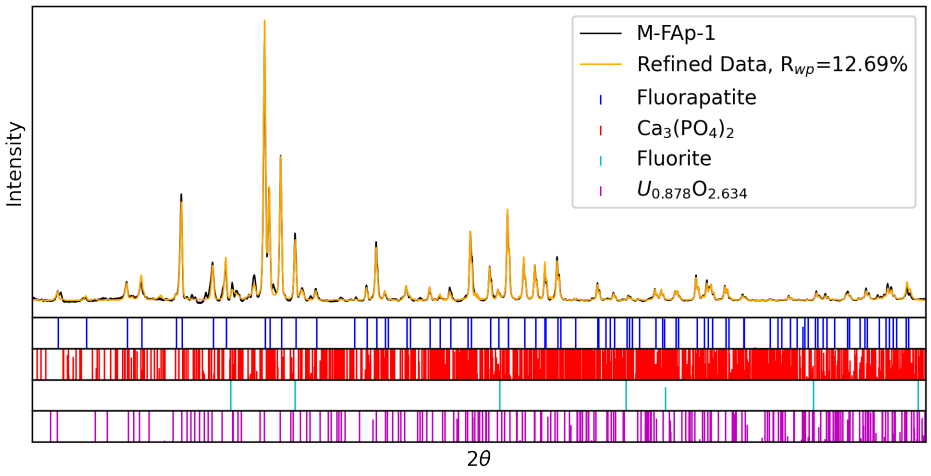

Figure 4.31: Observed XRD pattern and refinement of M-FAp substituted fluorapatite with associated phases.

4.3 Density

Densities were obtained using two different methods. The first method was conducted immediately after heat treating by obtaining the mass, heigth, and diameter to calculate a geometrical density. The geometric densities are shown in Table 4.1 below.

Table 4.1: Geometric densities obtained from dimensional measurements of pellets, averaged over three pellets for each waste form.

Geometric Density	
	(g/cm^3)
FAp-1	1.99
FAp-2	2.16
FAp-3	2.13
U-Fap-1	1.89
U-Fap-2	2.03
U-Fap-3	1.90
FAp-4	2.02
Cs-FAp	1.91
Sr-FAp	1.91
Gd-FAp	1.96
CsGd-FAp	1.97
M-FAp	1.89

The second method involved the use of a pycnometer. The results are listed below in Table 4.2.

Table 4.2: Pycnometer densities obtained for each waste form.

	(g/cm^3)	Error (g/cm^3)
FAp-1	3.00	4.00E-04
FAp-2	2.83	4.40E-03
FAp-3	2.97	0.00E+00
U-Fap-1	3.05	2.00E-04
U-Fap-2	2.98	1.50E-03
U-Fap-3	3.08	3.00E-03
FAp-4	2.95	4.80E-03
Cs-FAp	3.07	6.90E-03
Sr-FAp	3.07	1.90E-03
Gd-FAp	3.04	4.20E-03
CsGd-FAp	3.03	6.10E-03
M-FAp	3.03	5.20E-03

4.4 Fluoride and pH Changes of Leachate

Free fluoride and pH measurements were taken of the leachant liquid before and after a product consistency test. The pH measurements allowed for a quick identification if leaching was occurring, by comparing the initial pH value obtained at the start of a test and the final values after completion. The initial pH is presented below in Table 4.3 and the final pH's of each vessel is displayed in Figure 4.32.

Table 4.3: Initial pH of the Type-1 ASTM water used as the leachant for each waste form.

Fluorapatite	pH
FAp-1	7.35
FAp-2	6.97
FAp-3	7.16
U-FAp-1	6.98
U-FAp-2	6.98
U-FAp-3	7.35
FAp-4	6.94
Cs-FAp	6.96
Sr-FAp	6.96
Gd-FAp	7.13
CsGd-FAp	6.94
M-FAp	7.13

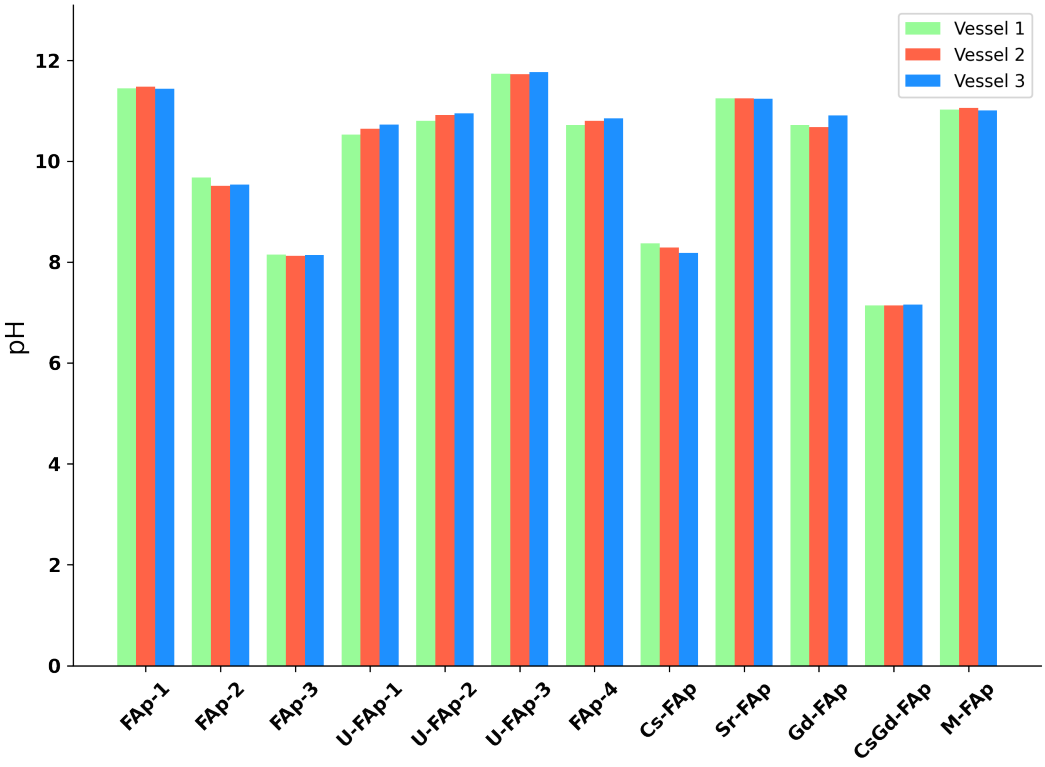

Figure 4.32: The pH in each vessel post leach test.

Fluorine is one of the major components of LiF-BeF_2 salts. Additionally, fluorine is also a major structural component of the fluorapatite ($Ca_5(PO_4)_3F$) that is being investigated as a surrogate waste form. Therefore, understanding if the fluorine is mobile during leach testing is crucial and was monitored using the Oakton select fluorine selective ion probe, the concentraion values in ppm obtained post PCT are show in Figure 4.33, and Figure 4.34 displays the same data in g/L.

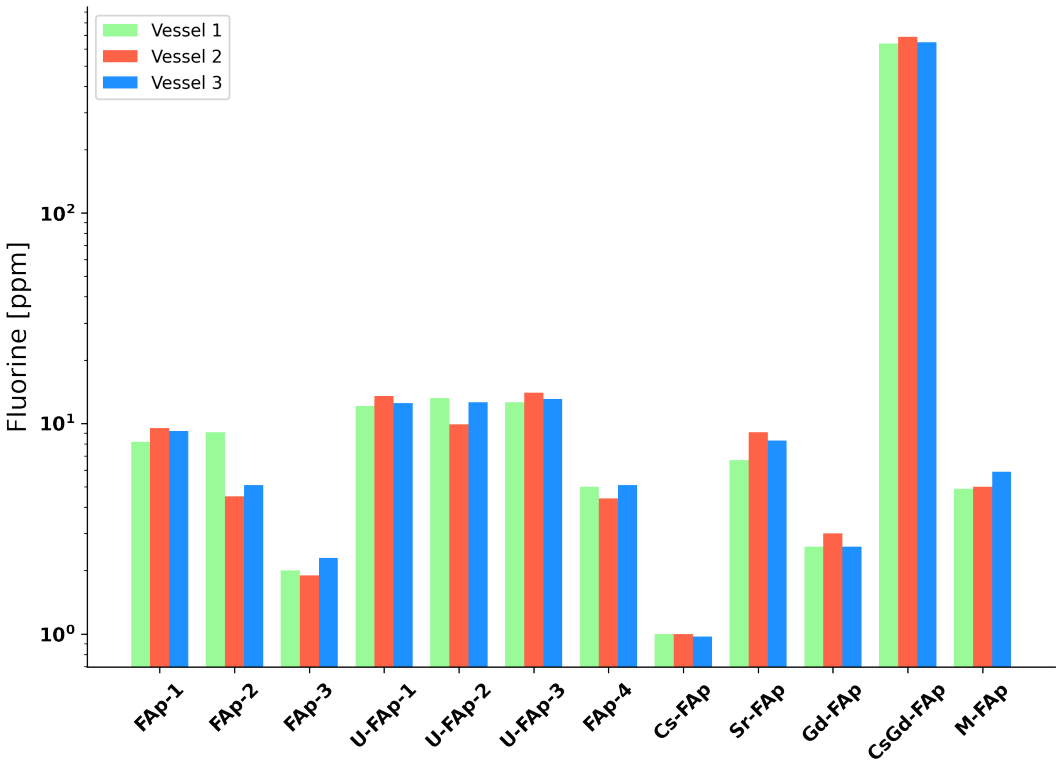

Figure 4.33: Concentration data in ppm of free fluorine present in leachate after PCTs.

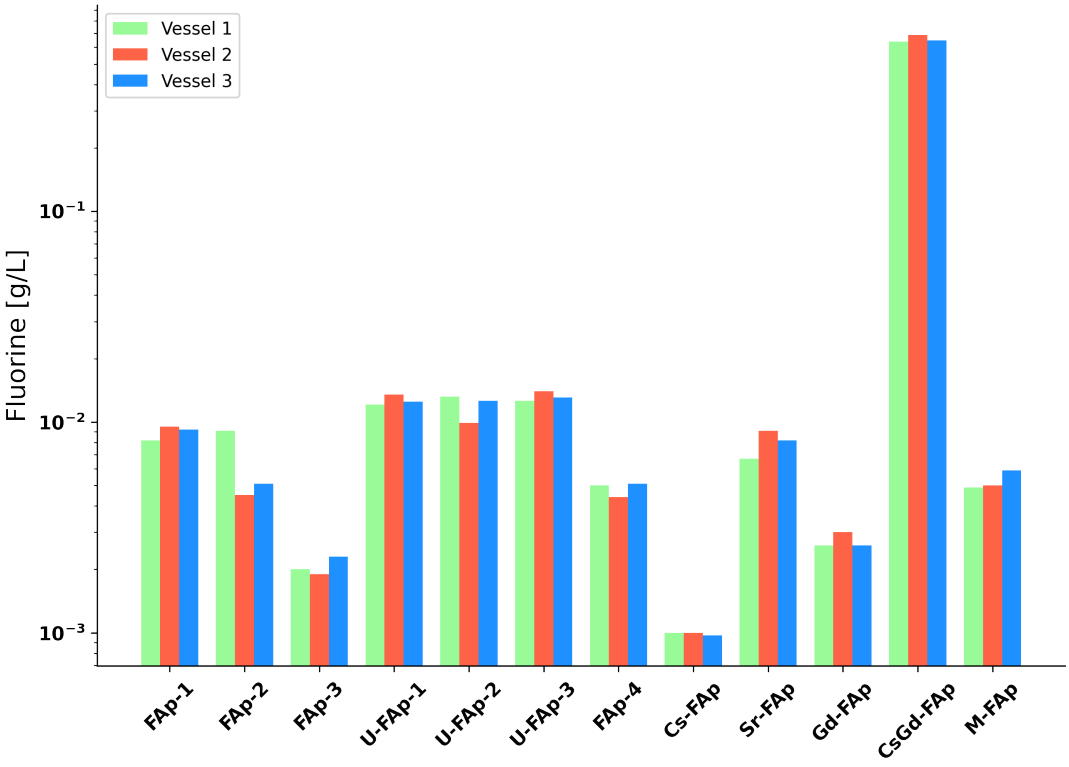

Figure 4.34: Concentration data in g/L of free fluorine present in leachate after PCTs.

4.5 ICP-MS

Additional structure components, the cations, of the substituted fluorapatite which include calcium, beryllium, and the surrogate fission products and fuel that may leach during a test were investigated by inductively coupled plasma mass spectroscopy (ICP-MS). The cation analysis was conducted at the Chemical Characterization Facility at Texas A&M using a Perkin Elmer NexION 350 by Dr. Bryan Tomlin. The concentration data, in ng/mL, obtained from the CCF is presented in Appendix 3. The following data is converted to g/L, and is used in calculating the normalized leach rates in Section 5.3. For all images the y-axis, is in log scale to properly display the range of leached specimens, unless otherwise noted.

4.5.1 Contamination in the control vessels

The following two images display the contaminates found in each control vessel for the PCTs that were conducted. Figure 4.35 shows the amount of beryllium, calcium, and cesium. While Figure 4.36 shows strontium, gadolinium. and uranium. Note that Figure 4.35 the y-axis is not log scale.

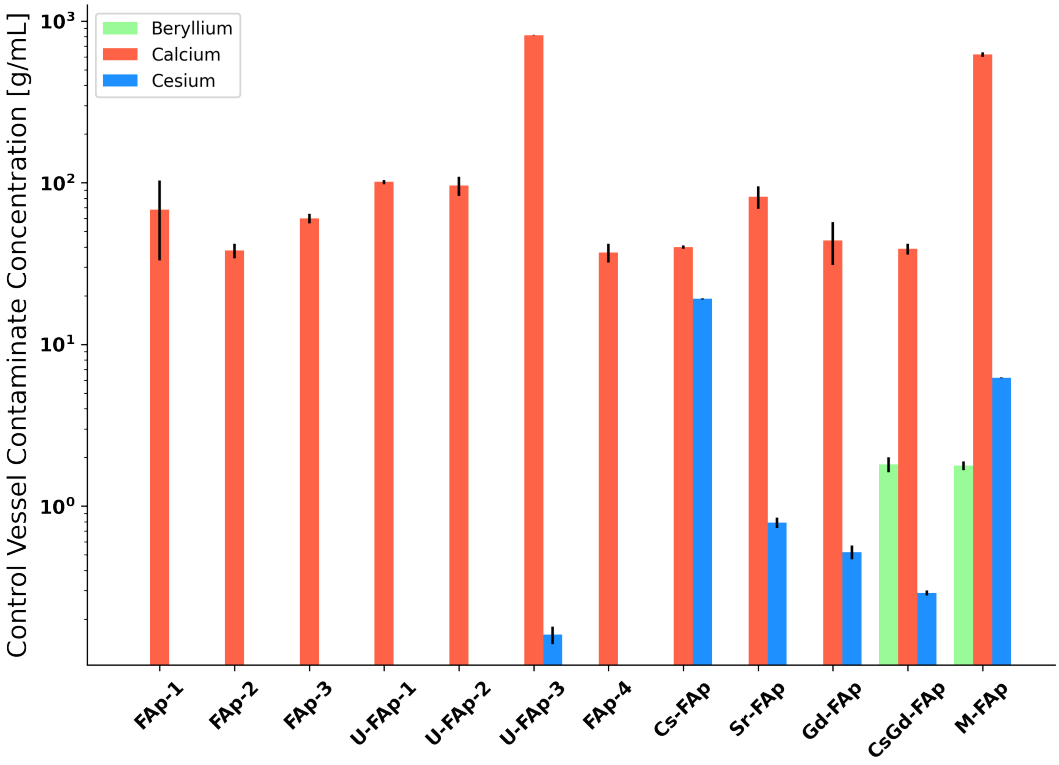

Figure 4.35: Concentration data in g/mL of contaminates found in the control vessels from ICP-MS for Be, Ca, and Cs.

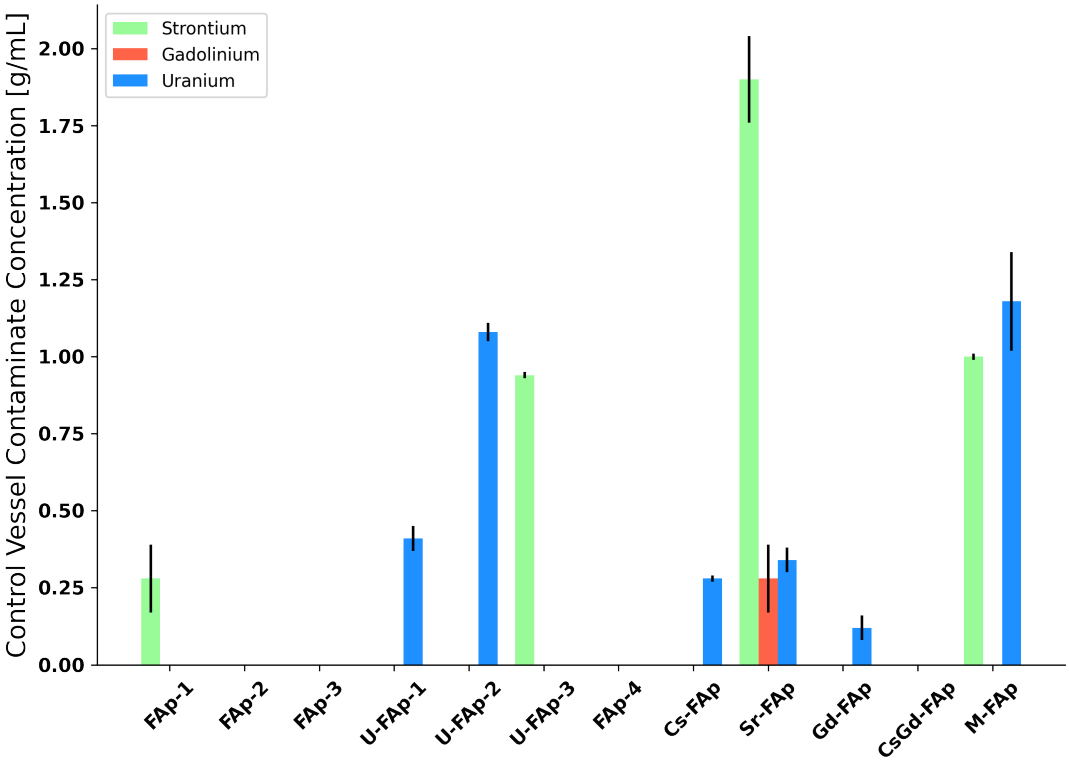

Figure 4.36: Concentration data in g/mL of contaminates found in the control vessels from ICP-MS for Sr, Gd, and U.

4.5.2 ICP Data

Each image below presents only one cation across the three waste filled test vessels for each apatite. Note in the following images that log scale was used on the y-axis to adaqately display the more excessive leaching behavior of some samples.

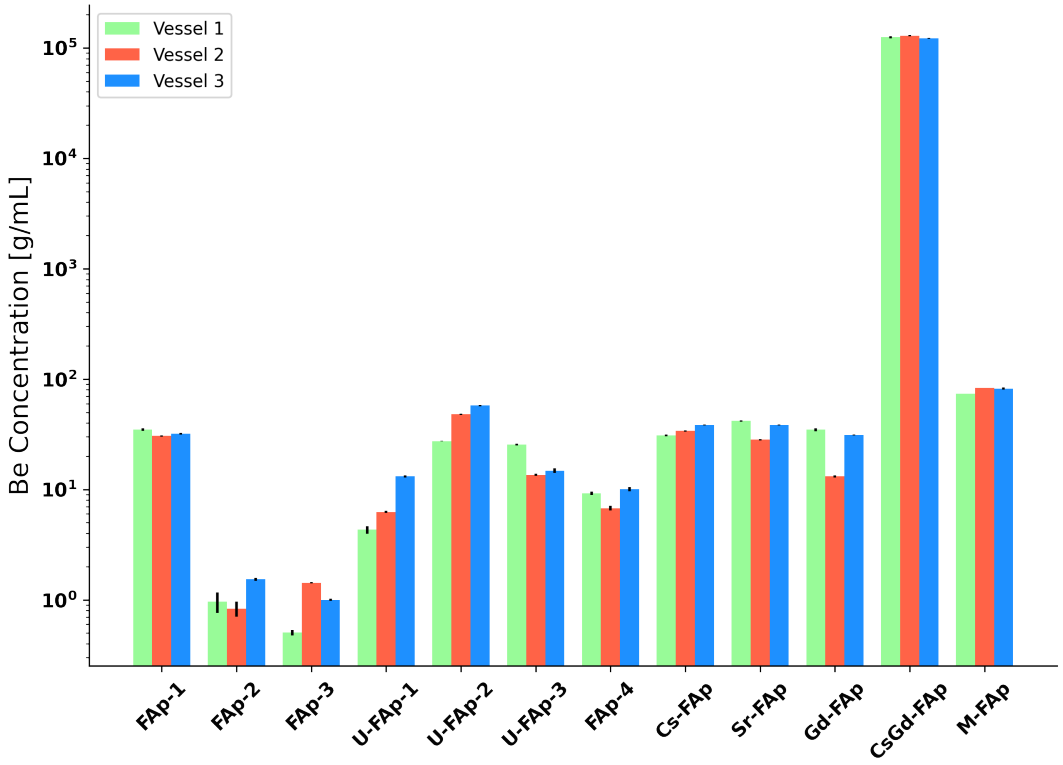

Figure 4.37: Concentration data in g/mL of of beryllium that leached from the surrogate waste forms.

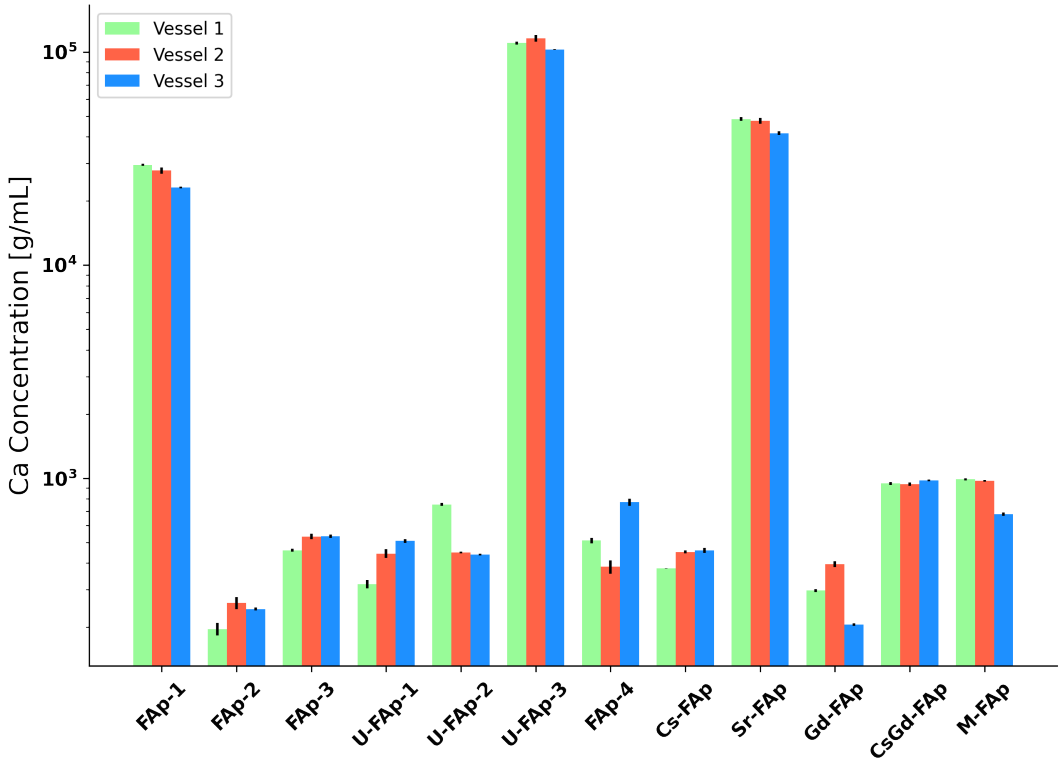

Figure 4.38: Concentration data in g/mL of calcium that leached from the surrogate waste forms.

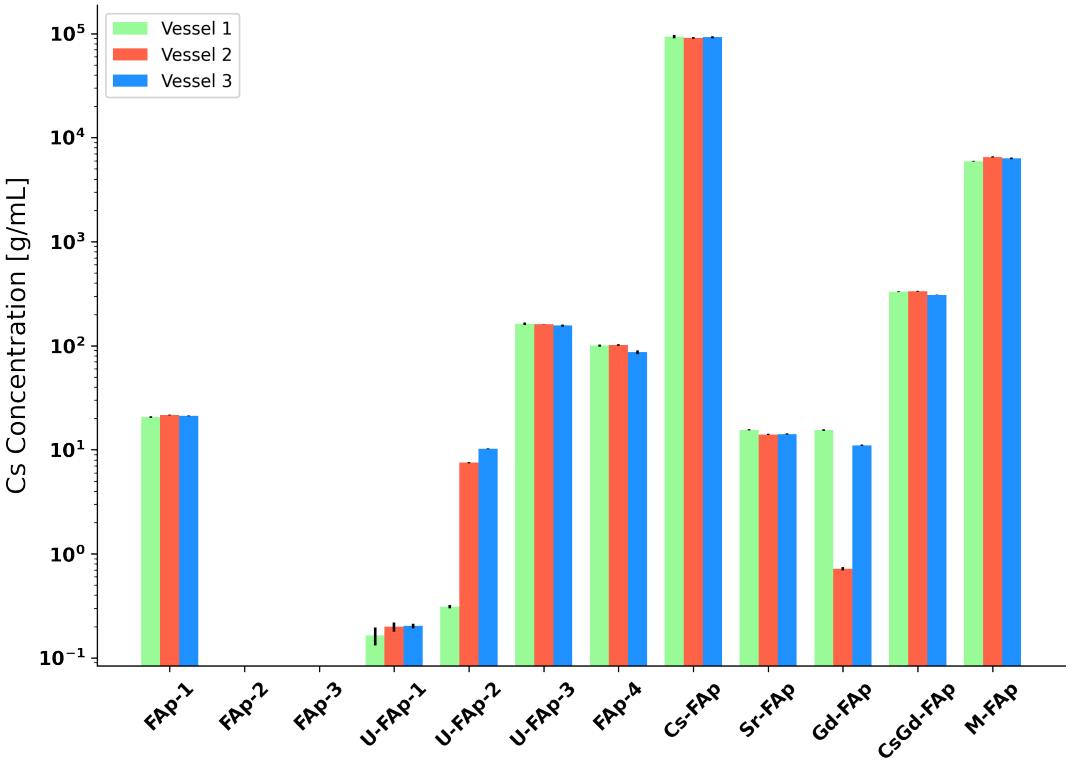

Figure 4.39: Concentration data in g/mL of cesium that leached from the surrogate waste forms.

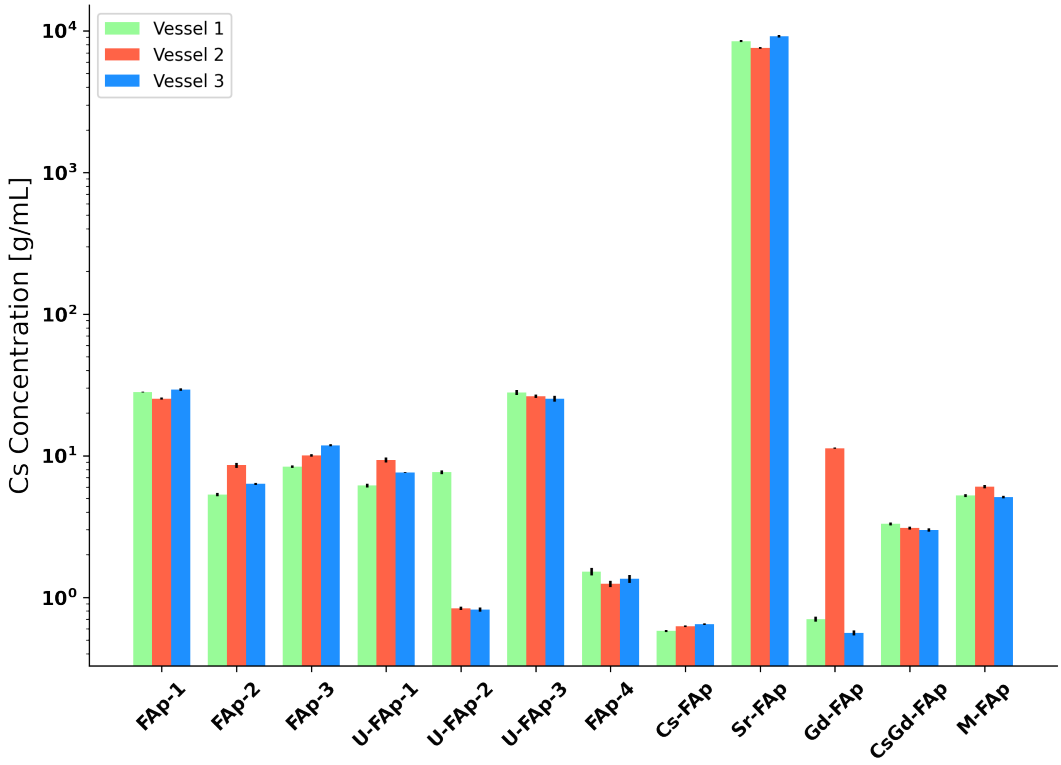

Figure 4.40: Concentration data in g/mL of strontium that leached from the surrogate waste forms.

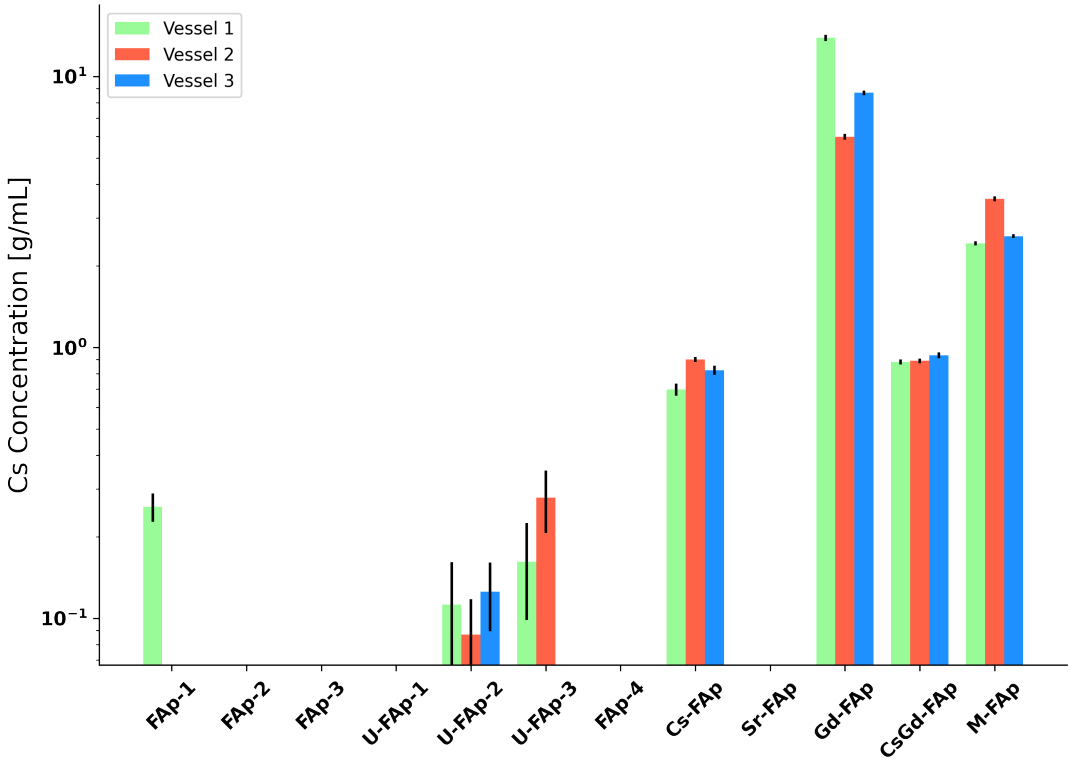

Figure 4.41: Concentration data in g/mL of gadolinium that leached from the surrogate waste forms.

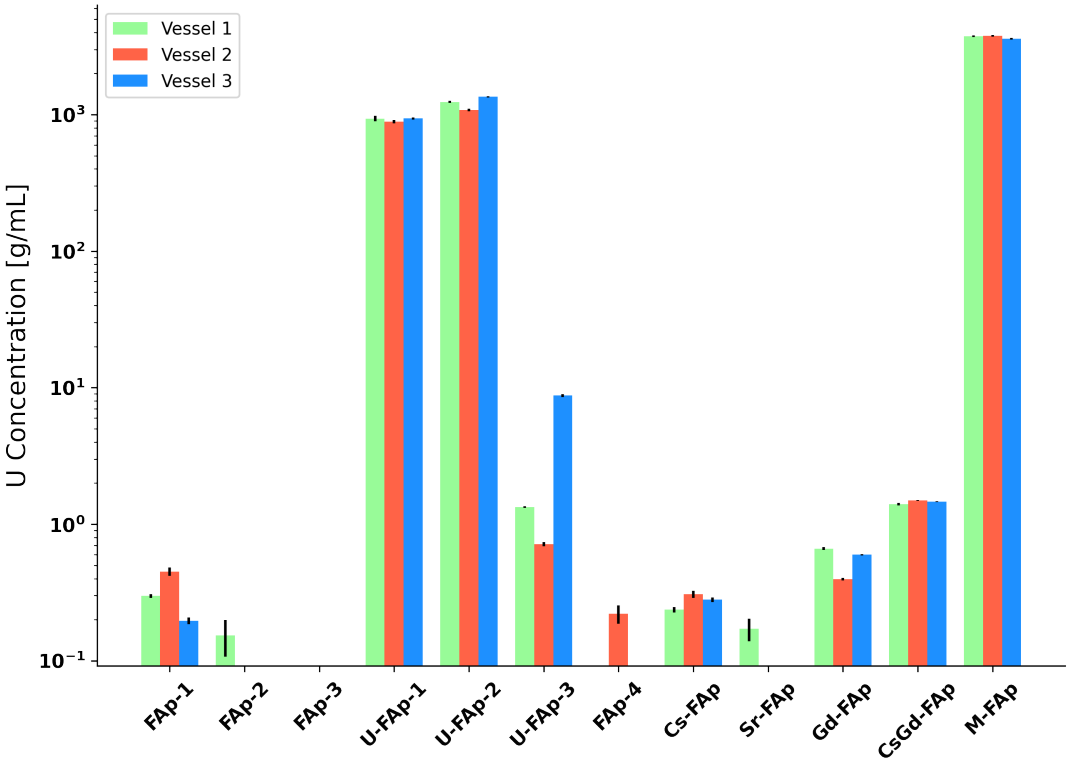

Figure 4.42: Concentration data in g/mL of uranium that leached from the surrogate waste forms.

5. Discussion

The following chapter presents a discussion of the results presented in Chapter 4 by addituin of context and interpretation of the results. Section 5.1 discusses the structural information of each apatite. Section 5.2 details the normalization leachate figures and compares the results to leaching data from other waste forms. Finally, Section 5.3 summarizes the results, introduces concluding remarks, and includes areas of future work regarding fluorapatite waste forms.

5.1 Microstructures of the Apatites

To obtain an accurate representation of the microstructures of each apatite, samples were subjected to EDS and XRD techniques. In general, EDS and XRD identified major phases of fluorapatite and calcium phosphates were present in most samples. Each sample additionally had its own minor phases and is associated with the chemical composition and the production conditions implemented. Theses minor phases are possibly metal oxides, fluoro-phosphates, and calcium fluoride compounds. The bulk structure is a dense body laced with sporadic porous regions, with the occasional large void, the large voids often being surrounded by a porous region. The three regions can be seen in Figure 5.1.

5.1.1 Fluorapatites

FAp-1 was synthesized at the lowest ball-milling and sintering time at 700°C, resulting in a waste form that contained fluorapatite and two distinct calcium phosphate phases: calcium diphosphate and tricalcium phosphate. Tricalcium phosphate is a precursor compound signifying that a significant portion of the surrogate waste form had not been converted to the ideal waste material. Finally, it contained an additional phase which is present in most of the waste forms, which is calcium fluoride, and is shown in Figure 5.2.

The second surrogate waste form, FAp-2, was produced under the same conditions as FAp-1. However it was sintered at a higher temperature, 800°C and displayed significant improvement in conversion to fluorapatite with minor phases of fluorite and hurlbutite. Hurlbutite has the chemical

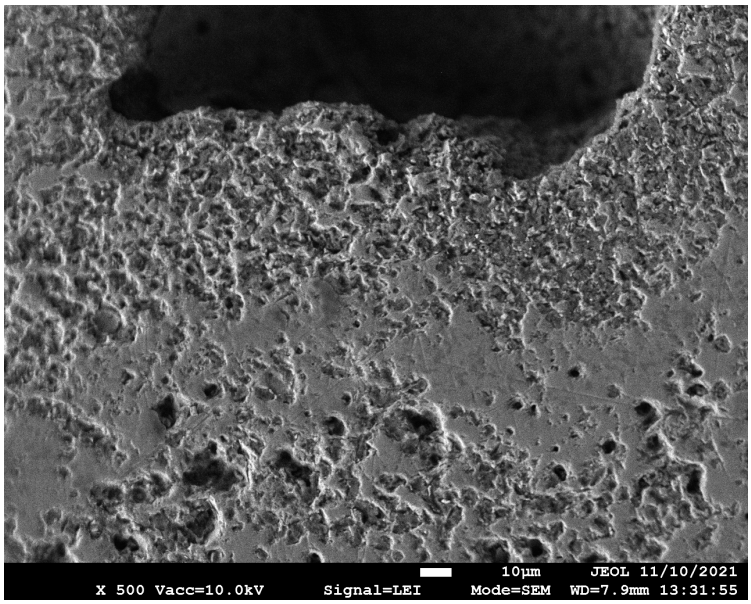

Figure 5.1: The dense phase, porous, and a void area displaying the different phases present in the apatites

formula of $CaBe_2(PO_4)_2$, indicating that enough beryllium had migrated to a calcium phosphate region to replace calcium in the structure and have sufficient quantity to detect the phase on the XRD, which can not detect beryllium of the concentration is below 10-mass%.

The FAp-3 surrogate waste form, was ball-milled for 10-hours and sintered for 10-hours at 700°C, showed high conversion to fluorapatite. Along side SEM-EDS data a small secondary phase was also identified that being calcium fluoride.

The final FLiBe only salt loaded surrogate waste form, FAp-4, which increased the amount of FLiBe salt to 51.1-mol%, found that the fluorapatite concentraion was less than FAp-3 and contained a fluorite and calcium diphosphate. The SEM images for FAp-4 found easily identifiable crystal structures in the open porous regions, and noticeable inclusions of the dicalcium phosphate within the bulk phase, seen in Figure 5.4 and Figure 5.5, correspondingly.

Once the phases present were identified, whole pattern powder fitting was conducted to determine the weight composition of each waste form. The refined weight fractions of identified phases found within the FAp-1 through FAp-4 surrogate waste forms are displayed in Figure 5.6. From

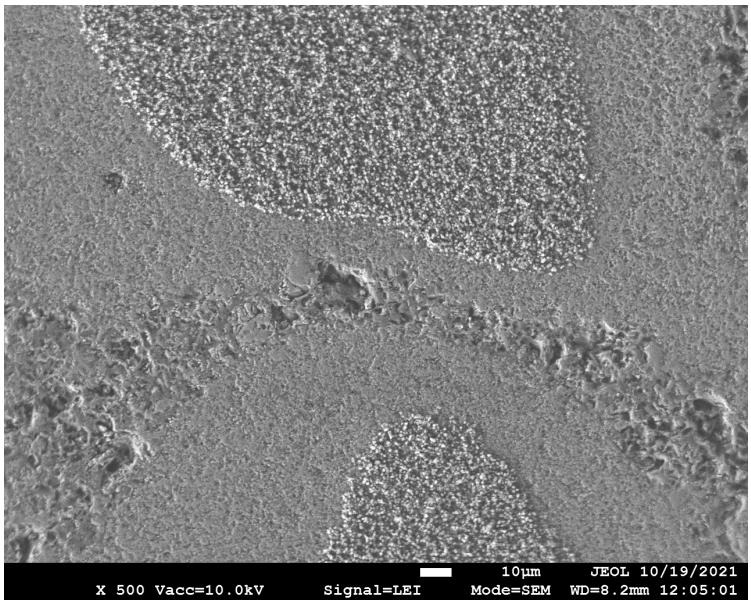

Figure 5.2: Two regions of fluorite surrounded by the calcium phosphate with the final region fluorapatite separating the two.

the image it is observed that as ball-milling, sintering time, or temperature increased fluorapatite content increased. With an increase in temperature from FAp-1 to FAp-2 beryllium appeared to mobilize creating Be rich regions, hurlbutite. Finally, in FAp-4 it was observed that a decrease of the fluorapatite and increases in fluorite and calcium phosphate phases, however no precursor (TCP) material was left, showing there may be a maximum loading of FLiBe salt to optimize fluorapatite or sintering time may need to be adjusted.

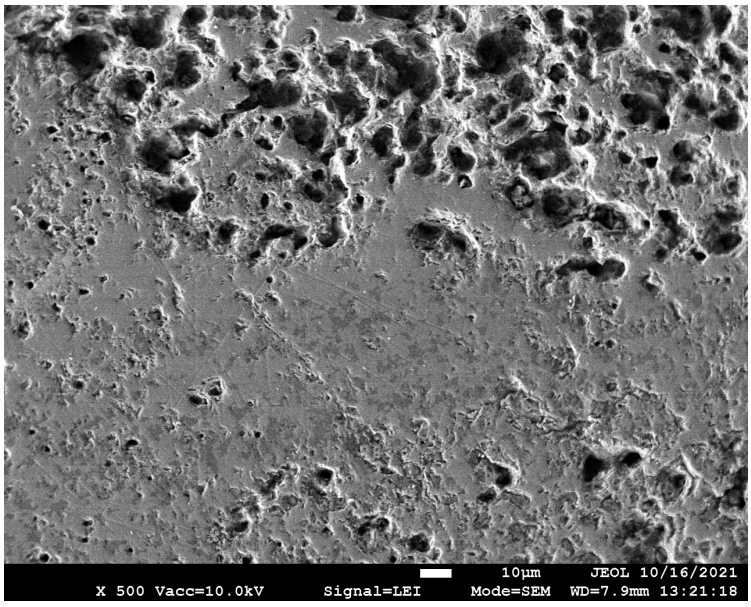

Figure 5.3: A region of FAp-2 showing two phases present in the bulk material, the smaller dark inclusions show where less calcium was found during EDS.

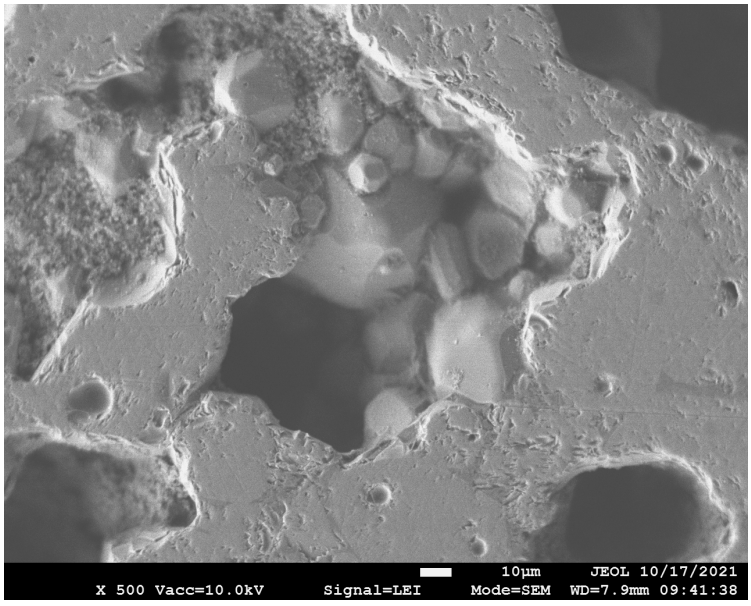

Figure 5.4: The fluorapatite region (light) and phosphate region (dark) found in FAp-4.

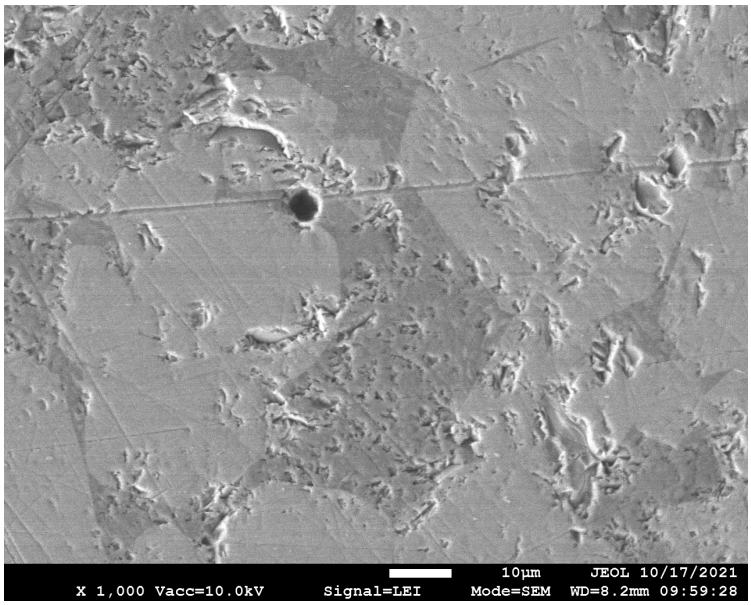

Figure 5.5: Crystals of fluorapatite found in the open pores FAp-4.

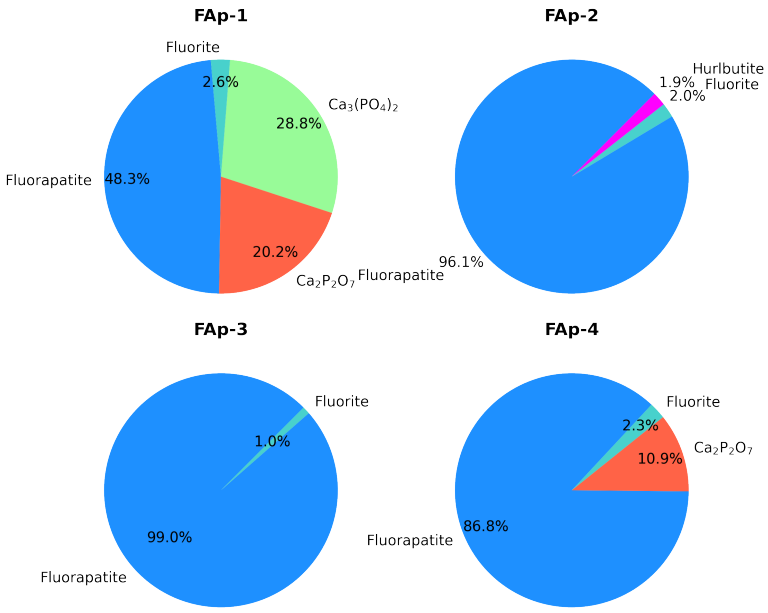

Figure 5.6: Weight percent of FAp-1 through FAp-4 compositions.

5.1.2 Uranium Fluorapatites

Three uranium fluoride doped surrogate waste forms were produced U-FAp-1 through U-FAp-3. These followed the same production conditions as FAp-1 through FAp-3, respectively. First EDS of the U-FAp surrogate waste forms found that a majority of the material contained calcium, phosphorous, oxygen, and uranium. However, fluorine was less densely located throughout the material and regions of a high concentrations of uranium were found. Subsequently, XRD found two major regions in U-FAp-1 of uranium substituted fluorapatite and TCP, with a final minor phase of a uranium oxide. A uranium oxide deposit is shown in Figure 5.7.

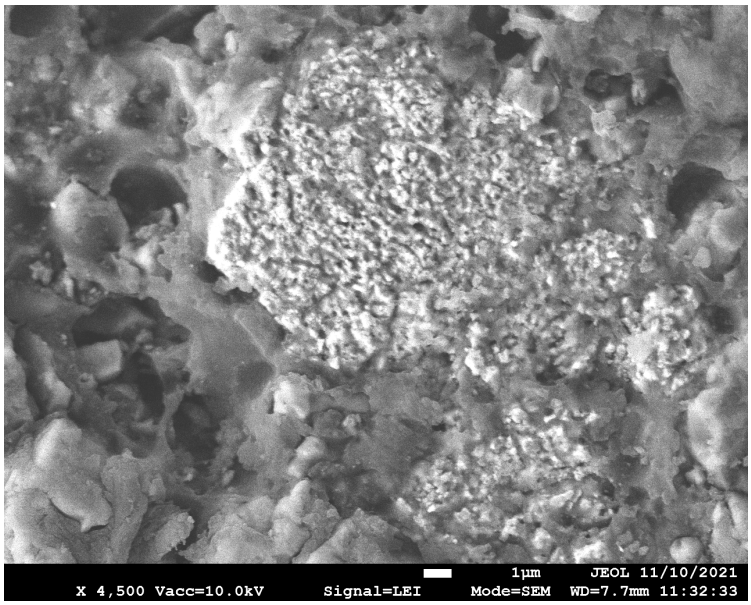

Figure 5.7: A phase of high concentrations of uranium found in U-FAp waste forms.

Further U-FAp-2 found that the uranium fluorapatite content increased with decreases in the TCP phase, however the fluorite phase re-appeared in the SEM-EDS mapping. Figure 5.8 shows a region of fluorapatite and TCP. In the final uranium surrogate waste form, U-FAp-3, the fluorapatite phase decreased, having the lowest concentration of the three uranium waste forms. This coincided with the creation a third major phase of dicalcium diphosphate, and an increase of the fluorite phase. The weight composition of all three U-FAp surrogate waste forms can be found in Figure 5.9. While the refined XRD weight percentages are found in Figure 5.9 for U-FAp-1 through U-FAp-3.

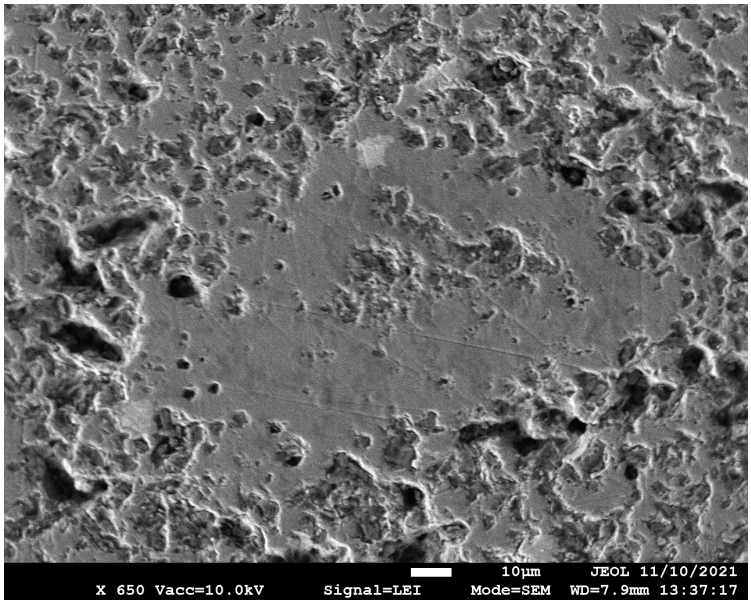

Figure 5.8: Sample of U-FAp-2 displaying the two phases fluorapatite (lighter) and the TCP phase (darker).

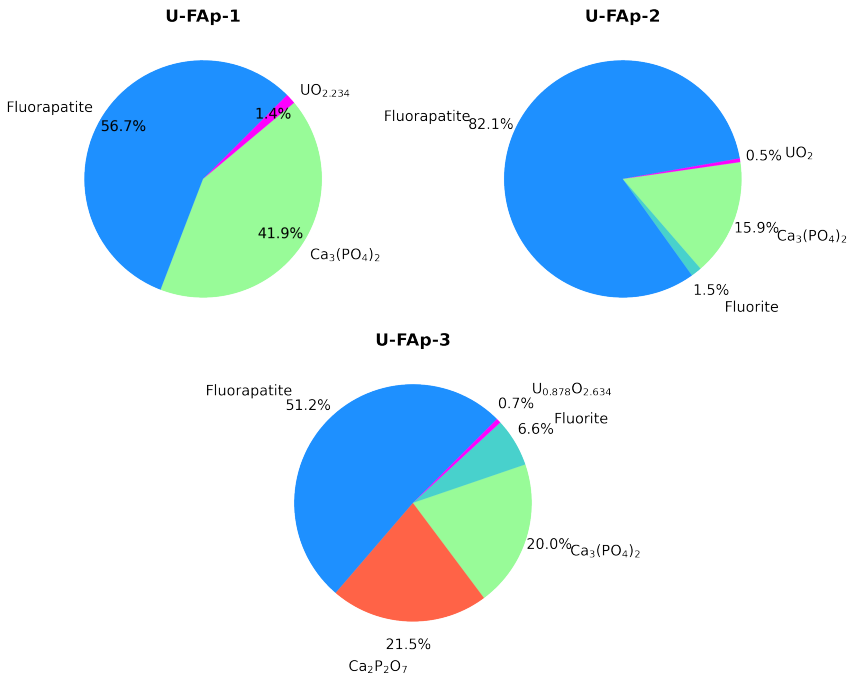

Figure 5.9: Weight percent of U-FAp1 through U-FAp-4 compositions.

5.1.3 Fission Product Fluorapatite

Fission product doped surrogate waste forms, X-FAp, were synthesized under the same conditions as FAp-3 and U-FAp-3 with 10-hours of ball-milling and sintering at 700°C. The first of these is Cs-FAp, SEM identified the most of the material contained cesium, calcium, oxygen, fluorine, and phosphorus. Two small phases identified calcium and fluorine rich regions, and one instance of high concentration of cesium and oxygen. The XRD identified that the major phase was a cesium doped fluorapatite with minor phases of fluorite, seen in Figure 5.10 and TCP. The XRD data could not identify the cesium oxide phase, but again only one instance was found through out all Cs bearing samples in the SEM-EDS analysis.

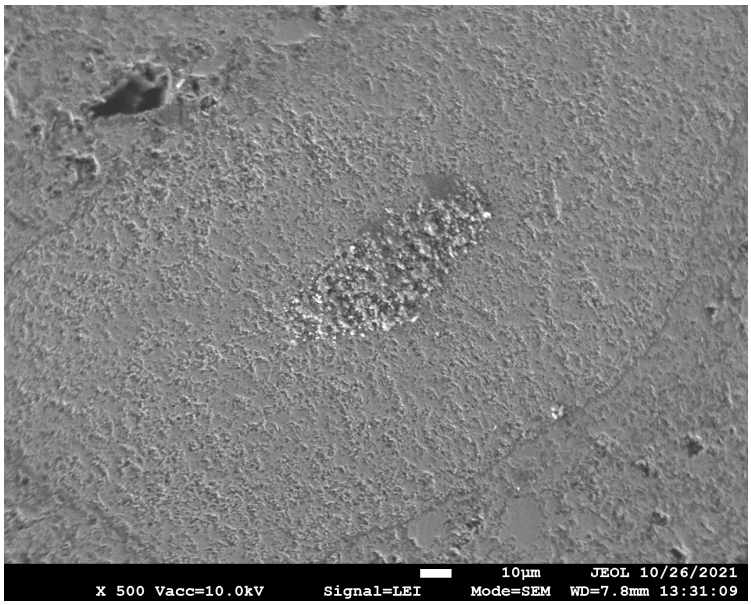

Figure 5.10: Fluorite region found in the Cs-FAp surrogate waste form surrounded by Cs-fluorapatite with a Cs-fluorapatite center.

For the strontium loaded surrogate waste form SEM-EDS confirmed the presennce of strountium through out the sample. Calcium, oxygen, fluorine, and phosphorus were found throughout the samples. With addiotional zones that contained calcium and fluorine rich ares and phosporous and oxgyen defficient area. XRD identified fluorostrophite, a strontium substituted fluorapatite,

and fluorapatite. With minor phases of fluorite and dicalcium phosphate. The fluorostrophite could not accurately describe the major peaks that are associated with fluorapatite, during refinement additional strontium sites were added to the fluorapatite.

Gadolinium fluoride was the final surrogate fission product tested EDS and SEM found one major phase consisting of gadolinium, oxygen, fluorine. and phosphorus. With minor regions with low concentrations of oxygen and phosporus and an increasein fluorine and clacium. XRD identified substituted fluorapatite with minor phases of fluorite and dicalcium phosphate.

Two additional surrogate waste forms were synthesized. the first contained equal mol% of Cs and Gd. Analysis showed that only Cs-Gd substituted fluorapatite and TCP were synthesized. The final surrogate watse form contained equal amounts of all dopants (Cs, Sr, Gd, and U). The EDS and XRD analysis identified a major phase of fluorapatite substituted with all four dopants. With minor phases of TCP, fluorite, and uranium oxide. In the EDS mapping, the high concentration uranium sites also contained an increase in cesium and was reflected in the refinement. Mapping also identified one small inclusion of a gadolinium rich region however XRD could not describe the phase. The refined weight percentages for X-FAp surrogate waste forms are found in Figure 5.11.

While beryllium is a major component in the FLiBe salt and consequently the surrogate waste form neither the XRD nor the SEM-EDS could accurately quantify the beryllium, with exception of FAp-2 were beryllium in sufficient amounts allowed for the detection of Be in a hurlbutite phase via the XRD. A small peak at 29.5-2θ is observed in most samples, which may be attibuted to the presence of Be in the fluorapatite or part of a hurlbutite phase that is not being observed appropriately. At this angle, hurlbutite contains a peak at this location, however even in the refinement of FAp-2 the peak was not fully resolved.

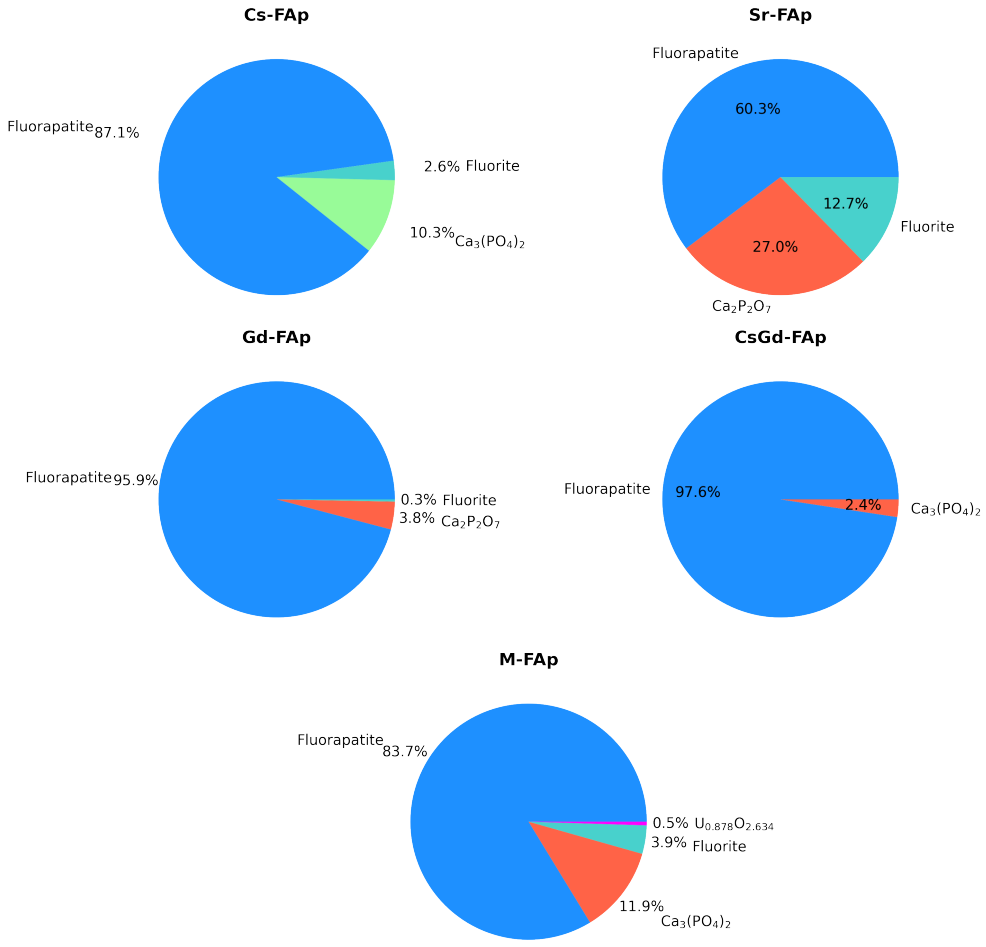

Figure 5.11: Compositional weight percent of fission product doped surrogate waste forms.

5.2 Normalized Leaching Behavior

Normalized leach rates NC_i, subsection 5.3.1, and NC_i, subsection 5.3.2, were tabulated from equations 3.9 and 3.12, respectively, from the ICP-MS data found in Section 4.5.2 and the free fluorine data found in Section 4.4. A comparison of the calculated leach rates for the flourapatites are then compared to published data from other waste forms in subsection 5.3.3.

From the ICP-MS leachate data, it is apparent that the samples contained contaminants of the other various fission products used in the study. However, to determine the normalized leach rates a starting known mass in the sample is required. The cross contamination is most likely due to in adaquate cleaning standards and procedures, most likely with the sieve used to separate the mixed powders from the milling media after ball milling inside the glove box. Thus, since no original value exists for the contaminants normalized leach rates were not tabulated for them. Further the EDS and XRD analysis did not identify these contaminants in the sample, signaling that the contamination amount is low.

Densities were obtained for the calculation of NL_i. Comparing the density values and methods employed to obtain the information in Section 4.3, pycnometer densities were used in determining the normalized elemental mass loss rates. The geometric densities, while great for initial density values, have various sources of error and is due to many factors: first is the slight dimensional changes because of the porosity of the surfaces of the sample, which cannot be accurately captured using this method. Second is issues associate with a more global aspect of the pellet being measured and slight dimensional differences from one side of a pellet compared to the same measurement at different points. Finally, is the errors associate to use of the calipers inside the glove box, which made working with them difficult. The calipers captured particles on the tips of the caliper testing surface interface introducing additional measurement errors. It is believed to be because of electrostatic forces inside the particular glove box because of the excessive salts present. In all, due to these issues it is shown that the average densities from one apatite to another are quiet variable. Where as the pycnometer densities, because of the method, ignores geometry wihtin its measurement and attained a more stable average density.

Normalized Concentration (NC_i)

The first normalized leaching figure of interest is the normalized concentration NC_i), which determines the total mass fraction of an element *i* in the waste form that has dissolved into the solution. Normalized concentration data can be found below in Figures 5.12 through Figure 5.18 for the beryllium, calcium, fluorine, cesium, strontium, gadolinium, and uranium found in each vessel for each PCT. Figures 5.19 through 5.20 condense the presented data from Figures 5.12 through 5.18 into average NC_i for each fluorapatite waste form.

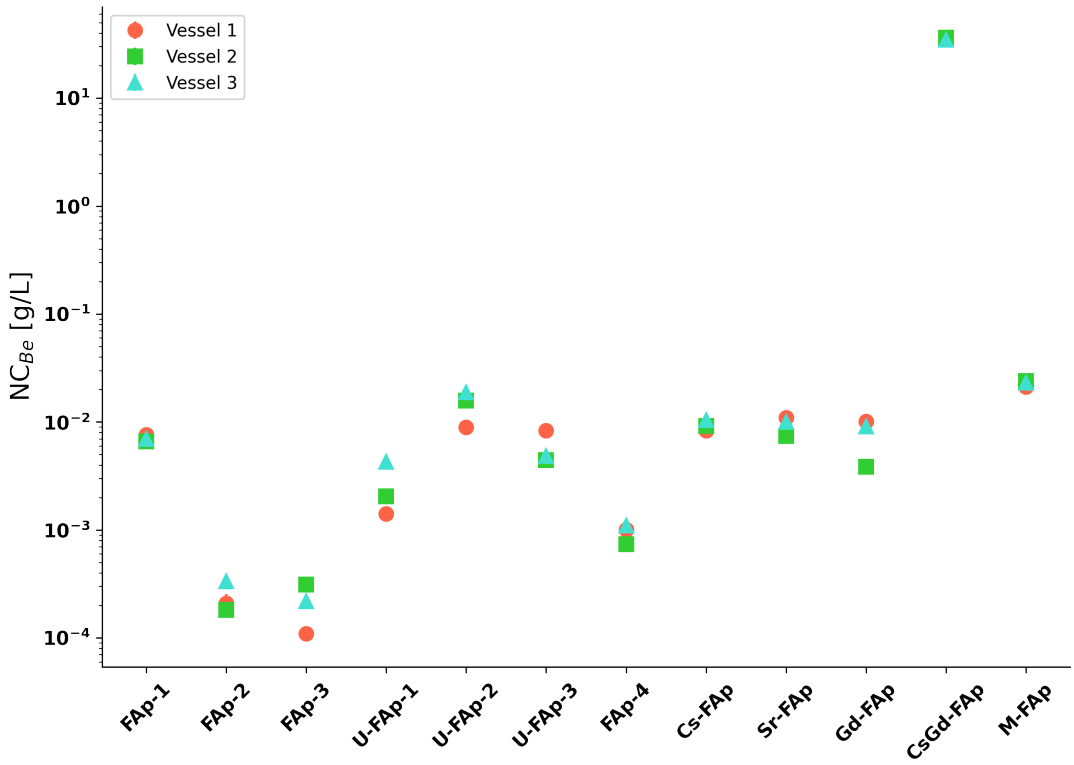

Figure 5.12: The normalized concentration of beryllium found in the surrogate waste form leachate, NC_{Be}.

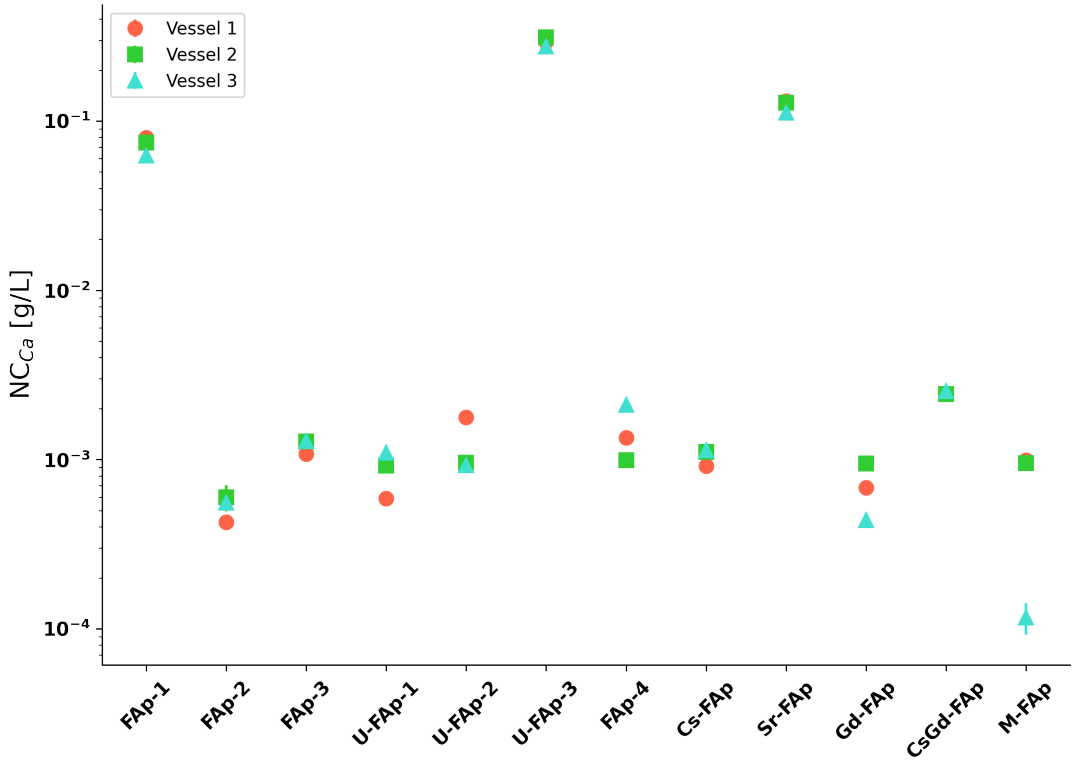

Figure 5.13: The normalized concentration of calcium found in the surrogate waste form leachate, NC_{Ca}.

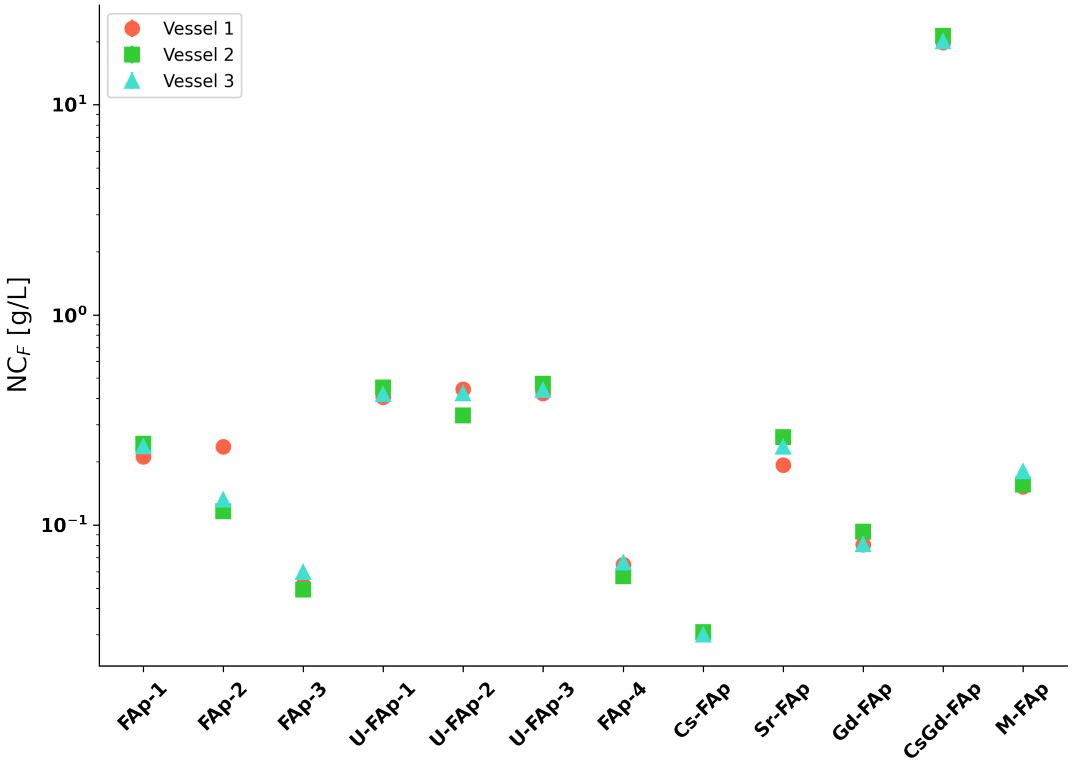

Figure 5.14: The normalized concentration of fluorine found in the leachate, NC_F.

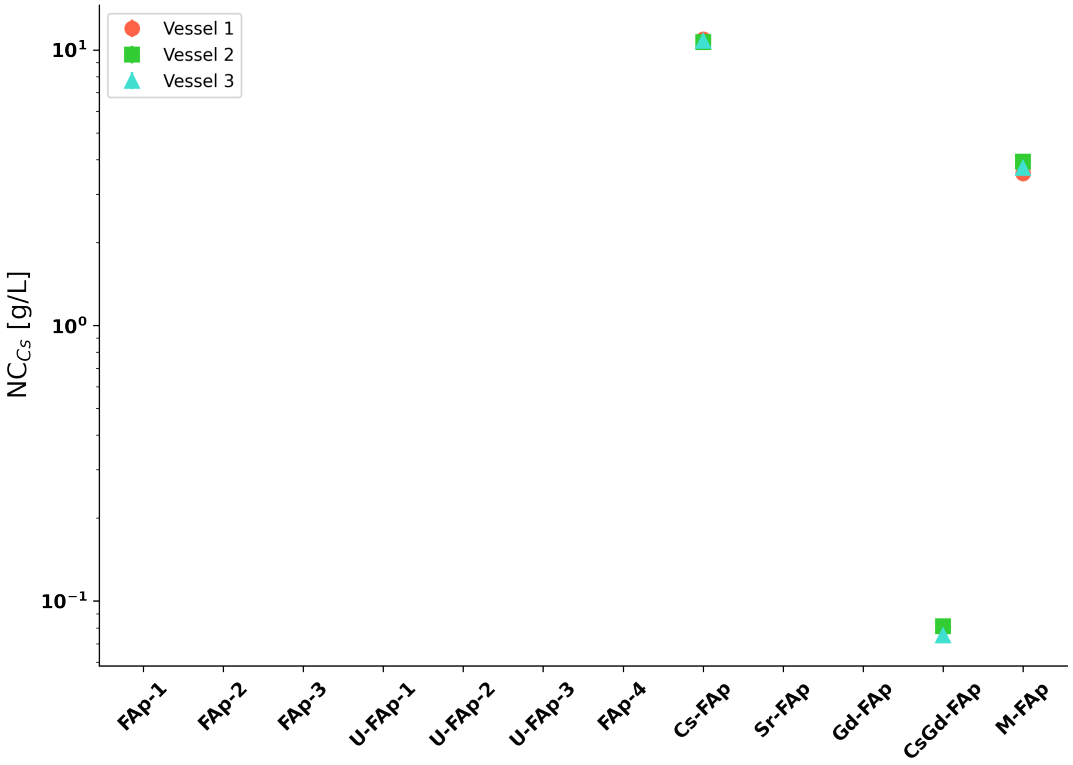

Figure 5.15: The normalized concentration of cesium found in the leachate after the PCT, NC_{Cs}.

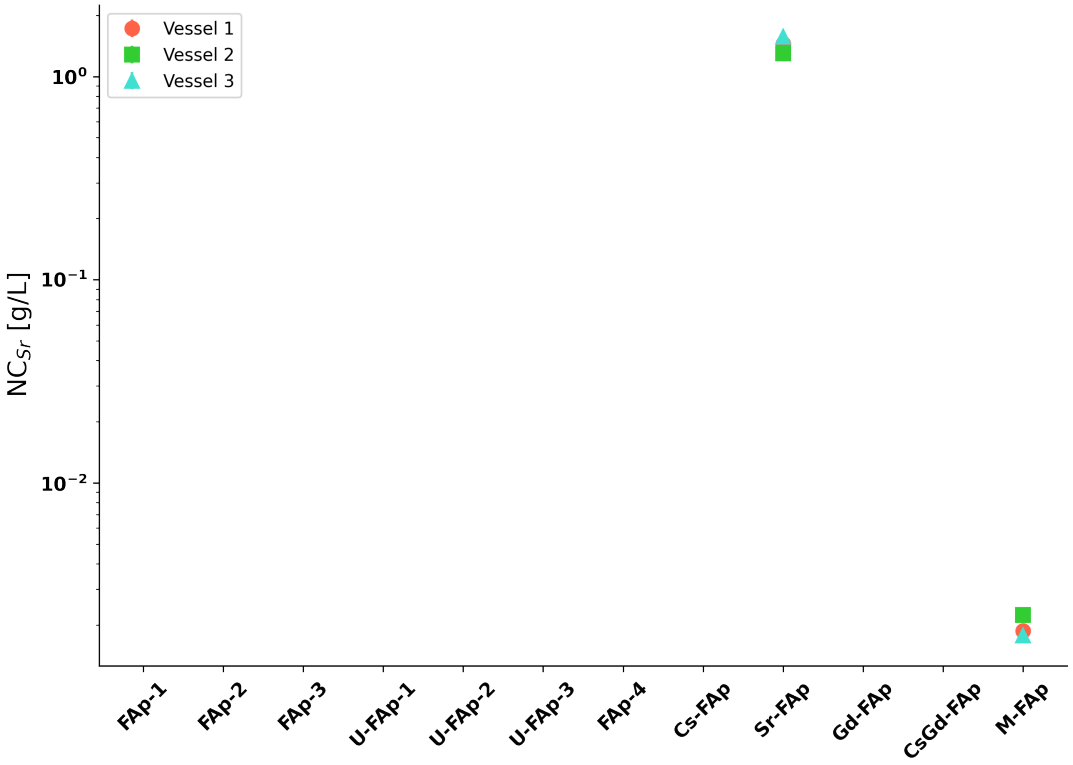

Figure 5.16: The normalized concentration of strontium found in the waste leachate, NC_{Sr}.

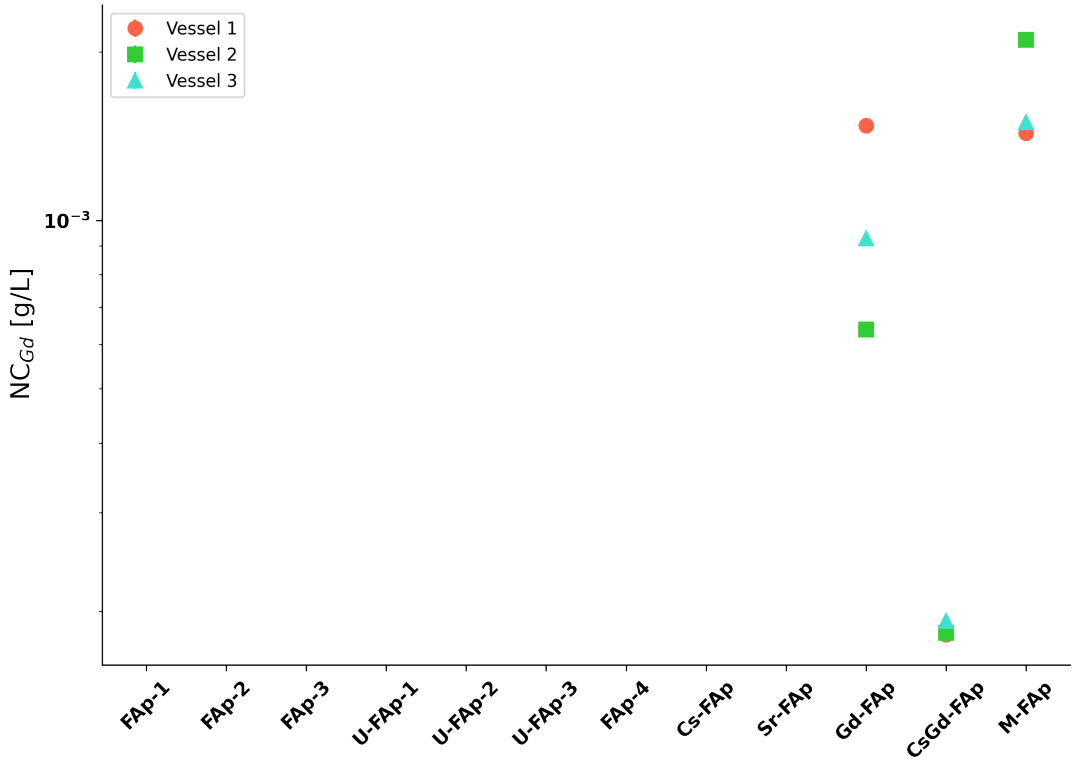

Figure 5.17: The normalized concentration of gadolinium found in the surrogate waste form leachate, NC_{Gd}.

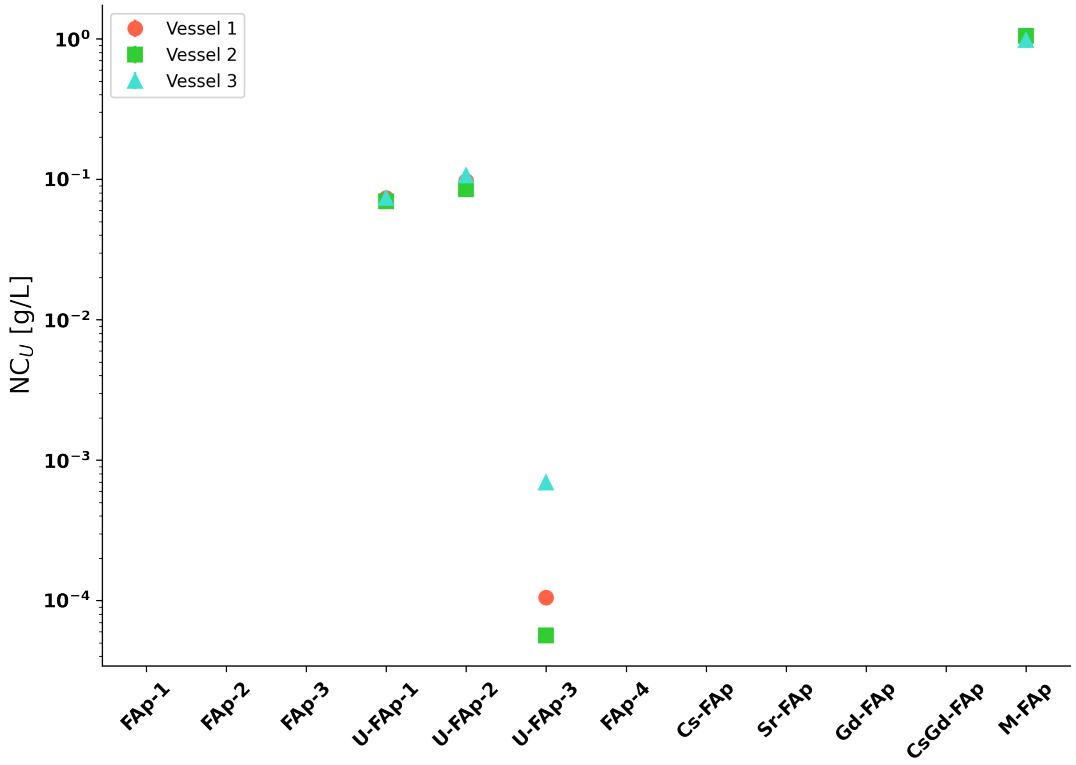

Figure 5.18: The normalized concentration of uranium found in the leachate post PCT, NC_U.

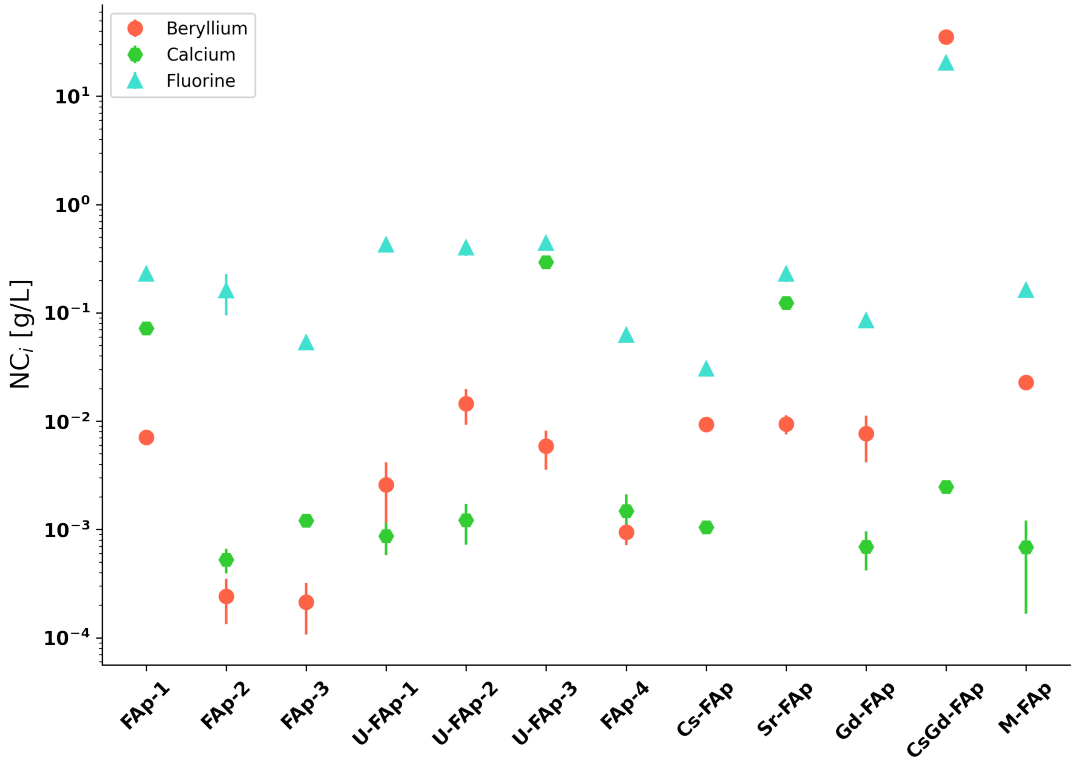

Figure 5.19: The average NC_i over the three vessels for each surrogate waste form for beryllium, calcium, and fluorine.

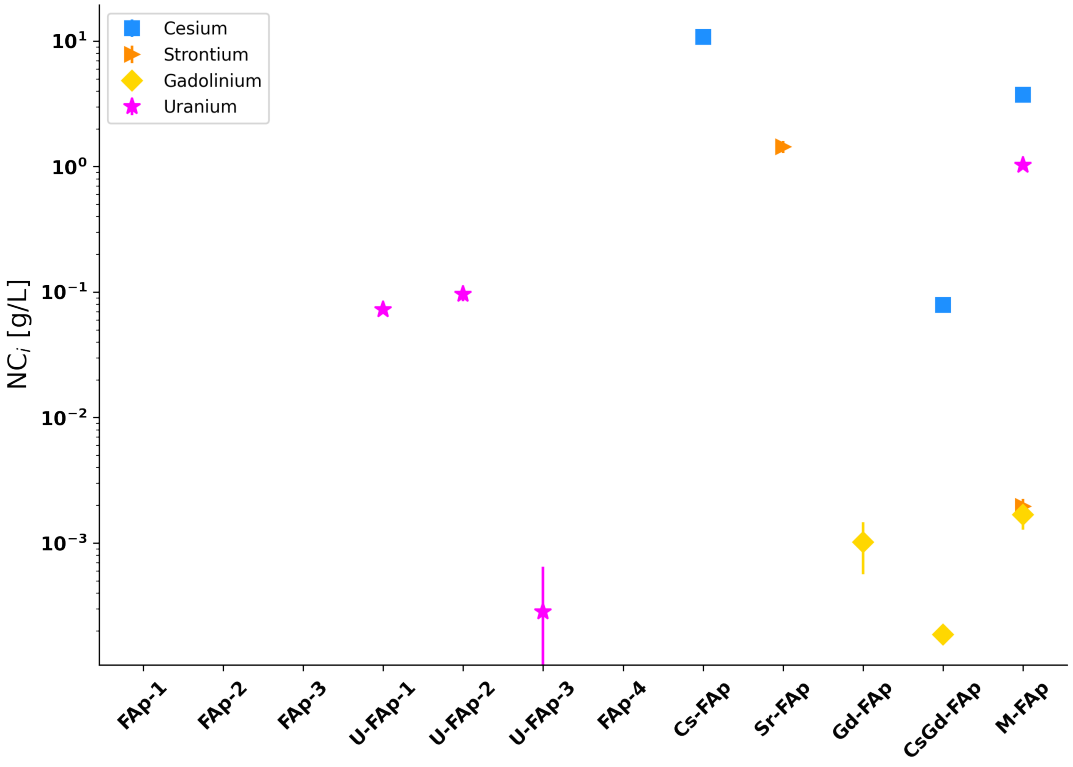

Figure 5.20: The average NC_i over the three vessels for each surrogate waste form for cesium, strontium, gadolinium, and uranium.

Normalized Elemental Mass Loss (NL_i)

The second normalized leaching figure of merit is the normalized elemental mass loss, which determines the total mass of element *i* dissolved into the leachant during the test duration. Normalized mass loss data can be found below in Figures 5.21 through Figure 5.27 display the beryllium, calcium, fluorine, cesium, strontium, gadolinium, and uranium found in each vessel for each PCT. Figures 5.28 and 5.29 condense the presented data from Figures 5.22 through 5.28 into average NL_i for each fluorapatite.

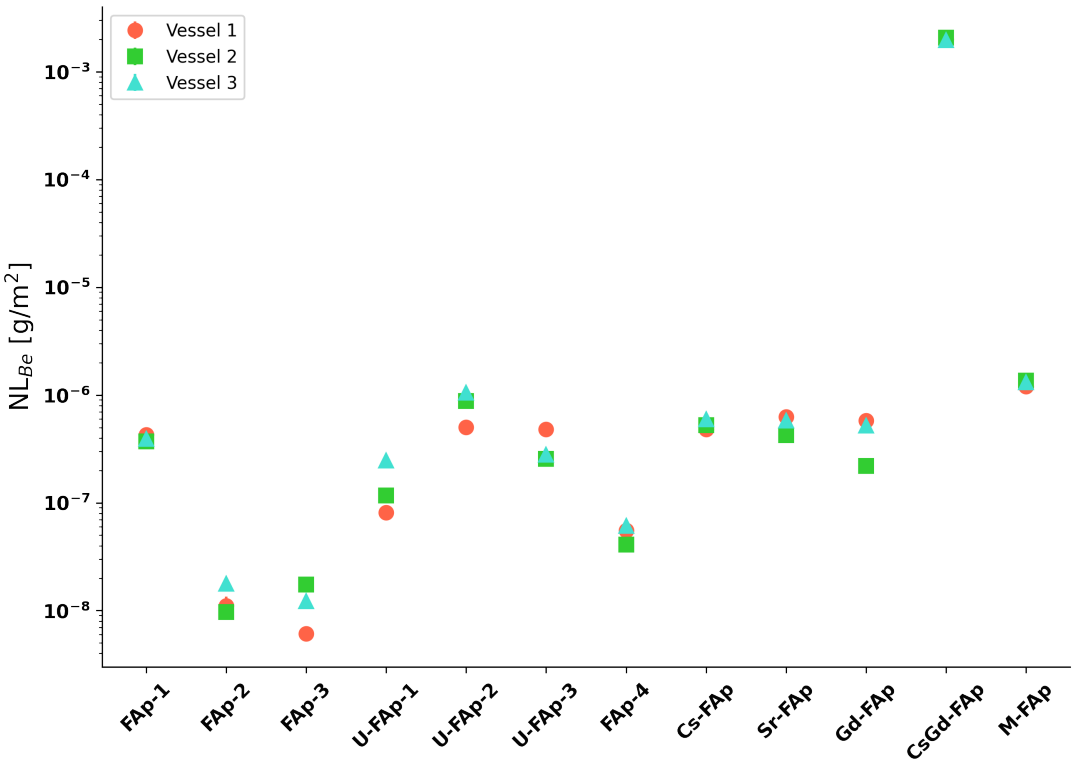

Figure 5.21: The normalized concentration of beryllium found in the surrogate waste form leachate, NL_{Be}.

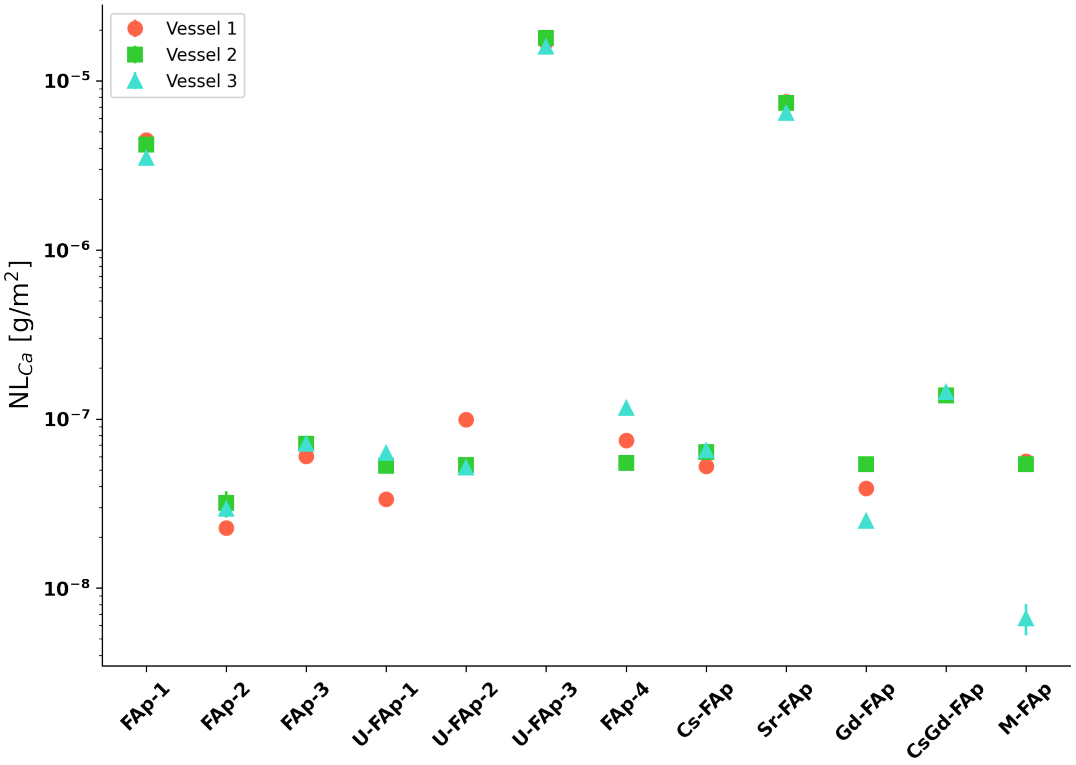

Figure 5.22: The normalized concentration of calcium found in the waste leachate, NL_{Ca}.

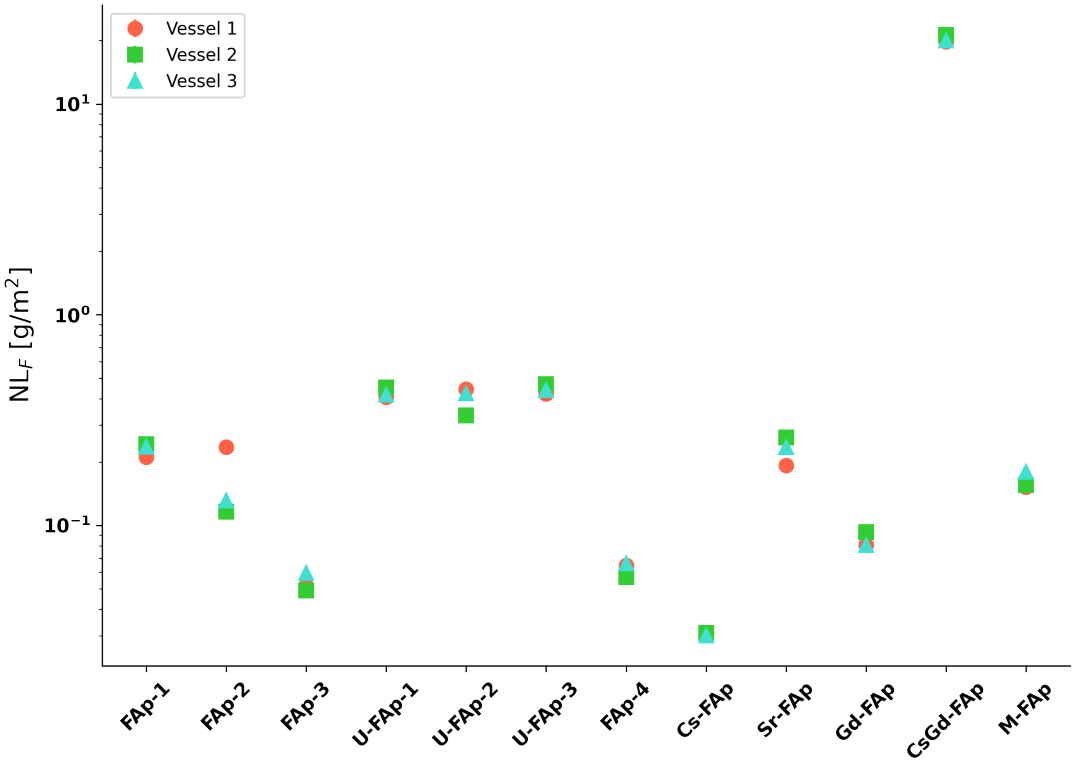

Figure 5.23: The normalized concentration of fluorine found in the leachate post PCT, NL_F.

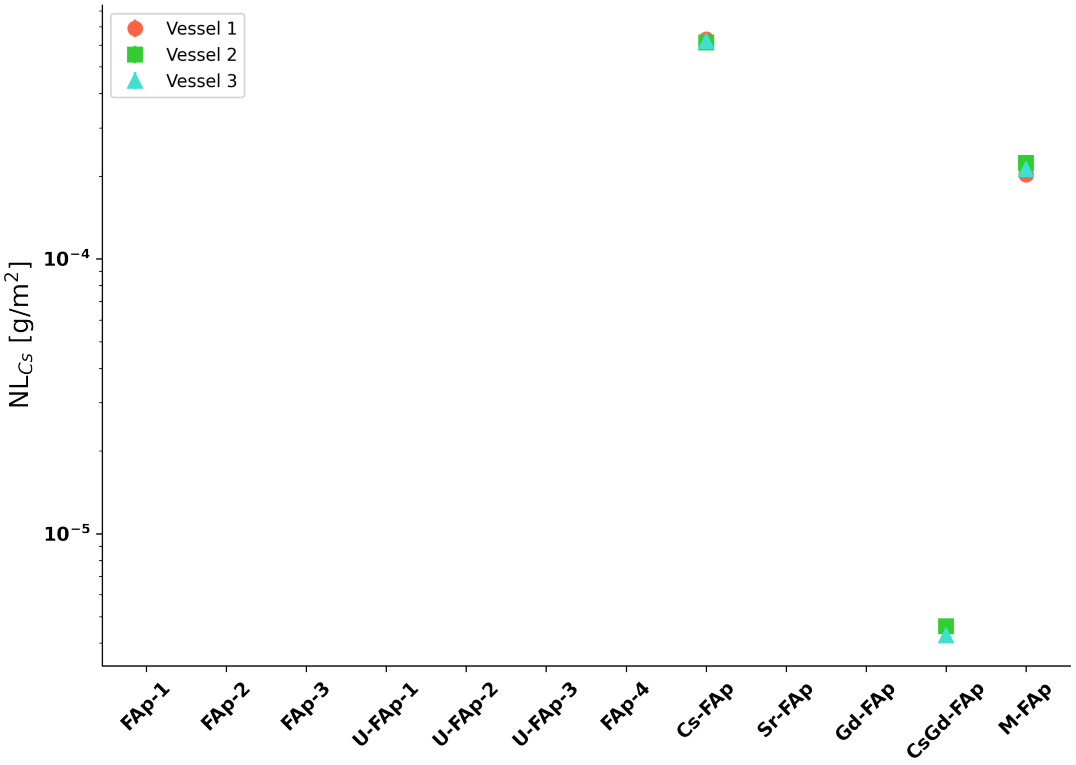

Figure 5.24: The normalized concentration of cesium found in the waste leachate after PCT, NL_{Cs}.

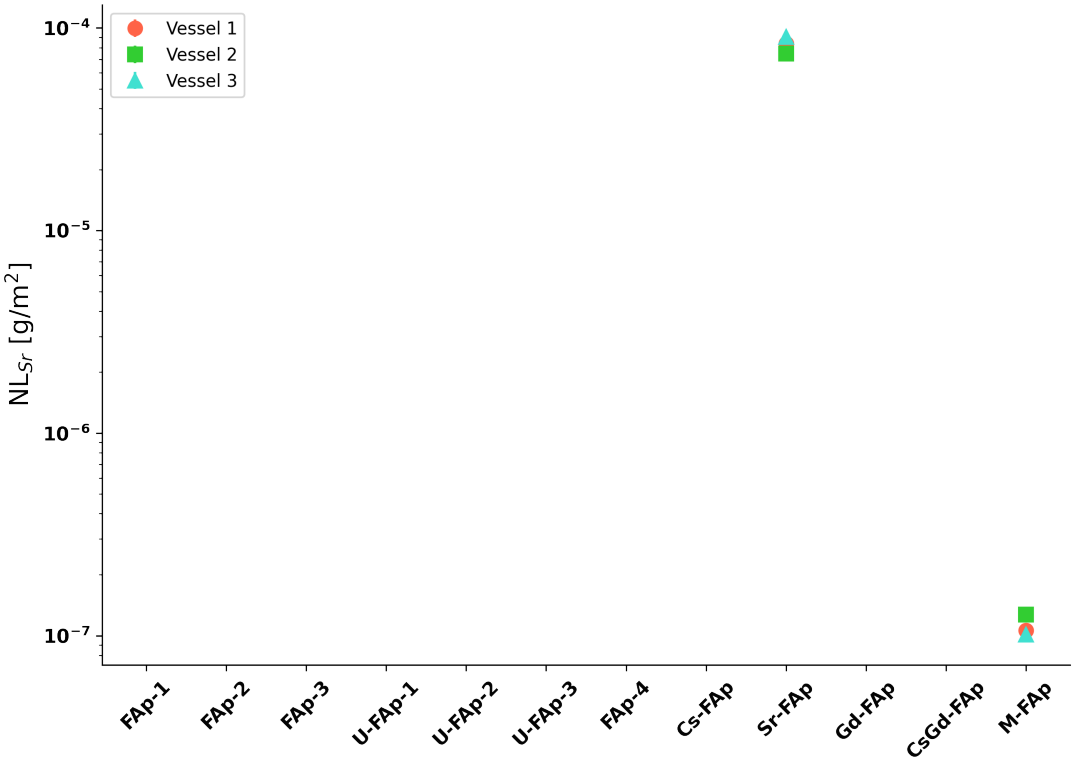

Figure 5.25: The normalized concentration of strontium found in the surrogate waste form leachate, NL_{Sr}.

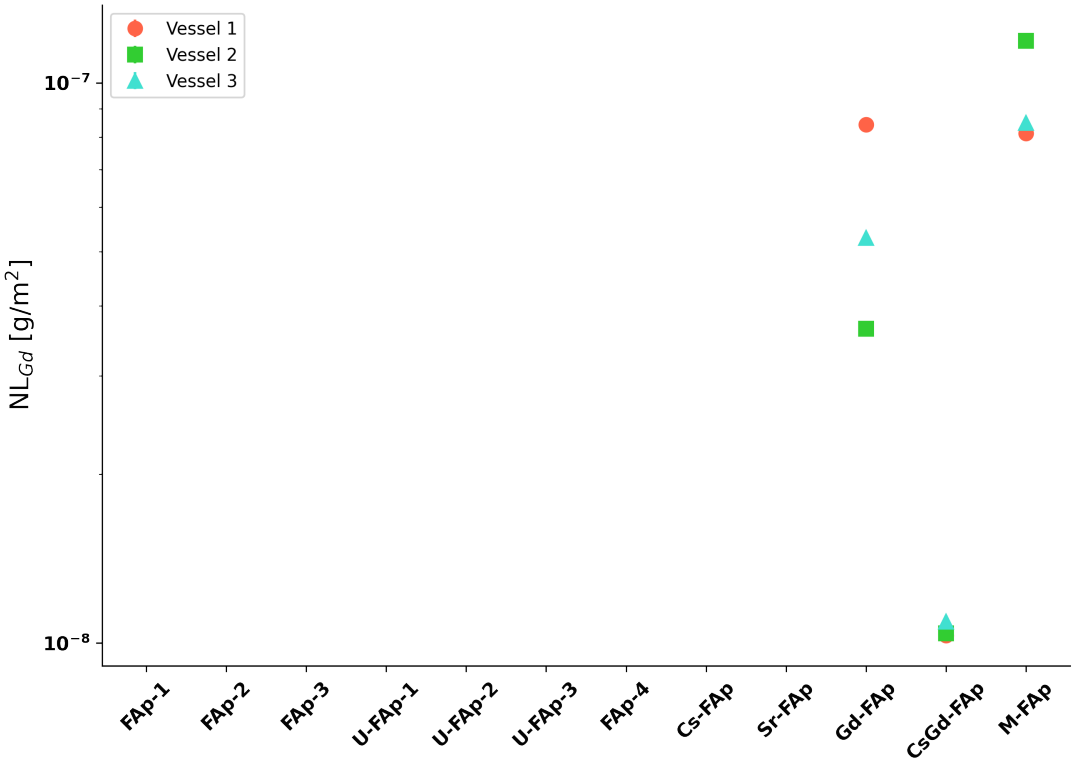

Figure 5.26: The normalized concentration of gadolinium found in the waste leachate, NL_{Gd}.

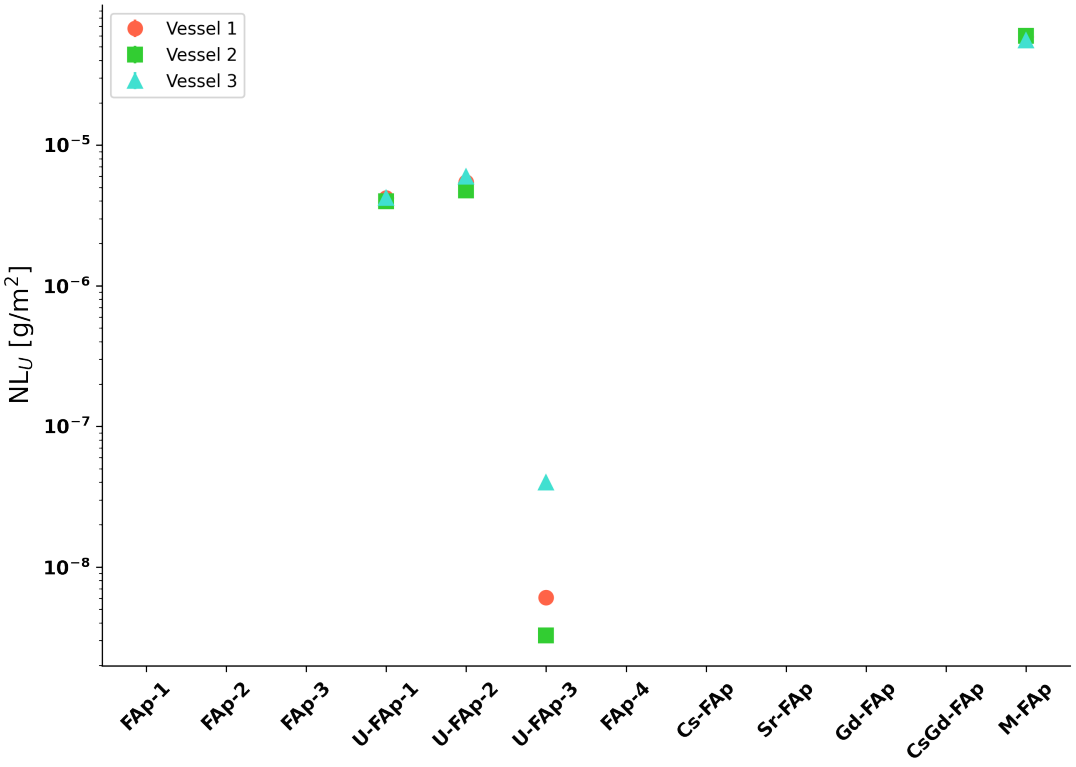

Figure 5.27: The normalized concentration of uranium found in the waste leachate, NL_U.

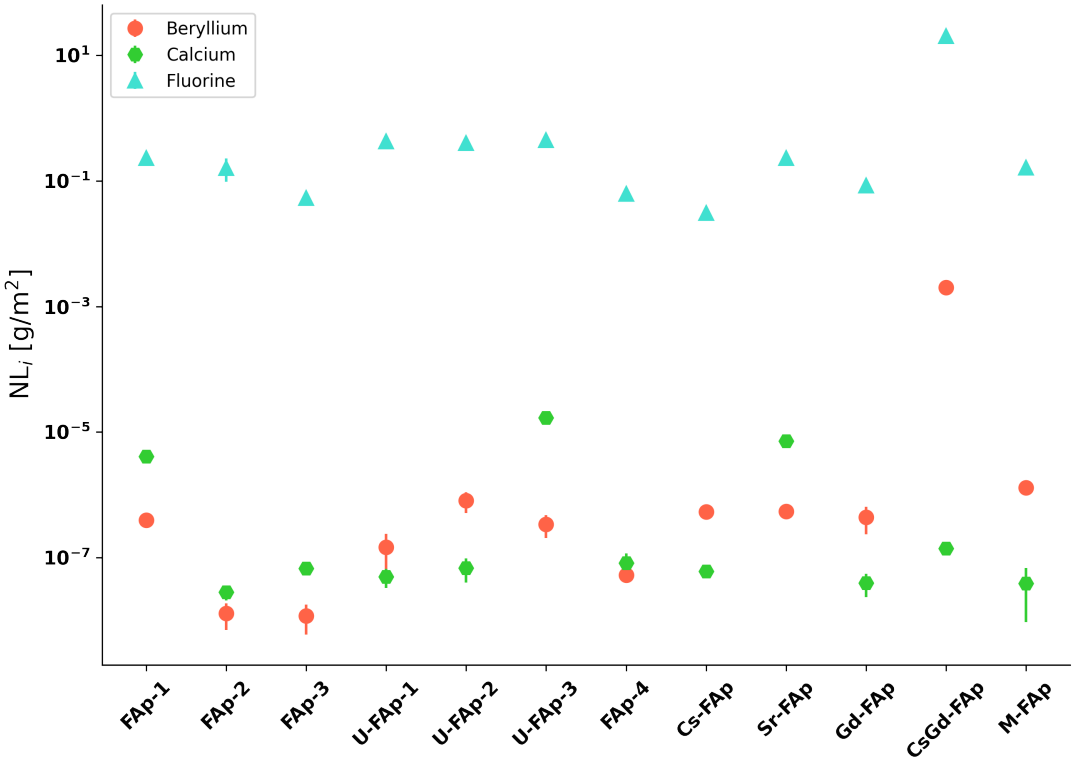

Figure 5.28: The average NL_i over the three vessels for each surrogate waste form for beryllium, calcium, and fluorine.

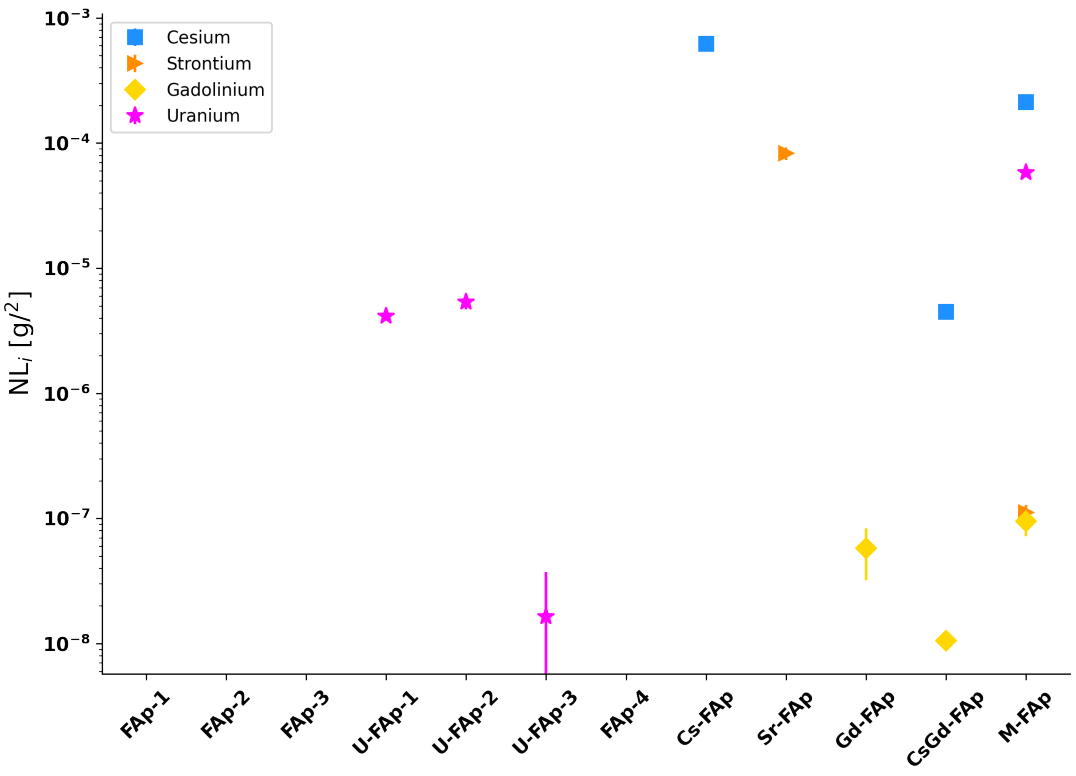

Figure 5.29: The average NL_i over the three vessels for each surrogate waste form for cesium, strontium, gadolinium, and uranium.

Observations of the above data show that the ability for the surrogate waste form to retain the common elements (Be, Ca, F) varies with sintering conditions and dopant. In FAp-1 through FAp-3 beryllium and fluorine release decreased with increasing temperature and time with FAp-3 having the lowest release of Be and F. Calcium decreased in both FAp-2 and FAp-3 however release was slightly higher in FAp-3. For FAp-4, which had a higher loading of FLiBe salt, the values increased for all three elements compare to FAp-3.

The uranium substitute surrogate waste forms however, showed a different trend. For beryllium, the release increased from U-FAp-1 to U-FAp-2 and decreased slightly for U-FAp-3. While calcium increased from U-FAp-1 through U-FAp-3. While fluorine was stable over all three uranium waste forms. For the remaining surrogate waste forms, all three elements were comparable to U-FAp-2, except for the CsGd, which displayed leach rates for Be and F two orders of magnitude greater than the other waste samples.

Cesium was present in three waste forms: Cs-FAp, CsGd-FAp, and M-FAp. The highest normalized concentration was found in the Cs-FAp and decreased for the other two. Strontium was found in Sr-FAp and M-FAp with a large decrease, approximately 2 orders of magnitude in the M-FAp sample. Uranium, found in U-FAp 1 through U-FAp-3 and M-FAp found the least release in U-FAp-2 and the highest concentration in M-FAp. Gadolinium found in Gd-FAp, CsGd-FAp, and M-FAp had low levels released across all waste forms and the lowest in the CsGd-FAp.

Comparison of Normalized Leachrates to Available Data

To begin comparisons, FLiBe salt was also subject to a PCT to obtain a baseline leaching rate and compared to the fluorapatite, dhoen Figure 5.32. Here, eith the exception of CsGd-FAp, the apatite surrogate waste forms outperformed the FLiBe salt. The beryllium content was not obtained for FLiBe PCT.

Further investigation compared the NC_i and NL_i of the fluorapatite surrogate waste forms to other published waste form data to understand the efficacy of the fluorapatite waste. Frequently, major structural components are investigated during leach testing. One such study looked at sodium, lithium, boron, etc. of the glass waste forms. In the fluorapatite however the major

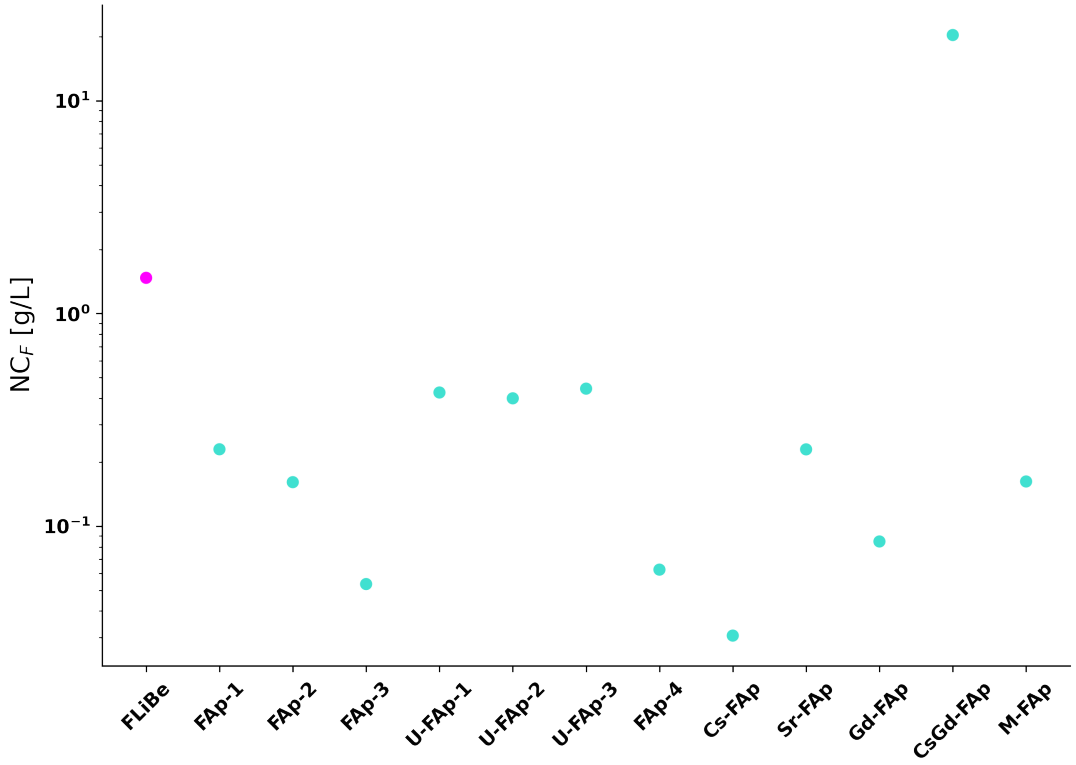

Figure 5.30: The average NC_F, including FLiBe (magenta).

structural components are all the components Li, Be, F, and fission products as they ideally should substitute into the fluorapatite structure.

In one study, by Bibler and Janzen determined the NC_i for a glass waste form in the interest if determining the role of the PCT in waste selection [45]. In another investigation by Fox et al., determined the structural component leach rate for a range of glass waste forms [46]. The data for these two studies is compared to the data collected in this study in Figure 5.33. The data points selected for display from this study show that the minimum leaching rates are 1 to 2 orders of magnitude less than Bobler or Fox, and that the upper bounds of the leach rates with the exception of Be are comparable to sodalite and glass waste forms.

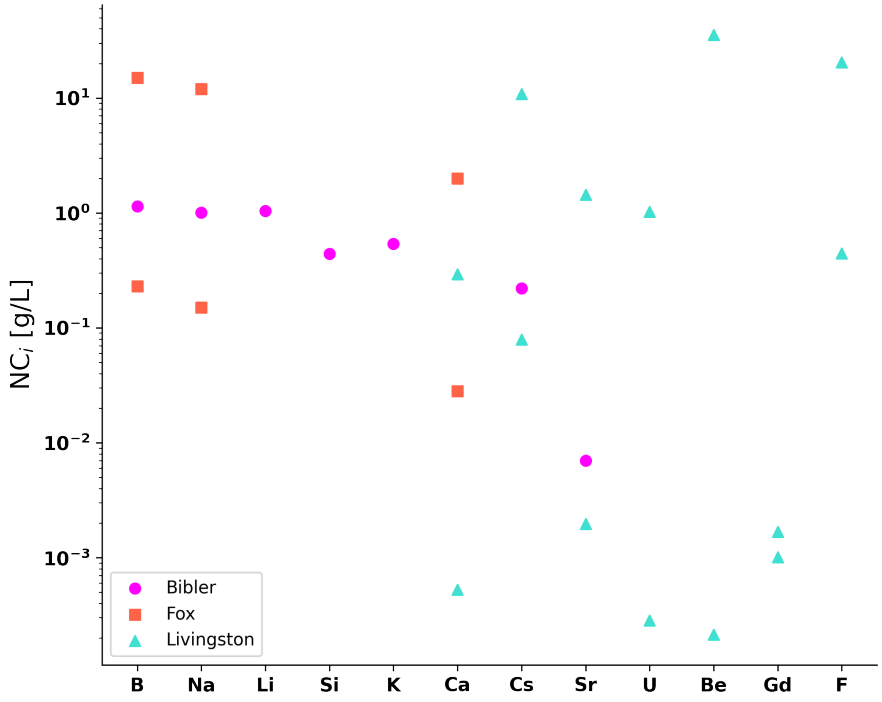

Figure 5.31: The average NC_i found in Bibler, the upper and lower limits determined by Fox, and the maximum and minimum observed rates obtained for fluorapatite surrogate waste forms.

While a third study, by Morss, found the leaching behavior of U in sodalite waste form [47]. The Morss data can be seen in Figure 5.34 and directly compared to the behavior of the fluorapatite surrogate waste forms. Here, it is seen that the uranium leaching is considerably lower in the apatites created in this study.

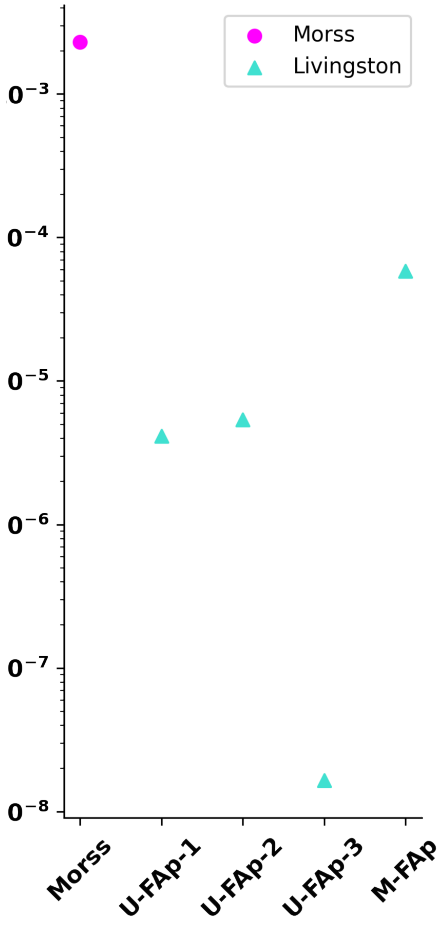

Figure 5.32: The NL_U found in the apatite surrogate waste forms compared to the Morss data (magenta).

5.3 Conclusion & Future Work

The leaching behavior of fission product and fuel incorporated fluorapatite minerals was investigated as a potential waste form for molten salt reactors. The surrogate waste forms were subjected to leach testing to determine the effectiveness of the apatites to retain the fission products, spent fuel, and structural components. Additionally, the surrogate waste forms were chracterized using SEM-EDS, XRD, and various density measurement techniques.

Basic fluorapatite surrogate waste forms were fabricated of 66.89-mol% tricalcium phosphate and 33.11-mol% FLiBe salt at varying sintering temperatures and duration. The FLiBe salt was composed of 66.4-mol% lithium fluoride and 33.4-mol% beryllium fluoride. Additional surrogate waste form pellets consisting of surrogate fuel and fission products were produced in the same manner in a ratio of 95-mol% tricalcium phosphate and 5-mol% FLiBe salt. Where the FliBe salt was mixed with the surrogate fission products at a 95-mol% FLiBe salt 5-mol% fluoride compound or compounds. A final pellet consisting of 48.9-mol% tricalcium phosphate and 51.1-mol% FLiBe salt was also created to identify if the fluorapatite could contain an additional loading of salt.

To understand the microstructures and phases developed during sintering SEM-EDS and powder XRD were conducted on the surrogate waste forms. The largest structural components within the waste forms were identified to be forms of substituted fluorapatites. Other phases were identified as calcium triphosphate, dicalcium diphosphate, fluorite, hurlbutite, and various metal oxides.

To determine leaching behavior the surrogate waste forms they were processed according to testing method B of the ASTM's C1285 standard "Standard Test Methods for Determining Chemical Durability of Nuclear, Hazardous, and Mixed Glasses and Multiphase Glass Ceramics: The Product Consistency Test (PCT)". Results showed that the apatites retained the fluorine better than FLiBe with the exception of the CsGd substituted fluorapatite. Comparison of the normalized leaching behaviors to published data avialable showed that the surrogate waste forms in most cases out perform glass and sodalite waste forms that were identified. Resulting in a waste form that maybe proved a direct method of waste neutralization for the soluble components of thermal molten salt reactors and the carrier salt.

This work did not investigate leachant wall interatcions, further work should identify if the vessel walls are contributing to an accelerated leaching of the cations. Additional future work related to fluorapatite waste forms should look into the leaching behavior of wet synthesized apatites. It may be that access to phosphates are a limiting factor in the uptake of the waste components into the crystal structure, thus it may be of interest to look at phosphate donors that the cation will completely volatilize out of the sample during synthesis. Their is also a lack of known crystal information for the substitutate fluorapatites that would be synthesiszed, further XRD investigation is need to completley characterize the apatites and produce CIF files for the substituted apatites. Moving on to monolith testing would be the next step for leaching behavior and idenitfy its assovaited leaching characteristings which will differ due to the lower surface area interation of a monolith. Finally, this study did not account for radiolysis effects that may induce changes in the cyrstal structure of the minerals. While the work completed on the natural apatites found at the Oklo-Gibbon site suggests fluorapatites are radiolysis resistance verification and study on synthesized waste should be investigated. Thus to summarize future work should investigate:

- Investigate the leaching behavior of the leachant and vessel wall interations to idenitfy possbile accelerated leaching pathways
- Investigation leaching behavior of west synthesized fluorapatites
- Identify a possible phosphate donor such that the cation fully volatilizes during heat treament
- Rigorous investigation into the XRD of substituted fluorapatites not present in the available databases
- Investigation into monolith leach testings of substituted fluorapaites
- Investigate the radiolysis effects on fluorapatites in a laboratory setting

REFERENCES

[1] E. Bettis, W. Cottrell, E. Mann, J. Meem, and G. Whitman, "The aircraft reactor experiment—operation," *Nuclear Science and Engineering*, vol. 2, no. 6, pp. 841–853, 1957.

[2] W. Ferguson, F. McQuilkin, G. Robinson, and R. Strulting, "Termination report for construction of the art facility," Tech. Rep. ORNL-2465, Oak Ridge Site Specific Advisory Board, November 1959.

[3] H. MacPherson, "The molten salt reactor adventure," *Nuclear Science and engineering*, vol. 90, no. 4, pp. 374–380, 1985.

[4] P. N. Haubenreich and J. Engel, "Experience with the molten-salt reactor experiment," *Nuclear Applications and technology*, vol. 8, no. 2, pp. 118–136, 1970.

[5] F. J. Peretz, "Disposition of the fluoride fuel and flush salts from the molten salt reactor experiment at oak ridge national laboratory," tech. rep., Oak Ridge National Lab., 1996.

[6] "Molten salt reactor continues to test skills and patience," tech. rep., Oak Ridge Site Specific Advisory Board, April 2010.

[7] D. Lexa, "Preparation and physical characteristics of a lithium-beryllium-substituted fluorapatite," *Metallurgical and Materials Transactions A*, vol. 30, no. 1, pp. 147–153, 1999.

[8] S. McDeavitt, J. Park, and J. Ackerman, "Defining a metal-based waste form for ifr pyroprocessing wastes," tech. rep., Argonne National Lab., IL (United States), 1994.

[9] I. W. Donald, B. Metcalfe, S. K. Fong, L. A. Gerrard, D. M. Strachan, and R. D. Scheele, "A glass-encapsulated calcium phosphate wasteform for the immobilization of actinide-, fluoride-, and chloride-containing radioactive wastes from the pyrochemical reprocessing of plutonium metal," *Journal of nuclear materials*, vol. 361, no. 1, pp. 78–93, 2007.

[10] B. J. Riley, J. McFarlane, G. D. DelCul, J. D. Vienna, C. I. Contescu, and C. W. Forsberg, "Molten salt reactor waste and effluent management strategies: A review," *Nuclear Engineering and Design*, vol. 345, pp. 94–109, 2019.

[11] S. Crichton, T. Barbieri, and M. Tomozawa, "Solubility limits for troublesome components in a simulated low level nuclear waste glass," *Ceram. Trans.*, vol. 61, pp. 283–290, 1995.

[12] E. R. Vance, D. T. Chavara, and D. J. Gregg, "Synroc development—past and present applications," *MRS Energy & Sustainability*, vol. 4, 2017.

[13] R. AE, K. SE, W. NG, H. WO, and A. Major, "The synroc process: A geochemical approach to nuclear waste immobilization," *Geochemical Journal*, vol. 13, no. 4, pp. 141–165, 1979.

[14] S. Priebe and K. Bateman, "The ceramic waste form process at idaho national laboratory," *Nuclear Technology*, vol. 162, no. 2, pp. 199–207, 2008.

[15] W. C. Lepry, B. J. Riley, J. V. Crum, C. P. Rodriguez, and D. A. Pierce, "Solution-based approaches for making high-density sodalite waste forms to immobilize spent electrochemical salts," *Journal of nuclear materials*, vol. 442, no. 1-3, pp. 350–359, 2013.

[16] L. Campayo, S. Le Gallet, Y. Grin, E. Courtois, F. Bernard, and F. Bart, "Spark plasma sintering of lead phosphovanadate pb3 (vo4) 1.6 (po4) 0.4," *Journal of the European Ceramic Society*, vol. 29, no. 8, pp. 1477–1484, 2009.

[17] J. Elliot, *Structure and Chemistry of the Apatites and Other Calcium Orthophosphates*. Elsevier, Netherlands, 1994.

[18] R. C. Ewing, "Nuclear waste forms for actinides," *Proceedings of the National Academy of Sciences*, vol. 96, no. 7, pp. 3432–3439, 1999.

[19] H. Hidaka, K. Takahashi, and P. Holliger, "Migration of fission products into micro-minerals of the oklo natural reactors," *Radiochimica Acta*, vol. 66, no. s1, pp. 463–468, 1994.

[20] C. Beevers and D. d. McIntyre, "The atomic structure of fluor-apatite and its relation to that of tooth and bone material.(with plates xvi-xviii.)," *Mineralogical magazine and journal of the Mineralogical Society*, vol. 27, no. 194, pp. 254–257, 1946.

[21] R. Wallaeys, *Contribution à l'étude des apatites phosphocalciques*. PhD thesis, Masson & Cie, 1952.

[22] H. McCann, "The solubility of fluorapatite and its relationship to that of calcium fluoride," *Archives of oral biology*, vol. 13, no. 8, pp. 987–1001, 1968.

[23] B. E. Burakov, "Development of fluorapatite as a waste form: Final report 1," tech. rep., University of Nevada Las Vegas, 2004.

[24] N. Senamaud, D. Bernache-Assollant, J. Carpena, and C. Pin, "Synthesis and characterization of cs-bearing apatites," *MRS Online Proceedings Library (OPL)*, vol. 556, 1999.

[25] E. Macerata, P. Innocente, M. Mariani, and M. Galletta, "Immobilization of radioactive isotopes in fluorapatite matrices," *MRS Online Proceedings Library (OPL)*, vol. 1193, 2009.

[26] E. Macerata, E. Pizzi, A. Ossola, M. Giola, and M. Mariani, "Fluorapatite as immobilization matrix for nuclear waste," *Radiation Effects and Defects in Solids*, vol. 173, no. 9-10, pp. 763–771, 2018.

[27] J. R. Long, *The Use of Ammonium Bifluoride in the Preparation of Fluorides from Oxides*, vol. 3203. US Atomic Energy Commission. Technical Information Service, 1948.

[28] D. MacFarlane, P. Mineely, and P. Newman, "Synthesis of zirconium tetrafluoride using ammonium bifluoride melts," *Journal of non-crystalline solids*, vol. 140, pp. 335–339, 1992.

[29] B. Wani, S. Patwe, U. Rao, and K. Venkateswarlu, "Fluorination of oxides of uranium and thorium by ammonium hydrogenfluoride," *Journal of fluorine chemistry*, vol. 44, no. 2, pp. 177–185, 1989.

[30] A. Mukherjee and A. Awasthi, "Fluorination of thorium oxide by ammonium bifluoride and its reduction to metal," in *Thorium—Energy for the Future*, pp. 225–232, Springer, 2019.

[31] A. D. Elliot, "Structure of pyrrhotite 5c (fe9s10)," *Acta Crystallographica Section B: Structural Science*, vol. 66, no. 3, pp. 271–279, 2010.

[32] M. Yashima, A. Sakai, T. Kamiyama, and A. Hoshikawa, "Crystal structure analysis of β-tricalcium phosphate ca3 (po4) 2 by neutron powder diffraction," *Journal of Solid State Chemistry*, vol. 175, no. 2, pp. 272–277, 2003.

[33] S. Boudin, A. Grandin, M. M. Borel, A. Leclaire, and B. Raveau, "Redetermination of the β-$Ca_2P_2O_7$ structure," *Acta Crystallographica Section C*, vol. 49, no. 12, pp. 2062–2064, 1993.

[34] M. Schreyer, L. Guo, S. Thirunahari, F. Gao, and M. Garland, "Simultaneous determination of several crystal structures from powder mixtures: the combination of powder x-ray diffraction, band-target entropy minimization and rietveld methods," *Journal of Applied Crystallography*, vol. 47, no. 2, pp. 659–667, 2014.

[35] J. Lindbloom, G. Gibbs, and P. Ribbe, "The crystal structure of hurlbutite: a comparison with danburite and anorthite," *American Mineralogist: Journal of Earth and Planetary Materials*, vol. 59, no. 11-12, pp. 1267–1271, 1974.

[36] S. Speziale and T. S. Duffy, "Single-crystal elastic constants of fluorite (caf2) to 9.3 gpa," *Physics and Chemistry of Minerals*, vol. 29, no. 7, pp. 465–472, 2002.

[37] A. Cheetham, B. Fender, and M. Cooper, "Defect structure of calcium fluoride containing excess anions i. bragg scattering," *Journal of Physics C: Solid State Physics*, vol. 4, no. 18, p. 3107, 1971.

[38] Y. Luo, J. M. Hughes, J. Rakovan, and Y. Pan, "Site preference of u and th in cl, f, and sr apatites," *American Mineralogist*, vol. 94, no. 2-3, pp. 345–351, 2009.

[39] J. Kim, Y. Choi, C. Lee, S. Kim, and Y. Lee, "Crystal structure analysis of uranium oxides," *Journal of the Korean Ceramic Society*, vol. 38, no. 11, pp. 967–972, 2001.

[40] B. Wasserstein, "Cube-edges of uraninites as a criterion of age," *Nature*, vol. 168, no. 4270, pp. 380–380, 1951.

[41] C. Greaves and B. E. F. Fender, "The structure of α-uo$_3$ by neutron and electron diffraction," *Acta Crystallographica Section B*, vol. 28, pp. 3609–3614, Dec 1972.

[42] R. Klevtsova, "The crystal structure of strontium-apatite," *Journal of Structural Chemistry*, vol. 5, pp. 318–320, 1964.

[43] J. Knowles, I. Gibson, and I. Abrahams, "High temperature phase transitions in ca$_3$(po$_4$)$_2$ measured by neutron diffraction," in *Bioceramics: Volume 12*, pp. 341–344, World Scientific, 1999.

[44] M. Mathew, L. W. Schroeder, B. Dickens, and W. E. Brown, "The crystal structure of αca$_3$(po$_4$)$_2$," *Acta Crystallographica Section B*, vol. 33, no. 5, pp. 1325–1333, 1977.

[45] N. Bibler and C. Jantzen, "The product consistency test and its role in the waste acceptance process," tech. rep., Savannah River Site (SRS), Aiken, SC (United States). Savannah River . . . , 1989.

[46] K. Fox and T. Edwards, "Chemical composition and pct data for the initial set of hanford enhanced waste loading glasses," *US Department of Energy Report SRNL-STI-2014-00063, Revision*, 2014.

[47] L. Morss, M. Lewis, M. Richmann, and D. Lexa, "Cerium, uranium, and plutonium behavior in glass-bonded sodalite, a ceramic nuclear waste form," *Journal of alloys and compounds*, vol. 303, pp. 42–48, 2000.

APPENDIX A

ICP-MS Data

The following section presents the raw ICP-MS data obtained for each PCT. The fourth value in each FAp PCT block is the control for that set of data.

Sample ID	Be		Ca	
	Conc. [ng/mL]	± u (1s)	Conc. [ng/mL]	± u (1s)
FAp-1	35.0	0.9	29570	329
	30.5	0.4	27831	931
	32.0	0.5	23164	189
	ND (0.5)	-	68	35
FAp-2	0.96	0.20	196	13
	0.83	0.13	260	17
	1.53	0.05	243	3
	ND (0.5)	-	38	4
FAp-3	0.50	0.03	459	8
	1.43	0.02	533	16
	1.00	0.02	534	9
	ND (0.1)	-	60	4
U-FAp-1	4.3	0.3	318	14
	6.3	0.2	443	21
	13.1	0.3	508	10
	ND (0.5)	-	101	3
U-FAp-2	27.4	0.1	753	13
	48.0	0.7	449	4
	57.6	0.8	438	4
	ND (0.5)	-	96	13
U-FAp-3	25.6	0.5	110186	1762
	13.6	0.2	116039	4165
	14.8	0.7	102813	402
	ND (0.5)	-	817	3
FAp-4	9.2	0.3	510	15
	6.8	0.3	384	28
	10.1	0.5	772	30
	ND (0.5)	-	37	5

Cs-FAp	30.8	0.5	377	1
	33.9	0.4	451	7
	38.4	0.4	459	12
	ND (0.5)	-	40	1
Sr-FAp	41.7	0.5	48506	986
	28.2	0.3	47542	1506
	38.3	0.3	41599	812
	ND (0.5)	-	82	13
Gd-FAp	34.7	0.9	297	5
	13.1	0.3	396	12
	31.1	0.3	206	3
	ND (0.5)	-	44	13
CsGd-FAp	125093	2531	945	14
	129219	1701	939	17
	122462	1204	977	7
	1.81	0.19	39	3
M-FAp	73.7	0.3	989	11
	83.3	0.2	972	9
	81.9	1.8	678	11
	1.78	0.11	620	20

Sample ID	Sr		Cs	
	Conc. [ng/mL]	± u (1s)	Conc. [ng/mL]	± u (1s)
FAp-1	28.1	0.2	20.6	0.3
	25.3	0.4	21.5	0.2
	29.2	0.6	21.2	0.2
	0.28	0.11	ND (0.1)	-
FAp-2	5.3	0.1	ND (0.1)	-
	8.6	0.3	ND (0.1)	-
	6.3	0.1	ND (0.1)	-
	ND (0.1)	-	ND (0.1)	-
FAp-3	8.4	0.2	ND (0.1)	-
	10.0	0.2	ND (0.1)	-
	11.8	0.2	ND (0.1)	-
	ND (0.1)	-	ND (0.1)	-
U-FAp-1	6.2	0.2	0.16	0.03
	9.3	0.4	0.20	0.02
	7.59	0.05	0.20	0.01
	ND (0.1)	-	ND (0.1)	-
U-FAp-2	7.64	0.22	0.31	0.01
	0.84	0.02	7.52	0.11
	0.82	0.03	10.2	0.1
	ND (0.1)	-	ND (0.1)	-
U-FAp-3	27.9	1.1	162	5
	26.3	0.6	161	1
	25.2	1.2	156	3
	0.94	0.01	0.16	0.02
FAp-4	1.52	0.09	100	2
	1.25	0.06	101	2
	1.35	0.09	87	4
	ND (0.1)	-	ND (0.1)	-
Cs-FAp	0.58	0.01	93573	3245
	0.63	0.01	91135	1565
	0.65	0.01	92115	1868
	ND (0.1)	-	19.1	0.2
Sr-FAp	8460	146	15.5	0.3
	7572	102	14.0	0.2
	9146	192	14.2	0.2
	1.90	0.14	0.79	0.06
Gd-FAp	0.70	0.03	15.5	0.3
	11.3	0.1	0.72	0.02

	0.56	0.02	11.0	0.1
	ND (0.1)	-	0.52	0.05
CsGd-FAp	3.3	0.1	331	3
	3.1	0.1	333	2
	3.0	0.1	308	1
	ND (0.1)	-	0.29	0.01
M-FAp	5.2	0.1	5937	61
	6.0	0.1	6521	87
	5.1	0.1	6336	113
	1.00	0.01	6.21	0.03

Sample ID	Gd		U	
	Conc. [ng/mL]	± u (1s)	Conc. [ng/mL]	± u (1s)
FAp-1	0.26	0.03	0.30	0.01
	ND (0.05)	-	0.45	0.03
	ND (0.05)	-	0.20	0.01
	ND (0.05)	-	ND (0.1)	-
FAp-2	ND (0.05)	-	0.15	0.05
	ND (0.05)	-	ND (0.1)	-
	ND (0.05)	-	ND (0.1)	-
	ND (0.05)	-	ND (0.1)	-
FAp-3	ND (0.05)	-	ND (0.1)	-
	ND (0.05)	-	ND (0.1)	-
	ND (0.05)	-	ND (0.1)	-
	ND (0.05)	-	ND (0.1)	-
U-FAp-1	ND (0.05)	-	934	42
	ND (0.05)	-	885	24
	ND (0.05)	-	935	15
	ND (0.05)	-	0.41	0.04
U-FAp-2	0.11	0.05	1238	20
	0.09	0.03	1080	21
	0.13	0.04	1348	10
	ND (0.05)	-	1.08	0.03
U-FAp-3	0.16	0.06	1.33	0.02
	0.28	0.07	0.71	0.03
	ND (0.05)	-	8.76	0.23
	ND (0.05)	-	ND (0.1)	-
FAp-4	ND (0.05)	-	ND (0.1)	-
	ND (0.05)	-	0.22	0.03
	ND (0.05)	-	ND (0.1)	-
	ND (0.05)	-	ND (0.1)	-
Cs-FAp	0.70	0.04	0.24	0.01
	0.90	0.02	0.31	0.02
	0.82	0.03	0.28	0.01
	ND (0.05)	-	0.28	0.01
Sr-FAp	ND (0.05)	-	0.17	0.03
	ND (0.05)	-	ND (0.1)	-
	ND (0.05)	-	ND (0.1)	-
	0.28	0.11	0.34	0.04
Gd-FAp	13.9	0.4	0.66	0.02
	6.0	0.1	0.40	0.01

	8.7	0.2	0.60	0.01
	ND (0.05)	-	0.12	0.04
CsGd-FAp	0.88	0.02	1.40	0.03
	0.89	0.02	1.49	0.01
	0.93	0.02	1.47	0.01
	ND (0.05)	-	ND (0.1)	-
M-FAp	2.42	0.04	3748	56
	3.53	0.07	3774	50
	2.57	0.04	3593	43
	ND (0.05)	-	1.18	0.16

APPENDIX B

PCT Vessel Cleaning Log

The table below lists the cleaning log of the PTFE vessels.

Vessel Cleaning Log

Date	Vessel #	T°C	pH	F- (ppm)	Pass	Initial
12/18/18	1	21.70	7.53	0.05		x
	2	21.70	7.78	0.03		x
	3	21.70	7.93	0.02		x
	4	21.70	7.81	0.01		x
	5	21.80	7.90	0.01		x
	6	21.70	7.84	0.01		x
	7	21.80	7.93	0.00		x
	8	21.70	7.80	0.02		x
	9	21.60	7.93	0.02		x
	10	21.70	7.81	0.02		x
	11	21.70	7.21	0.01		x
	12	21.60	7.39	0.01		x
1/25/19	1	23.30	5.83	0.00	x	x
	2	23.90	5.90	0.01	x	x
	3	23.90	6.12	0.02	x	x
	4	23.10	6.15	0.00	x	x
10/23/20	1	22.50	6.89	0.03	x	x
	2	22.50	5.51	0.01	x	x
	3	22.50	6.01	0.03	x	x
	4	22.40	6.05	0.01	x	x
	5	22.40	6.04	0.01	x	x
	6	22.50	5.97	0.01	x	x
	7	22.50	6.01	0.00	x	x
	8	22.40	5.98	0.00	x	x
2/2/21	1	23.00	5.39	0.00	x	
	2	23.10	5.57	0.00	x	
	3	23.10	5.60	0.00	x	
	4	23.10	5.39	0.00	x	
	5	23.10	5.42	0.00	x	
	6	23.10	5.50	0.00	x	
	7	23.10	5.61	0.00	x	

	8	23.10	5.62	0.00	x
3/2/21	9	21.40	6.64	0.00	x
	10	21.40	5.92	0.00	x
	11	21.40	5.06	0.00	x
	12	21.40	5.91	0.00	x
6/13/21	1	19.80	6.92	0.00	x
	2	19.80	6.89	0.00	x
	3	19.80	6.42	0.00	x
	4	19.80	6.94	0.00	x
	5	19.80	6.71	0.00	x
	6	19.80	6.89	0.00	x
	7	19.80	6.92	0.00	x
	8	19.80	6.62	0.00	x
	9	19.80	6.90	0.00	x
	10	19.80	6.94	0.00	x
	11	19.80	6.85	0.00	x
	12	19.80	6.84	0.00	x
6/18/21	1	21.80	6.88	0.00	x
	2	22.00	6.97	0.00	x
	3	22.00	6.92	0.00	x
	4	21.80	6.90	0.00	x
6/22/21	5	21.60	6.95	0.00	x
	6	21.70	6.84	0.00	x
	7	21.90	6.82	0.00	x
	8	21.60	6.88	0.00	x
	9	21.60	6.93	0.00	x
	10	21.60	6.95	0.00	x
	11	21.90	6.77	0.00	x
	12	21.60	6.92	0.00	x
6/29/21	1	22.00	6.13	0.00	x
	2	22.00	6.04	0.00	x
	3	22.00	6.29	0.00	x
	4	22.00	6.29	0.00	x
7/6/21	5	22.00	6.56	0.00	x
	6	22.10	5.98	0.00	x
	7	22.00	6.02	0.00	x
	8	22.10	5.95	0.00	x
	9	22.10	5.86	0.00	x
	10	22.10	5.85	0.00	x
	11	22.10	5.86	0.00	x
	12	22.10	5.94	0.00	x
7/23/21	1	21.80	5.99	0.00	x

	2	21.80	5.33	0.00	x
	3	21.80	5.55	0.00	x
	4	21.90	5.34	0.00	x
	5	21.80	5.64	0.00	x
	6	21.90	5.30	0.00	x
	7	21.80	5.73	0.00	x
	8	21.90	5.43	0.00	x
	9	21.90	5.19	0.00	x
	10	21.90	5.44	0.00	x
	11	22.00	5.29	0.00	x
	12	22.00	5.24	0.00	x
8/26/21	1	20.10	6.33	0.00	x
	2	20.10	6.73	0.00	x
	3	20.10	6.74	0.00	x
	4	19.90	6.53	0.00	x

APPENDIX C

List of Equipment

The following is a list of equipment, manufacturer, model number, and function of equipment in this study listed by location.

Equipment used for work inside the glovebox:

Equipment	**Manufacturer**	**Model**
Glovebox	MBraun	MBraun Pro
Scale	Mettler Toldedo	MS304T7S/00
Die	Precision Die Sets	Stainless Steel 20-mm
Press	Carver	3192
Furnace	Watlow	VC404AOGA 120-V
Furnace Controller	Watlow	Watlow SD
Ceramic Tube	McDaniels	50.8-mm Alumina Tube
Milling Media	MSE Supplies	6-mm Zirconia
Sieve	Dual Manufacturing	US3-14B
Sieves Lid Manufacturing	Dual	SC-3
Sieves Pan Manufacturing	Dual	SP3-1
Calipers	Mitutoyo	CD-6"PSX
Mortar and Pestle	Fisherbrand	AFB-970E

Equipment Used Outside the Globe Box

Equipment	**Manufacturer**	**Model**
Scale	Sartorius	GD-503-NTEP
Scale	A&D	GR-202
Scale	Mettler Toledo	XSR105
PCT Vessel	Savillex	300-060-03
PCT Vessel Lid	Savillex	600-058-04
Vessel Wrench	Savillex	730-0055
Furnace	Linberg Blue	BF51442C
Oven	Yamato	ADP-21
XRD	Rigaku	MiniFlex II
SEM	JEOL	JSM-7500F
EDS	Oxford Instruments	ULTIM MAX
ICP-MS	Perkin Elmore	NexION 350
Sieves	Dual Manufacturing	US3-100S, US3-200S
Sieve Lid	Dual Manufacturing	SC-3
Sieve Pan	Dual Manufacturing	SP3-1
Sieve Shaker	Dual Manufacturing	D-4326
pH Meter	Oakton	01X099314
Fluorine Selective Ion Probe	Oakton	UX-27504-14
pH Probe Reader	Oakton	pH5+
Fluorine Probe Reader	Oakton	pH6+ Ion
Thermocouple Reader	Omega	RDXL4SD
Pycnometer	Quantachrome	ULTRAPYC 1200e
Hot Plate	ThermoScientific	HP131225
Mortar and Pestle	Fisherbrand	FB970E
Bath Sonicator	L&R	PC3
Bath Sonicator	L&R	Q210H
Pipette	Eppendorf	Research Plus 1000